# Linear encoding of the spatiotemporal cat

**B Gutkin, P Cvitanović, R Jafari, A K Saremi and L Han**

Center for Nonlinear Cat Science, School of Cat Physics, Georgia Institute of Technology, Atlanta, GA 30332-0430, USA

E-mail: predrag.cvitanovic@physics.gatech.edu

6 August 2019

**Abstract.** The dynamics of an extended, spatiotemporally chaotic systems might appear extremely complex. Nevertheless, the local dynamics, observed through a finite spatiotemporal window, can often be thought of as a visitation sequence through a finite repertoire of finite patterns. To make statistical predictions about the system, one needs to know how often a given pattern occurs. Here we address this fundamental question within a model of a 1D spatial lattice of coupled cat maps evolving in time. In this model any spatiotemporal state is labeled by a unique 2D lattice of symbols from a finite alphabet, with the lattice states and their symbolic representation related linearly (hence "linear encoding"). We show that the state of the system over a finite spatiotemporal region can be described with exponentially increasing precision by a finite pattern of symbols, and we provide a systematic, lattice Green's function methodology to calculate the frequency (i.e., the measure) of such state.

PACS numbers: RECHECK! Do they still use them? 02.20.-a, 05.45.-a, 05.45.Jn, 47.27.ed

Submitted to: *Nonlinearity*

## 1. Introduction

While the technical novelty of this paper is in working out details of the spatiotemporal cat, an elegant, but very special model of many-particle dynamics (or discretization of a classical $d$-dimensional field theory), the vision that motivates it is much broader. We address here the long standing problem of how to describe, by means of discrete symbolic dynamics, the spatiotemporal chaos (or turbulence) in spatially extended, strongly nonlinear field theories.

One way to capture the essential features of turbulent motions of a physical flow is offered by coupled map lattice models, in which the spacetime is coarsely discretized, with the dynamics of domains that capture important small-scale spatial structures modeled by discrete time maps (Poincaré sections of a single "particle" dynamics) attached to lattice sites, and the coupling to neighboring sites consistent with the

translational and reflection symmetries of the problem. Here we shall follow this path by investigating the Gutkin and Osipov [48] $d$-dimensional coupled cat maps lattice ("spatiotemporal cat" for short, in what follows), a $d$-dimensional lattice screened Poisson equation

$$(-\Box + s - 2d)\, x_z = m_z$$

built from the Anosov-Arnol'd-Sinai cat maps (modeling the Hamiltonian dynamics of individual "particles") at sites of a $(d-1)$-dimensional spatial lattice, linearly coupled to their nearest neighbors. The remarkable feature of the spatiotemporal cat is that its every solution is uniquely encoded by a linear transformation to the corresponding finite alphabet $d$-dimensional symbol lattice, a spatiotemporal generalization of the linear code for temporal evolution of a single cat map, introduced in the beautiful 1987 paper by Percival and Vivaldi [76].

[2019-01-19 Predrag] This paper builds explicit phase space partitions using Green's functions with Dirichlet b.c.'s. Explain that the Adler-Weiss partitions and periodic orbit theory are discussed in the kittens paper [27].

Within this model, a spatial-temporal window into system dynamics is provided by a finite block of symbols, and the central question is to understand which symbol blocks are admissible, and what is the likelihood of a given block's occurrence. It was already noted in [48] that two spatiotemporal orbits that sharing a same finite symbol block shadow each other exponentially well within the corresponding spatial-temporal window. This is the key property of hyperbolic spatiotemporal dynamics that we explore in detail in this paper. The linearity of the spatiotemporal cat enables us to go far analytically; lattice Green's function methods enable us to compute explicitly the measures of a large set of spatiotemporally finite blocks, and give an algorithm for exact computation of the rest (so far computationally feasible only for small blocks).

We start by formulating our "spatiotemporal cat" and stating the main results of the paper.

## 2. Model and overview of the main results

*Spatiotemporal cat*

Consider a linear, phase space (area) preserving map of a 2-torus $\mathbb{T}^2 = \mathbb{R}^2/\mathbb{Z}^2$ onto itself

$$\begin{pmatrix} x_{t+1} \\ p_{t+1} \end{pmatrix} = A \begin{pmatrix} x_t \\ p_t \end{pmatrix} \mod 1\,, \qquad A = \begin{pmatrix} s-1 & 1 \\ s-2 & 1 \end{pmatrix}\,, \tag{1}$$

where both $x_t$ and $p_t$ belong to the unit interval. For integer $s = \operatorname{tr} A > 2$ the map is referred to as a cat map [2]. It is a fully chaotic Hamiltonian dynamical system, which, rewritten as a 2-step difference equation in $(x_{t-1}, x_t)$ takes a particularly simple form [76]

$$x_{t+1} - s\, x_t + x_{t-1} = -m_t\,, \tag{2}$$

with the unique integer "winding number" $m_t$ at every time step $t$ ensuring that $x_{t+1}$ lands in the given covering partition of the unit torus. While the dynamics is linear, the nonlinearity comes through the (mod 1) operation, encoded in $m_t \in \mathcal{A}$, where $\mathcal{A}$ is finite alphabet of possible values for $m_t$.

The single cat map is generalized to the *spatiotemporal* cat map by considering a 1-dimensional spatial lattice, with field $x_{n,t}$ at site $n$. If each site couples only to its nearest neighbors $x_{n\pm1,t}$, and if we require (1) invariance under spatial translations, (2) invariance under spatial reflections, and (3) invariance under the space-time exchange, we arrive at the 2-dimensional Euclidean cat map lattice:

$$x_{n,t+1} + x_{n,t-1} - s\, x_{n,t} + x_{n+1,t} + x_{n-1,t} = -m_{n,t}\,. \tag{3}$$

The temporal cat map (2), and the spatiotemporal cat (3) can be brought into uniform notation and generalized to $d$ dimensions by converting the spatialtemporal differences to discrete derivatives. This yields the discrete screened Poisson equation equation for the $d$-dimensional *spatiotemporal cat*

$$\begin{aligned}(-\Box + s - 2d)\, x_z = m_z\,, \qquad & m_z \in \mathcal{A}\,, \\ \mathcal{A} = \{-2d+1, -2d+2, \cdots, s-2, s-1\}\,, & \end{aligned} \tag{4}$$

$x_z \in \mathbb{T}^1$, $z \in \mathbb{Z}^d$, where the map is smooth and fully hyperbolic for integer $s > 2d$. For a discrete Euclidean space-time the Laplacian is given by

$$\Box\, x_t \equiv x_{t+1} - 2\, x_t + x_{t-1} \tag{5}$$

$$\Box\, x_{n,t} \equiv x_{n,t+1} + x_{n+1,t} - 4\, x_{n,t} + x_{n,t-1} + x_{n-1,t} \tag{6}$$

in $d = 1$ and 2 dimensions, respectively. The key insight (an insight that applies to coupled-map lattices [79–81], and PDEs modeled by them, not only the system considered here) is that a $d$-dimensional spatiotemporal pattern $\{x_z\} = \{x_z, z \in \mathbb{Z}^d\}$ is best described by the corresponding *d-dimensional* spatiotemporal symbol block $\{m_z\} = \{m_z, z \in \mathbb{Z}^d\}$, rather than a *single* temporal symbol sequence, as one usually does when describing a finite coupled "$N$-particle" system.

As the relation (4) between the trajectory $x_z$ and its symbolic dynamics encoding $m_z$ is linear, we refer to $m_z$ as the "linear code" [76], both for the cat map (2) in one dimension (temporal dynamics of a single "particle") and for the spatiotemporal cat (4) in $d$ dimensions (temporal dynamics of a ($d$-1)-dimensional spatial lattice of $N^{d-1}$ interacting "particles," $N \to \infty$). Given a set of $\{m_z\}$, the linearity of (4) enables us to find solution for $\{x_z\}$ by lattice Green's function methods.

However, the requirement that all $x_z \in [0, 1)$ introduces an infinite set of grammar rules for admissible symbol blocks $\{m_z\}$.

[2018-02-16 Predrag] Dropped this: Refer elsewhere to [27] where it is shown that the Adler-Weiss partition yields the full solution as a finite subshift.

*Statement of the problem*

Let $\mathsf{X} = \{x_z \in \mathbb{T}^1, z \in \mathbb{Z}^2\}$ be a spatiotemporally infinite solution of spatiotemporal cat (4) for $d = 2$, in the fully hyperbolic regime $s > 4$, and let $\mathsf{M} = \{m_z \in \mathcal{A}\,,\ z \in \mathbb{Z}^2\}$

be its symbolic representation. By the linear connection between $\mathsf{X}$ and $\mathsf{M}$, the corresponding symbolic dynamics block $\mathsf{M}$ is unique and admissible, i.e., $\mathsf{M}$ defines the unique spatiotemporal state $\mathsf{X}$ and vice-versa.

Assume now that only partial information is available, and we know only a finite block of symbols $\mathsf{M}_\mathcal{R} \subset \mathsf{M}$, over a finite lattice region $\mathcal{R} \subset \mathbb{Z}^2$. What information about the local spatiotemporal pattern $\mathsf{X}_\mathcal{R} = \{x_z \in \mathbb{T}^1,\, z \in \mathcal{R}\}$ does this give us? To be specific, let $\mathcal{R}$ be a rectangular $[\ell_1 \times \ell_2]$ region, and let $\mathsf{M}_\mathcal{R}$ be the $[\ell_1 \times \ell_2]$ block of $\mathsf{M}$ symbols. For the standard cat map symbolic dynamics based on a finite Markov partition of the cat map phase space, a finite block of symbols defines the corresponding trajectory points up to an error which decreases exponentially with the length of the symbol block [16, 18, 84]. We would like to know whether the corresponding result holds for 2-dimensional linear symbolic dynamics:

**Q1.** *To what precision does* $\mathsf{M}_\mathcal{R}$ *define the values of* $x_z, z \in \mathcal{R}$*?*

The central question studied in this paper is the measure of the partition corresponding to given finite symbol block within the symbolic representation of a generic spatiotemporal pattern.

Let $\mathsf{M}_\mathcal{R}$ be a fixed $[\ell_1 \times \ell_2]$ block of symbols from the alphabet $\mathcal{A}$. Let $\mathcal{N}(\mathsf{M}_\mathcal{R}|\mathsf{M}_{[L\times T]})$ be the number of times a given symbol block $\mathsf{M}_\mathcal{R}$ appears anywhere within a much larger admissible symbol block $\mathsf{M}_{[L\times T]}$ cut out from a spatiotemporally infinite generic solution $\mathsf{M}$ of the spatiotemporal cat (4). The $d = 1$ cat map is known to be fully hyperbolic and ergodic for $s > 2$, with a unique invariant natural measure $\mu$ in the phase space (1) of the system.

Similarly, the $d = 2$ spatiotemporal cat is fully hyperbolic and ergodic for $s > 4$, see (B.3). In the language of spatially extended systems, we assume that a steady state "turbulent" solution is on average spatiotemporally invariant, so the number of times a *given* admissible block $\mathsf{M}_\mathcal{R}$ shows up over a region $[L \times T]$ is expected to grow linearly with the area $LT$. Hence a *relative* frequency of the occurrence of the block $\mathsf{M}_\mathcal{R}$ can be defined as

$$f(\mathsf{M}_\mathcal{R}|\mathsf{M}_{[L\times T]}) = \frac{1}{LT}\mathcal{N}(\mathsf{M}_\mathcal{R}|\mathsf{M}_{[L\times T]})\,. \tag{7}$$

With $L$ and $T$ increasing at comparable rates (for example, take a square $[L \times T]$, i.e., $L = T$), the ergodic measure of finding the block $\mathsf{M}_\mathcal{R}$ across the infinite spatiotemporal domain is given by

$$\mu(\mathsf{M}_\mathcal{R}) = \lim_{L,T\to\infty} f(\mathsf{M}_\mathcal{R}|\mathsf{M}_{[L\times T]})\,, \qquad \sum_{\mathsf{M}_\mathcal{R}} \mu(\mathsf{M}_\mathcal{R}) = 1\,. \tag{8}$$

For an ergodic system with a unique invariant natural measure $\mu$, the limiting frequencies $f(\mathsf{M}_\mathcal{R})$ are equal to the measures $\mu(\mathcal{M}_\mathcal{R})$ of the cylinder sets $\mathcal{M}_\mathcal{R}$, defined as sets of phase space points $\mathsf{X}_\mathcal{R}$ having $\mathsf{M}_\mathcal{R}$ symbolic representation over the region $\mathcal{R}$. For this reason we sometimes refer, with a slight abuse of notation, to the frequencies $f(\mathsf{M}_\mathcal{R})$ defined by (7) as measures of $\mathsf{M}_\mathcal{R}$ in the limit $L, T \to \infty$, and denote them by $\mu(\mathsf{M}_\mathcal{R})$ in what follows. So our second question is:

**Q2.** *How often does a prescribed finite symbol block* $\mathsf{M}_\mathcal{R}$ *occur in the symbolic representation* $\mathsf{M}$ *of a generic state* $\mathsf{X}$*?*

*Main results*

**Answer to Q1.** *The block of symbols* $\mathsf{M}_\mathcal{R}$ *defines the phase space points of* $\mathsf{X}$ *within* $\mathcal{R}$ *up to an error which decreases exponentially with the size of the block* $\mathcal{R}$*.*

The linear code has no simple, finite set of grammar rules. Nevertheless, the spatiotemporal cat alphabet is finite, and we find it helpful to split it into two parts,

$$\mathcal{A} = \mathcal{A}_0 \cup \mathcal{A}_1 \,,$$

where the number of symbols in the exterior alphabet $\mathcal{A}_1$ is finite, and the interior alphabet $\mathcal{A}_0$ is a full shift, with the number of symbols in $\mathcal{A}_0$ growing linearly with $s$. The following hold:

- Any block of symbols from $\mathcal{A}_0$ is admissible.
- Measures of blocks $\mathsf{M}_\mathcal{R}$ are given by rational numbers and factorize into products of constant and geometrical parts:

  $$\mu(\mathsf{M}_\mathcal{R}) = d_\mathcal{R} |\mathcal{P}(\mathsf{M}_\mathcal{R})| \,.$$

  The constant $d_\mathcal{R}$ depends only on the shape of $\mathcal{R}$, independent of the symbolic content $M_\mathcal{R}$. The factor $|\mathcal{P}(\mathsf{M}_\mathcal{R})|$ admits geometrical interpretation as the volume of polytope $\mathcal{P}(\mathsf{M}_\mathcal{R})$ in the $|\partial\mathcal{R}|$-dimensional Euclidean space, where $|\partial\mathcal{R}|$ is the number of boundary points of the domain $\mathcal{R}$. The shape of $\mathcal{P}(\mathsf{M}_\mathcal{R})$ is determined by the content of $\mathsf{M}_\mathcal{R}$. For small $\mathcal{R}$, $\mu(\mathsf{M}_\mathcal{R})$ can be evaluated analytically.
- If $\mathsf{M}_\mathcal{R}$ is composed only of symbols from $\mathcal{A}_0$, then $|\mathcal{P}(\mathsf{M}_\mathcal{R})| = 1$ and $\mu(\mathsf{M}_\mathcal{R}) = d_\mathcal{R}$.
- The difference between any solution $x_{z_0}$ of (4) for $z_0 \in \mathcal{R}$ and the "average coordinate" $\bar{x}(\mathsf{M}_\mathcal{R})$, determined solely by $\mathsf{M}_\mathcal{R}$, is bounded by

  $$|x_{z_0} - \bar{x}(\mathsf{M}_\mathcal{R})| \leq C e^{-\nu \ell(z_0, \partial\mathcal{R})} \,, \qquad \nu > 0, \tag{9}$$

  where $\ell(z_0, \partial\mathcal{R})$ is the minimal Euclidean distance between $z_0$ and the boundary $\partial\mathcal{R}$. For explicit formulas for $\bar{x}(\mathsf{M}_\mathcal{R})$ in terms of the block of symbols $\mathsf{M}_\mathcal{R}$ see (24) and (41).

**Answer to Q2.** *The spatiotemporal cat admits a natural two-dimensional linear symbolic code with a finite alphabet. We show how to compute analytically the measure of a given finite spatiotemporal symbol block* $\mathsf{M}_\mathcal{R}$ *over a region* $\mathcal{R}$*.*

The key conceptual ingredient that underpins this calculation, hidden in much algebra in what follows, are the transformations (30) and (45) from the Hamiltonian initial state formulation to the Lagrangian end points formulation. This replaces the

exponentially unstable Hamiltonian time evolution problem by a robustly convergent Lagrangian boundary value problem.

In principle, having answers to Q1 and Q2 allows for a calculation of the expectation values of observables by means of symbolic dynamics. As $\mathsf{M}_{\mathcal{R}}$ defines positions of points in the center $z_0$ of region $\mathcal{R}$ with exponential precision, any observable $A(z)$ can be viewed as a function of $\mathsf{M}_{\mathcal{R}}$, $A(z_0) \approx A\left(\mathsf{M}_{\mathcal{R}}\right)$, where the quality of the approximation increases exponentially with the size of $\mathcal{R}$. In the limit of large region size $|\mathcal{R}|$, one approximates the sum over states of the lattice with exponentially increasing accuracy, and has for the average of $A$

$$\langle A \rangle = \lim_{|\mathcal{R}|\to\infty} \sum_{\mathsf{M}_{\mathcal{R}}} \mu(\mathsf{M}_{\mathcal{R}}) A\left(\mathsf{M}_{\mathcal{R}}\right) \ , \tag{10}$$

where the sum is over all admissible blocks of symbols within $\mathcal{R}$. In particular, for $A = -\frac{1}{|\mathcal{R}|}\log\mu(\mathsf{M}_{\mathcal{R}})$ the above expression defines the spatiotemporal entropy of the system.

For any general spatiotemporal system, relative frequencies $f(\mathsf{M}_{\mathcal{R}})$ defined by (7) provide a practical, numerical way to estimate measures $\mu(\mathsf{M}_{\mathcal{R}})$, by generating solutions on finite $[L\times T]$ regions, compatible everywhere locally with the defining equation (4), and counting the number of times $\mathsf{M}_{\mathcal{R}}$ occurs within each such solution. However, due to the linear relation between a lattice state $\mathsf{X}$ and its symbolic encoding $\mathsf{M}$, for the spatiotemporal cat one can do much better, and compute measures $\mu(\mathsf{M}_{\mathcal{R}})$ *analytically and explicitly*, see sections 3.5 and 4.3.

All the above results hold for the $d = 1$ temporal cat map if $s > 2$, see section 3. In this case, the region $\mathcal{R}$ is just an interval at $\mathbb{Z}$ with two endpoints, $|\partial\mathcal{R}| = 2$. The resulting regions $\mathcal{P}(\mathsf{M}_{\mathcal{R}})$ are polygons whose areas can be easily evaluated. It is plausible that similar results hold for (4) on the lattice of dimension $d$, provided that the system is in the chaotic regime. However, in order to streamline the exposition, we discuss here only the two lowest dimensional cases.

The paper is organized as follows: In section 3 we introduce the single cat map, and its linear code formulation (section 3.1). The new results follow from our determination of phase space partitions generated by the iterations of the temporal cat map, for different integer values of the stretching parameter $s$. In section 3.4 we investigate the measures corresponding to admissible finite symbolic blocks, and in section 3.5 we demonstrate the splitting of the alphabet into interior and exterior parts, and show that block measures factorize into a geometric part, and a constant part which depends only on the length of the block. These measures correspond to the areas of partitions in phase space, labelled by the admissible blocks of cat map symbolic dynamics. We evaluate explicitly the geometrical factor for short blocks of symbols and estimate the single cat map metric entropy.

In section 4 we extend these results to the spatiotemporal cat. We show in section 4.1 that the system admits a natural two-dimensional linear symbolic code with a

finite alphabet, and then compute the measures of finite spatiotemporal symbol blocks in section 4.2. In section 5 we use these results to construct sets of spatiotemporal invariant 2-tori that partially shadow each other. Implementing this program requires several tools not standard in dynamicist's tool box: lattice Green's functions, new kinds of determinants, new relations between propagation of temporal vs. spatial disturbances; some of these are derived in Appendix A. The results are summarized and some open questions discussed in the section 6.

## 3. Life of a single cat

Before turning to the "many-particle" case it is instructive to motivate our formulation of the spatiotemporal cat by investigating the single cat map ($L = 1$ particle case; a "spatial lattice" with only one site). We start by a brief review of the physical origin of cat maps.

Area-preserving maps that describe kicked rotors subject to a discrete time sequence of angle-dependent impulses $F(x_t)$, $t \in \mathbb{Z}$,

$$x_{t+1} = x_t + p_{t+1} \qquad \mod 1, \tag{11}$$

$$p_{t+1} = p_t + F(x_t)\,, \tag{12}$$

play important role in the theory of chaos in Hamiltonian systems, from the Taylor, Chirikov and Greene standard map [20, 69], to the cat maps that we study here. Here $2\pi x$ is the angle of the rotor, $p$ is the momentum conjugate to the configuration coordinate $x$, $F(x) = F(x+1)$ is periodic with period 1, and the time step has been set to $\Delta t = 1$. Eq. (11) says that in one time step $\Delta t$ the configuration trajectory starting at $x_t$ reaches $x_{t+1} = x_t + p_{t+1}\Delta t$, and (12) says that at each kick the angular momentum $p_t$ is accelerated to $p_{t+1}$ by the force pulse $F(x_t)\Delta t$. As the values of $x$ differing by integers are identified, and the momentum $p$ is unbounded, the phase space is a cylinder. However, to analyse the dynamics, one can just as well compactify the phase space by folding the momentum dynamics onto a circle, by adding "mod 1" to (12). This reduces the dynamics to a toral automorphism acting on a $(0,1] \times (0,1]$ square of unit area, with the opposite sides identified.

The simplest example of (11,12) is a rotor subject to a force $F(x) = Kx$ linear in the displacement $x$. The mod 1 added to (12) makes this a discontinuous "sawtooth," unless $K$ is an integer. In that case the map (11,12) is a continuous automorphism of the torus, or a "cat map" [2], a linear symplectic map on the unit 2-torus phase space, $(x \mapsto Ax \,|\, x \in \mathbb{T}^2 = \mathbb{R}^2/\mathbb{Z}^2\,;\ A \in SL(2,\mathbb{Z}))$, with coordinates $x = (x_t, p_t)$ interpreted as the angular position variable and its conjugate momentum at time instant $t$. Explicitly:

$$\begin{pmatrix} x_{t+1} \\ p_{t+1} \end{pmatrix} = A \begin{pmatrix} x_t \\ p_t \end{pmatrix} \quad \mod 1\,, \qquad A = \begin{pmatrix} a & c \\ d & b \end{pmatrix}\,, \tag{13}$$

where $a, b, c, d$ are integers whose precise values do not matter, as long as $\det A = 1$, so that the map is symplectic (area preserving).

A cat map is a fully chaotic Hamiltonian dynamical system if its stability multipliers $(\Lambda\,,\ \Lambda^{-1})$, where

$$\Lambda = (s + \sqrt{(s-2)(s+2)})/2\,, \qquad \Lambda = e^{\lambda}\,, \tag{14}$$

are real, with a positive Lyapunov exponent $\lambda > 0$. The eigenvalues are functions of a single parameter $s = \mathrm{tr}\, A = \Lambda + \Lambda^{-1}$, and the map is chaotic if and only if $|s| > 2$. We shall refer here to the least unstable of the cat maps (13), with $s = 3$, as the "Arnol'd", or "Arnol'd-Sinai cat map" [2, 32], and to general maps with integer $s \geq 3$ as "cat maps". Cat maps have been extensively analyzed as particularly simple examples of chaotic Hamiltonian dynamics. They exhibit ergodicity, mixing, exponential sensitivity to variation of the initial conditions (the positivity of the Lyapunov exponent), and the positivity of the Kolmogorov-Sinai entropy [89]. Detailed understanding of dynamics of cat maps is important also for the much richer world of nonlinear hyperbolic toral automorphisms, see [24, 40, 88] for examples.

### *3.1. Linear code*

Eqs. (11,12) are the discrete-time Hamilton's equations, which induce temporal evolution on the 2-torus $(x_t, p_t)$ *phase space*. For the problem at hand, it pays to go from the Hamiltonian $(x_t, p_t)$ phase space formulation to the Newtonian (or Lagrangian) $(x_{t-1}, x_t)$ *state space* formulation [76], with $p_t$ replaced by $p_t = (x_t - x_{t-1})/\Delta t$ . Eq. (12) then takes the 2-step difference form (the discrete time Laplacian $\Box$ formula for the second order time derivative $d^2/dt^2$, with the time step set to $\Delta t = 1$),

$$\Box\, x_t \equiv x_{t+1} - 2x_t + x_{t-1} = F(x_t) \qquad \mod 1\,, \tag{15}$$

i.e., Newton's Second Law: "acceleration equals force." For a cat map, with force $F(x)$ linear in the displacement $x$, the Newton's equation of motion (15) takes form

$$(\Box + 2 - s)\, x_t = -m_t\,, \tag{16}$$

with $\mod 1$ enforced by $m_t$'s, integers from the alphabet

$$\mathcal{A} = \{\underline{1}, 0, \ldots s-1\}\,, \tag{17}$$

necessary to keep $x_t$ for all times $t$ within the unit interval $[0, 1)$. The genesis of this alphabet is illustrated by figure 1. We have introduced here the symbol $\underline{|m_t|}$ to denote $m_t$ with the negative sign, i.e., '$\underline{1}$' stands for symbol '$-1$'.

### *3.2. Percival-Vivaldi linear code partition of the phase space*

To interpret $m_t$'s, consider the action of the Newtonian cat map (16) on a 2-dimensional state space point $(x_{t-1}, x_t)$,

$$\begin{pmatrix} x_t \\ x_{t+1} \end{pmatrix} = A' \begin{pmatrix} x_{t-1} \\ x_t \end{pmatrix} - \begin{pmatrix} 0 \\ m_t \end{pmatrix}\,, \qquad A' = \begin{pmatrix} 0 & 1 \\ -1 & s \end{pmatrix}. \tag{18}$$

In Percival and Vivaldi [76] this representation of cat map is referred to as "the two-configuration representation". As illustrated in figure 1, in one time step the area

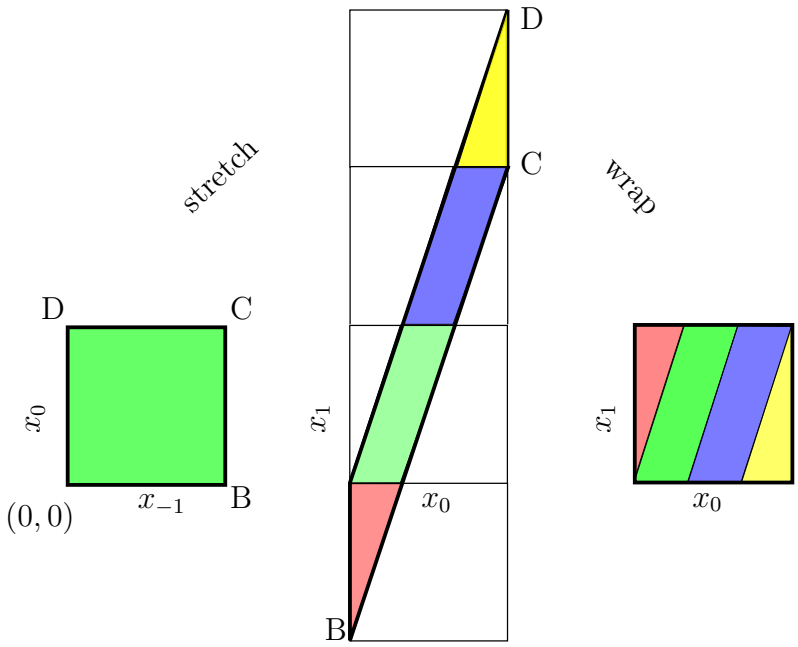


**Figure 1.** (Color online) The Newtonian $s = 3$ Arnol'd cat map matrix $A'$ (18) keeps the origin $(0, 0)$ fixed, but otherwise stretches the unit square into a parallelepiped. Translations by $m_0$ from alphabet $\mathcal{A} = \{\underline{1}, 0, 1, 2\}$ = {red, green, blue, yellow} bring stray regions back onto the torus.

preserving map $A'$ stretches the unit square into a parallelogram, and a point $(x_0, x_1)$ within the initial unit square in general lands outside it, in another unit square $m_t$ steps away. As they shepherd such stray points back into the unit torus, the integers $m_t$ can be interpreted as "winding numbers" [62], or "stabilising impulses" [76]. The $m_t$ translations reshuffle the state space, thus partitioning it into $|\mathcal{A}|$ regions $\mathcal{M}_m$, $m \in \mathcal{A}$.

There are the two kinds of pieces within partitions of figure 1 and figure 2 (a): the two interior parallelepipeds $\mathcal{M}_0$, $\mathcal{M}_1$, and the two exterior triangles $\mathcal{M}_{\underline{1}}$, $\mathcal{M}_2$, a result of cutting the third parallelepiped into two triangles. Hence one distinguishes the 1/3 of the square partitions, labeled here by the $(s-1)$-letter *interior* alphabet $\mathcal{A}_0$, and the 1/6 partitions, labeled by the two-letter *exterior* alphabet $\mathcal{A}_1$. For integer $s \geq 2$ these alphabets are

$$\mathcal{A} = \mathcal{A}_0 \cup \mathcal{A}_1 \,, \qquad \mathcal{A}_0 = \{0, \cdots, s-2\} \,, \qquad \mathcal{A}_1 = \{\underline{1}, s-1\} \,. \tag{19}$$

The interior alphabet $\mathcal{A}_0$ is a full shift, corresponding to a Smale horseshoe repeller (its phase space portraits are shown in figure 2 (g)-(i)), with any sequence of $m_t \in \mathcal{A}_0$ admissible. All grammar rules ("pruning" of inadmissible blocks) will involve the exterior alphabet symbols.

Refinements of these partitions work very much like they do for the baker's map and the Smale horseshoe, by peering further into the future and the past, and constructing the intersections of the future and past partitions [30]. The "$\ell$-th level" of partition $\mathcal{M} = \cup \mathcal{M}_b$ is labeled by the set of all admissible blocks $b$ of length $\ell$, composed of the

past $\ell - t - 1$ steps, and future $t$ steps, with 'decimal point' denoting the present,

$$b = m_{t-\ell+1} \cdots m_{-1} m_0 . m_1 m_2 \cdots m_t \,.$$

How the blocks partition the state space is best understood by inspecting figure 2.

[2017-09-04 Predrag] Please reformat the LaTeX layout of figure 2 (not the plots themselves! and without decreasing the sizes of individual plots) so each plot has in the lower left corner a label (a), (b), ..., (h), (i)

The state space coordinates $(x_0, x_1)$ are, up to the linear shift $p_t = x_t - x_{t-1} \to x_t$, equivalent to the Hamiltonian $(x_0, p_0)$ phase space, and as the cat map is invertible, ergodic, and area preserving, with the invariant measure $d\mu = dx_t dp_t = dx_t\, dx_{t-1}$ and uniform invariant density $\rho(x_0, x_1) = 1$, the measure $\mu(b)$ corresponding to a block $b$ equals to the area $|\mathcal{M}_b|$ of a state space region $\mathcal{M}_b$. The $(x_0, x_1)$ state space is composed of a disjoint union of regions $\mathcal{M} = \cup \mathcal{M}_b$ labelled by all admissible blocks of a fixed length $|b| = \ell$, so the sum of all measures $\mu(b)$ equals the total area of the state space $|\mathcal{M}| = 1$,

$$\sum_{|b|=\ell} \mu(b) = 1 \,. \tag{20}$$

The area $|\mathcal{M}_b|$ can be evaluated, for example, using Mathematica geometric computation tools [93]. Area sums over subpartitions, such as

$$\begin{aligned} \sum_{m_1} \mu(m_1 m_2 \cdots m_\ell) &= \mu(m_2 \cdots m_\ell) \\ \sum_{m_\ell} \mu(m_1 m_2 \cdots m_\ell) &= \mu(m_1 \cdots m_{\ell-1}) \,, \end{aligned} \tag{21}$$

provide consistency checks for such computations.

By the ergodic theorem, the relative frequency of appearances of a block $b$ in a generic ergodic trajectory equals $\mu(b)$. This allows for a numerical estimate of $\mu(b)$ by long ergodic trajectories, as illustrated in table 1. For the problem at hand, there is, in principle, no need for such simulations, as the areas of partitions are given analytically and, if evaluated with the integer arithmetic, exactly. We have computed such tables for partitions up to block length $|b| = 12$, but the results are quickly too unwieldy and unilluminating to tabulate here. We visualize instead the measures by their areas in the $(x_0, x_1)$ plane, as illustrated in figure 2.

### *3.3. From itineraries to orbits and back*

The power of the linear code for a cat map [76] is that one can use integers $m_t$ to encode its state space trajectories. Since the connection (16) between sequences of $m_t$ and $x_t$ is linear, it is straightforward to go back and forth between state space and symbolic representation of an orbit. In particular, if $\{m_t\}$ is an admissible itinerary, the corresponding state space point at the $t$ time instant is given by the inverse of (16),

$$x_t = \sum_{t'=-\infty}^{\infty} g_{tt'} m_{t'} \,, \qquad g_{tt'} = \left( \frac{1}{-\Box - 2 + s} \right)_{tt'} \,. \tag{22}$$

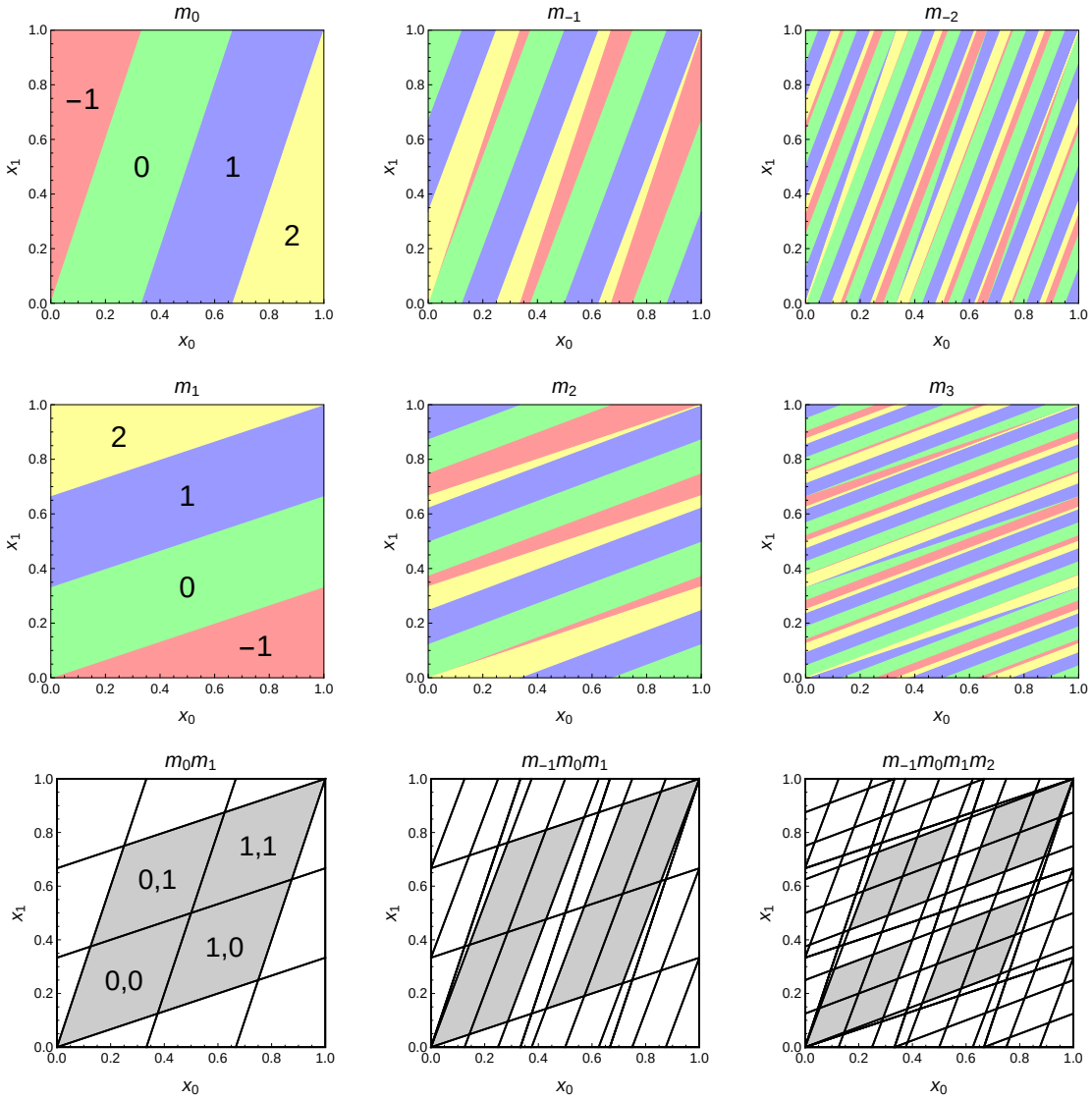


**Figure 2.** (Color online) Arnol'd cat map $(x_0, x_1)$ state space partition into (a) 4 regions labeled by $m_0$. , obtained from $(x_{-1}, x_0)$ state space by one iteration (the same as figure 1). (b) 14 regions labeled by past block $m_{-1}m_0$., obtained from $(x_{-2}, x_{-1})$ state space by two iterations. (c) 44 regions, past block $m_{-2}m_{-1}m_0$. (d) 4 regions labeled by $.m_1$ , obtained from $(x_2, x_1)$ state space by one backward iteration. (e) 14 regions labeled by future block $.m_1m_2$ , obtained from $(x_3, x_2)$ state space by two backward iterations. (f) 44 regions, future block $m_3m_2m_1$. Each color has the same total area (1/6 for $m_t = \underline{1}, 2$, and 1/3 for $m_t = 0, 1$). State space partition into (g) 14 regions labeled by block $b = m_0.m_1$, the intersection of one past (a) and one future iteration (d). (h) block $b = m_{-1}m_0.m_1$, the intersection of two past (b) and one future iteration (d). (i) block $b = m_{-1}m_0.m_1m_2$, the intersection of two past (b) and two future iterations (e). Note that while some regions involving external alphabet (such as _22_ in (g)) are pruned, the interior alphabet labels a horseshoe, indicated by the shaded regions. The first three covers of the horseshoe have areas (g) $4 \times 1/8$, (h) $8 \times 1/21$, and (i) $16 \times 1/55$. All boundaries are straight lines with rational slopes.

| | $\underline{1}$ | 0 | 1 | 2 |
|---|---|---|---|---|
| $\underline{1}$ | 0 | 0.0208 | 0.0625 | 0.0833 |
| 0 | 0.0208 | 0.1250 | 0.1250 | 0.0625 |
| 1 | 0.0625 | 0.1250 | 0.1250 | 0.0208 |
| 2 | 0.0833 | 0.0625 | 0.0208 | 0 |

| | $\underline{1}$ | 0 | 1 | 2 |
|---|---|---|---|---|
| $\underline{1}$ | 0 | 1/48 | 1/16 | 1/12 |
| 0 | 1/48 | 1/8 | 1/8 | 1/16 |
| 1 | 1/16 | 1/8 | 1/8 | 1/48 |
| 2 | 1 /12 | 1/16 | 1/48 | 0 |

**Table 1.** The measures $\mu(m_i m_{i+1})$ of the 16 distinct 2-symbol blocks $m_i m_{i+1}$ for the $s = 3$ Arnol'd cat map, (left) obtained from a long-time ($\sim 10^9$ iterations) numerical simulation rounded off to four significant digits; (right) the exact values given by (34), or read off as sub-partition areas in figure 2 (g). Column: $m_i$. Row: $m_{i+1}$. See figure 2 for a geometric picture of why blocks $\underline{11}$ and 22 are pruned.

The matrix $g_{tt'}$ is the Green's function for one-dimensional discretized heat equation [73, 76] given explicitly by $g_{tt'} = \Lambda^{-|t-t'|}/(\Lambda - \Lambda^{-1})$, $s = \Lambda + \Lambda^{-1}$, see (14) and Appendix A.

Although the recovery of state space periodic orbits from finite symbol blocks is straightforward for the linear code, it is not easy to describe the grammar rules for which symbol blocks are admissible [77]. For the linear code as presented here there is no finite set of short pruned block grammar rules (in contrast, as explained in [27], linear code for the Adler–Weiss Markov partition of the phase space cat map is a generating partition). An itinerary $\ldots m_{-1} m_0 m_1 \ldots$ is admissible if and only if each of the corresponding state space orbit points $x_t$ in (22) is in the unit interval $[0, 1)$. Therefore, there is an infinite number of conditions to satisfy.

All these conditions, however, are automatically satisfied if the symbols $m_t$ belong to the interior alphabet $\mathcal{A}_0$ (19): if $0 \le m_t \le s-2$ for all $t$, then

$$0 \le \sum_{n=-\infty}^{\infty} \frac{m_n \Lambda^{-|n|}}{\Lambda - \Lambda^{-1}} \le \sum_{n=-\infty}^{\infty} \frac{(\Lambda^{-1} + \Lambda - 2)\Lambda^{-|n|}}{\Lambda - \Lambda^{-1}} = 1\,, \tag{23}$$

and all $x_i$ generated by (22) fall into $[0, 1)$.

The number of letters of the interior alphabet $\mathcal{A}_0$ grows linearly with the increasing stretching parameter $s$, while the exterior alphabet $\mathcal{A}_1$ always consists of only two letters. This implies that in entropy estimates for large values of $s$, the orbits affected by the exterior letters pruning rules can be neglected, and the dynamics of the cat map approaches a Bernoulli process.

### *3.4. Measures of symbolic sequences*

While an admissible infinite itinerary defines a unique trajectory in the state space, a finite block $b = m_1 m_2 \ldots m_\ell$ determines the cylinder set of $\mathsf{M}_b$, a state space region of all points with itineraries of the form

$$\cdots a_{-2} a_{-1} \,.\, m_1 m_2 \cdots m_\ell a_{\ell+1} a_{\ell+2} \cdots\,,$$

with fixed $m_i$'s, and arbitrary $a_i \in \mathcal{A}$. One is interested in the measures $\mu(b) = |\mathcal{M}_b|$ of these regions in the phase space. Figure 1 illustrates how these measures are generated.

Stretching of the initial unit square and wrapping it onto the torus results in the exterior alphabet labelled triangles $\mathcal{M}_{\underline{1}}$ and $\mathcal{M}_2$, i.e., variations in partition areas, as well as to *pruning* rules, such as inadmissibility of itineraries that contain blocks $\_\underline{11}\_$ and/or $\_22\_$, see figure 2 (g). The number of partitions grows exponentially with the number of time steps, while their areas $|\mathcal{M}_b|$ shrink exponentially. Furthermore, for larger $|b|$, the domains $\mathcal{M}_b$ split into disjoint sets making it hard to determine their areas and the pruning rules for longer blocks.

For that calculation, the Lagrangian reformulation of the trajectory determination as a variational problem for a trajectory fixed by the boundary points $x_0$ and $x_{\ell+1}$ is, as we now show, more natural. Furthermore, as we show in section 4.2, the Lagrangian formulation applies in a natural way to the spatiotemporal cat, in any spatial dimension.

Let $\{x_t\}$ be a trajectory generated by the cat map and let $\{m_t\}$ be its symbolic representation. The state $x_t$ at time $t \in \{1, \dots \ell\}$ can be expressed through the block $b = m_1 m_2 \dots m_\ell$ at the times $1, \dots \ell$, and the boundary coordinates $(x_0, x_{\ell+1})$:

$$x_t = \sum_{t'=1}^{\ell} \mathsf{g}_{tt'} m_{t'} + \mathsf{g}_{t1} x_0 + \mathsf{g}_{t\ell} x_{\ell+1} \,, \qquad t = 1, \dots \ell. \tag{24}$$

[2017-09-04 Predrag] Border notation conflicts with (40). Shouldn't it be $+\mathsf{g}_{t,0}x_0 + \mathsf{g}_{t,\ell+1}x_{\ell+1}$ ?

[2017-09-26 Boris] Most probably (24) is correct, while (40) should be corrected. Going to check it anyway.

Here $\mathsf{g}$ is the discrete Green's function with the Dirichlet boundary conditions at $t = 0$ and $t = \ell + 1$, i.e., it connects the partition boundary at time 0 to the partition boundary at time $\ell + 1$. As we show in Appendix A, $\mathsf{g}_{tt'}$ can be expressed in terms of Chebyshev polynomials of the second kind $U_n(s/2) = \sinh(n+1)\lambda/\sinh\lambda$:

$$\mathsf{g}_{ij} = \begin{cases} \frac{U_{i-1}(s/2)U_{\ell-j}(s/2)}{U_\ell(s/2)}, & \text{for } i \le j \\ \frac{U_{j-1}(s/2)U_{\ell-i}(s/2)}{U_\ell(s/2)}, & \text{for } i > j. \end{cases}$$

The first term on the right hand side of (24),

$$\bar{x}_i(b) = \sum_{j=1}^{\ell} \mathsf{g}_{ij} m_j \,, \tag{25}$$

can be thought of as the "average coordinate" at time $i$. Indeed, by (24) we have

$$|x_i - \bar{x}_i(b)| = \left| \frac{U_{\ell-i}(s/2)}{U_\ell(s/2)} x_0 + \frac{U_{i-1}(s/2)}{U_\ell(s/2)} x_{\ell+1} \right| \le \frac{\cosh(\frac{1}{2}(\ell+1) - i)\lambda}{\cosh\frac{1}{2}(\ell+1)\lambda} \,. \tag{26}$$

Hence the block $b$ determines the state space position at the center of the block $\lfloor \ell/2 \rfloor$, up to an exponentially small error in $\ell$, of the order $e^{-\ell\lambda/2}$.

[2017-09-25 Predrag] It would be "average coordinate" for the periodic boundary conditions, i.e., the periodic point (with repeats of the defining block correctly summed. Here $\bar{x}_i(b)$ is at the lower edge (lower corner?) of the admissible polytope.

From (24) it follows that in the plane spanned by $(x_0, x_{\ell+1})$, the element $\mathcal{M}_b$ of the partition $\mathcal{M}$ is defined by the inequalities

$$0 \le \bar{x}_i(b) + \frac{U_{\ell-i}(s/2)}{U_\ell(s/2)} x_0 + \frac{U_{i-1}(s/2)}{U_\ell(s/2)} x_{\ell+1} < 1\,, \qquad i = 1, \ldots, \ell, \tag{27}$$

$$0 \le x_0 < 1, \qquad 0 \le x_{\ell+1} < 1\,. \tag{28}$$

In general, this defines a polygon $\mathcal{P}_b$ in the $(x_0, x_{\ell+1})$ plane, bounded by the straight lines (27) cut out of the unit square (28). As a result, the measure of $b$ is given by the product

$$\mu(b) = |\mathcal{M}_b| = d_\ell |\mathcal{P}_b| \tag{29}$$

of the area $|\mathcal{P}_b|$ of the polygon $\mathcal{P}_b$ and the Jacobian $d_\ell$ of the transformation of the invariant phase space measure $d\mu = dx_0 dp_0$ to the Lagrangian end points measure $dx_0 dx_{\ell+1}$. The $\mathcal{M}_b$ are partitions of the $(x_0, x_1)$ phase space, in contrast to the polygons $\mathcal{P}_b$, plotted in the Lagrangian coordinates $(x_0, x_{\ell+1})$, see figure 3. Hence the interior alphabet measures $\mu(b)$, $m_i \in \mathcal{A}_0$, are given by the Jacobian (30) of coordinate transformation from the Lagrangian coordinates $(x_0, x_{\ell+1})$ to the phase space $(x_0, x_1)$, $\mu(b) = U_{|b|}(s/2)^{-1}$. The value of $U_{|b|}(s/2)$ is always an integer greater than 1, and thus the $(x_0, x_1)$ state space is "magnified" and wrapped around the $(x_0, x_{\ell+1})$ state space $U_{|b|}(s/2)$ times through $\ell$ iterations of the cat map. Lagrangian coordinates $(x_0, x_{\ell+1})$ are related to phase space coordinates $(x_k, p_k)$, $p_t = (x_t - x_{t-1})/\Delta t$, at time $t \in (0, \ell+1)$ by

$$\begin{aligned} x_t &= \bar{x}_t(b) + \frac{U_{\ell-t}(\frac{s}{2})}{U_\ell(\frac{s}{2})}\, x_0 + \frac{U_{t-1}(\frac{s}{2})}{U_\ell(\frac{s}{2})}\, x_{\ell+1} \\ p_t &= \bar{x}_{t+1}(b) - \bar{x}_t(b) + \frac{U_{\ell-t-1}(\frac{s}{2}) - U_{\ell-t}(\frac{s}{2})}{U_\ell(\frac{s}{2})}\, x_0 + \frac{U_t(\frac{s}{2}) - U_{t-1}(\frac{s}{2})}{U_\ell(\frac{s}{2})}\, x_{\ell+1}. \end{aligned}$$

This is a linear map, so its Jacobian $d_\ell = |\partial(x_0, x_1)/\partial(x_0, x_{\ell+1})|$ is simply

$$d_\ell = \frac{1}{U_\ell(\frac{s}{2})^2} \det \begin{pmatrix} U_{\ell-1}(\frac{s}{2}) - U_\ell(\frac{s}{2}) & U_\ell(\frac{s}{2}) \\ U_0(\frac{s}{2}) - U_{-1}(\frac{s}{2}) & U_{-1}(\frac{s}{2}) \end{pmatrix} = \frac{1}{U_\ell(\frac{s}{2})}\,. \tag{30}$$

Only the areas $|\mathcal{P}_b|$ in (29) depend on the particular block $b$; the Jacobian $d_\ell$ is the same for all $b$'s of length $\ell$. The view from $(x_0, x_{\ell+1})$ state space has a natural interpretation of area as the relative measure to sequence of all interior symbols, i.e., the geometrical factor $|\mathcal{P}_b|$. In other words, as illustrated by comparing figure 2 with figure 3, the Hamiltonian and the Lagrangian partition areas are the same up to the overall Jacobian factor $d_\ell$. The power of the Lagrangian reformulation is now evident: in contrast to the exponentially shrinking and disjoint (for sufficiently large $|b|$) $\mathcal{M}_b$ of figure 2, $\mathcal{P}_b$ are always simply connected convex polygons cut out of the unit square, see figure 3.

### *3.5. Evaluation of measures*

As the factor $d_\ell$ in (29) is known explicitly, the evaluation of $\mu(b)$ relies on the knowledge of the areas $|\mathcal{P}_b|$ which can be easily found analytically for small $\ell$. Before working out

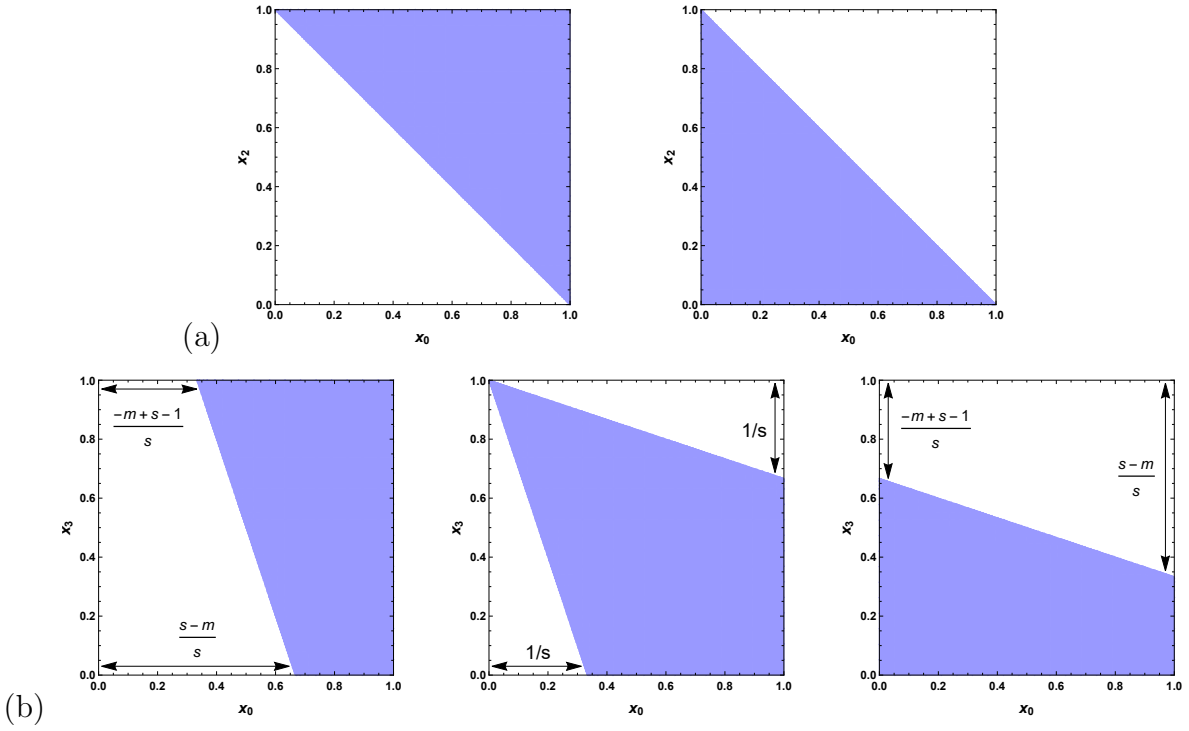


**Figure 3.** (a) Polygons $\mathcal{P}_m$ (shaded areas) for a single symbol, Lagrangian $(x_0, x_2)$ plane, exterior letters $m \in \mathcal{A}_1$: (left) $m = \underline{1}$, (right) $m = s-1$. (b) Polygons $\mathcal{P}_{m_1 m_2}$ (shaded areas) in Lagrangian $(x_0, x_3)$ plane for blocks $m_1 m_2$ of length 2, $m_1 = \underline{1}, m_2 = m \in \mathcal{A}_0$ (left); $m_1 = \underline{1}, m_2 = s-1$ (middle); $m_1 = s-1, m_2 = m \in \mathcal{A}_0$ (right). Repeated exterior alphabet symbols are pruned, $\mathcal{P}_{mm} = \emptyset$ if $m \in \mathcal{A}_1$. For blocks composed of only interior symbols $m_1, m_2 \in \mathcal{A}_0$, $\mathcal{P}_{m_1 m_2}$ is the entire unit square (full shift, no pruning). Note that $\mu(b) = \mu(\bar{b})$ by the symmetry (31). Compare also with the phase space representation figure 2.

specific examples, we list several properties of measures $\mu(b)$ valid for any block length $\ell$.

*Reflection symmetries.* Symmetries of the cat map induce invariance with respect to corresponding symbol exchanges. Define $\bar{m} = s-m-2$ to be the conjugate of symbol $m \in \mathcal{A}$. For example, the two exterior alphabet $\mathcal{A}_1$ symbols are conjugate to each other, as illustrated by figure 1. If $b = m_1 m_2 \dots m_\ell$ is a block, and $\bar{b} = \bar{m}_1 \bar{m}_2 \dots \bar{m}_\ell$ its conjugate, then by reflection symmetry of the cat map we have $|\mathcal{P}_b| = |\mathcal{P}_{\bar{b}}|$. Similarly, if $b^* = m_l m_{l-1} \dots m_1$, the time reversal invariance implies $|\mathcal{P}_b| = |\mathcal{P}_{b^*}|$. Accordingly, blocks $b$, $b^*$, and $\bar{b}$ have the same measure,

$$\mu(b) = \mu(\bar{b}) = \mu(b^*)\,. \tag{31}$$

*Interior symbols.* For blocks composed of interior symbols only, the inequalities (27) are always satisfied, and $\mathcal{P}_b$ are unit squares of area 1. The corresponding measure

$$\mu(b) = 1/U_{|b|}(s/2), \qquad m_i \in \mathcal{A}_0\,, \quad i = 1, \dots |b|$$

depends only on the length of the block $b$.

*Rationality.* Since all coefficients in (27) are given by rational numbers, the polygon areas $|\mathcal{P}_b|$ are rational too. The same holds for the $d_\ell$ factor. As a result, measures $\mu(b)$ are always rational (see, for example, table 1). This allows for their exact evaluation by integer arithmetic.

*Normalization.* For a fixed block length $\ell$

$$\sum \mu(b) = 1\,, \tag{32}$$

where the sum is over all admissible blocks $b$ of length $|b| = \ell$, see (20).

*3.5.1. Example: Measure of blocks of length $\ell = 1$.* The defining, single symbol block Lagrangian equation (2) is the simplest example of the Lagrangian, two-point boundary values formulation,

$$x_1 = \mathsf{g}_{11} m_1 + \mathsf{g}_{10} x_0 + \mathsf{g}_{12} x_2\,,$$

with $\ell = 1$, $\mathsf{g}_{10} = \mathsf{g}_{11} = \mathsf{g}_{12} = 1/s$ verifying the general Green's function formula (24).

[2017-09-21 Predrag] $\ell = 2$, etc., is obtained by chaining these together.

[2017-09-26 Boris] I think it should be $x_1 = \mathsf{g}_{11} m_1 + \mathsf{g}_{11} x_0 + \mathsf{g}_{11} x_2$. Note $\mathsf{g}_{10} = \mathsf{g}_{12} = 0$ - this is Dirichlet Green's function!

For single symbol $m_1 \equiv m$ the set of inequalities (27) thus reduces to

$$-m \le x_0 + x_2 < s - m\,.$$

This constraint is always fulfilled for interior symbols $m \in \mathcal{A}_0$. For $m \in \mathcal{A}_1$, polygon $\mathcal{P}_m$ is the upper and lower triangle, respectively, shown in figure 3 (a). As a result, we have $|\mathcal{P}_m| = 1$ if $m \in \mathcal{A}_0$ and $|\mathcal{P}_m| = 1/2$ if $m \in \mathcal{A}_1$, giving measures

$$\mu(m) = \begin{cases} 1/s, & \text{for } m \in \mathcal{A}_0 \\ 1/2s, & \text{for } m \in \mathcal{A}_1\,, \end{cases}$$

which indeed add up to (32), with the numbers of letters in the alphabet $\mathcal{A}$ given by (17).

[2016-11-07 Predrag] figure 2: Note 5th bullet on page 48 and Appendix E.16. Refer here (within this comment) to the source code (in the repository) that generates these figures.

*3.5.2. Example: Measure of blocks of length $\ell = 2$:* For blocks $m_1 m_2$, bounds (27) give four inequalities

$$\begin{aligned} -sm_1 - m_2 \le sx_0 + x_3 < s^2 - 1 - sm_1 - m_2 \\ -sm_2 - m_1 \le sx_3 + x_0 < s^2 - 1 - sm_2 - m_1 \,, \end{aligned} \tag{33}$$

where we have used $u_2(s/2) = s^2 - 1$. A constraint arises whenever at least one of the symbols belongs to the exterior alphabet $\mathcal{A}_1$. By the symmetry (31) it is sufficient to analyze the case when $m_1 = \underline{1}$. If $m_2 \in \mathcal{A}_0$, the region $\mathcal{P}_{\underline{1}m_2}$ is determined by (see figure 3 (b)):

$$s - m_2 \le sx_0 + x_3, \qquad 0 \le x_0, x_3 < 1.$$

The area of the resulting polygon is equal to $|\mathcal{P}_{\underline{1}m_2}| = (1 + 2m_2)/2s$, where $m_2 \in \mathcal{A}_0$. If both $m_1 \neq m_2$ belong to $\mathcal{A}_1$, i.e., $m_1 = \underline{1}$, $m_2 = s-1$, then the corresponding polygon is determined by the conditions:

$$1 \le sx_0 + x_3, \qquad sx_3 + x_0 \le s, \qquad 0 \le x_0, x_3 < 1.$$

with the corresponding area $|\mathcal{P}_{m_1 m_2}| = 1 - 1/s$. Finally, if both $m_1 = m_2$ belong to $\mathcal{A}_1$ and they are equal, then block is pruned, $\mathcal{P}_{m_1 m_2} = \emptyset$; there are two pruned blocks of length 2. In summary,

$$\mu(m_1 m_2) = \begin{cases} 1/s^2 - 1 & \text{for } m_1, m_2 \in \mathcal{A}_0 \\ (1 + 2m_2)/2s(s^2 - 1) & \text{for } m_1 = \underline{1}, m_2 \in \mathcal{A}_0 \\ 1/s(s+1) & \text{for } m_1 = \underline{1}, m_2 = s-1 \\ 0 & \text{for } m_1 = \underline{1}, m_2 = \underline{1}. \end{cases} \tag{34}$$

The measures for the remaining symbol combinations can be obtained by the symmetries, see (31) and table 1 for the $s = 3$ case.

[2016-11-08 Predrag] To Rana: In caption of table 1, state how many iterations total did you use to generate these measures.

*3.5.3. Pruning.* As shown in (23), any sequence of $\mathcal{A}_0$ symbols is admissible. If, on the other hand, one or more symbols from $m$ belong to $\mathcal{A}_1$, such a sequence might be forbidden, with the region $\mathcal{P}_m$ defined by (27,28) empty, and thus $\mu(m) = 0$. An example are the pruned blocks $\_\underline{11}\_$ and $\_22\_$, missing from figure 2 (g). While here we do not attempt to solve the number-theoretic problem of determining the number of pruned blocks for arbitrary $\ell$, the count of pruning rules given in table 2 indicates that for the linear code the number of pruned blocks grows exponentially with their length. Thus the linear code is not a subshift of finite type, and it does not yield a finite Markov partition; its grammar consists of an infinity of arbitrarily long pruned (i.e., inadmissible) blocks.

[2017-07-31 Boris] Should we change layout of table 2 to the horizontal one?

[2017-08-11 Predrag] Not sure - easier to see the exponential growth in this format. but perhaps it could be the left panel of the (finalized) figure B1.

**Table 2.** $N_n$ is the total number of pruned blocks of length $n = |b|$ for the $s = 3$ Arnol'd cat map. $\tilde{N}_n$ is the number of *new* pruned blocks of length $|b|$, with all length $|b|$ blocks that contain shorter pruned blocks already eliminated. Empirically there is a single new pruning rule for each prime-number block length (it is listed as two rules, but by the reflection symmetry there is only one).

| $n$ | $N_n$ | $\tilde{N}_{n-1}$ |
|---|---|---|
| 2 | 2 | 0 |
| 3 | 22 | 2 |
| 4 | 132 | 8 |
| 5 | 684 | 2 |
| 6 | 3164 | 30 |
| 7 | 13894 | 2 |
| 8 | 58912 | 70 |
| 9 | 244678 | 16 |
| 10 | 1002558 | 198 |
| 11 | 4073528 | 2 |
| 12 | 16460290 | 528 |
| 13 | | 2 |

[2017-09-01 Li] How about including list of new pruning rules for small lengths as an Appendix?

## 4. Spatiotemporal cat

[2016-11-08 Predrag] Say: THE BIG DEAL is
for $d$-dimensional field theory, symbolic dynamics is not one temporal sequence with a huge alphabet, but $d$-dimensional spatiotemporal tiling by a finite alphabet

We now turn to the study of the spatiotemporal cat (4), with cat maps on sites ("particles") coupled isotropically to their nearest neighbors on a 2-dimensional spatiotemporally infinite $\mathbb{Z}^2$ lattice. To motivate the model, we briefly review the early work on coupled map lattices (CMLs), and then describe the new results (the core of this paper) specific to the spatiotemporal cat, an elegant $L$-"particle," $L \to \infty$ coupled map lattice.

The conventional CML models [58, 59], mostly motivated by discretizations of dissipative PDEs, start out with chaotic on-site dynamics weakly coupled to neighboring sites, with strong space-time asymmetry. Spatially homogenous lattice models also invariant under discrete *space translations* were studied by Bunimovich and Sinai [19]. Pesin and Sinai [78] were the first to study Hamiltonian lattices, with chains of coupled Anosov maps. In order to establishe rigorously the desired statistical properties of coupled map lattices, such as the continuity of their SRB measures, they, and most of the subsequent statistical mechanics literature, relied on the structural stability of Anosov automorphisms under small perturbations. Contrast this with the 2-dimensional

Gutkin and Osipov [48] *spatiotemporal cat* (4):

$$(-\Box + s - 4)\, x_z = m_z\,, \qquad m_z \in \mathcal{A}\,,$$
$$\mathcal{A} = \{-3, -2, \cdots, s-2, s-1\}\,, \tag{35}$$

integer $s > 4$, $x_z \in \mathbb{T}^1$, $z \in \mathbb{Z}^2$, derived here in section 2. The map is space $\leftrightarrow$ time symmetric and has the temporal and spatial dynamics strongly coupled. Unlike the systems studied in [19], spatiotemporal cat cannot be conjugated to a product of non-interacting cat maps; a way to see that is to compare the numbers of periodic orbits in the two cases – they differ.

[2017-09-14 Boris] More straightforward argument is that $\mathcal{B}_L$ (see (B.2) in Appendix B) is not conjugated to any feline with $B = 0$).

In this paper we focus on learning how to enumerate admissible spatiotemporal patterns, compute their measures, and identify their recurrences (shadowing of a large invariant 2-torus by smaller invariant 2-tori), rather than any rigorous proofs.

### *4.1. Linear symbolic dynamics*

The key advantage of the linear code is illustrated already by the $d = 2$ case. While the size of the alphabet $\bar{\mathcal{A}}$ based on a Markov partition grows exponentially with the "particle number" $L$, the number of letters (4) of the linear code $\mathcal{A}$ is finite and the same for any $L$, including the $L \to \infty$ spatiotemporal cat. For the linear code an invariant 2-torus is encoded by a doubly periodic $d = 2$ block $\mathsf{M}$ of symbols from a small alphabet, rather then by a 1-dimensional temporal string of symbols from the exponentially large (in $L$) Adler-Weiss alphabet $\bar{\mathcal{A}}$.

While the $d = 2$ spatiotemporal cat has a Hamiltonian formulation (see section Appendix B), it is instructive to write down its equations of motion in the Lagrangian form (35), as in the single cat map case of section 3.1,

$$(-\Box + s - 4)\, x_{n,t} = m_{n,t}\,, \qquad m_z \in \mathcal{A}\,, \tag{36}$$

with $\Box$ being the discrete space-time Laplacian (6) on $\mathbb{Z}^2$,

$$\Box\, x_{n,t} := x_{n,t-1} + x_{n-1,t} - 4\, x_{n,t} + x_{n,t+1} + x_{n+1,t}\,.$$

The symbols $m_{n,t}$ from the set $\mathcal{A} = \{\underline{3}, \underline{2}, \cdots, s-2, s-1\}$ on the right hand side of (36) are necessary to keep $x_{n,t}$ within the interval $[0, 1)$ The symbol $\underline{|m_t|}$ here denotes $m_t$ with the negative sign, i.e., '$\underline{3}$' stands for symbol '$-3$'. As we now show, the block $\mathsf{M} = \{m_{n,t} \in \mathcal{A}\,,\ (n,t) \in \mathbb{Z}^2\}$ can be used as a 2-dimensional symbolic representation of the lattice system state.

First, we show that any solution $\mathsf{X}$ of (36) can be uniquely recovered from its symbolic representation $\mathsf{M}$. By inverting (36) we obtain

$$x_z = \sum_{z' \in \mathbb{Z}^2} g_{zz'} m_{z'}, \qquad g_{zz'} = \left( \frac{1}{-\Box + s - 4} \right)_{zz'}\,, \tag{37}$$

where $g_{zz'}$ is the Green's function for the 2-dimensional discretized heat equation, see Appendix A. A lattice state $\mathsf{M}$ is admissible if and only if all $x_z$ given by (37) fall into the interval $[0,1)$.

As for the single cat map, we split the $s+3$ letter alphabet $\mathcal{A} = \mathcal{A}_0 \cup \mathcal{A}_1$ into the interior $\mathcal{A}_0$ and exterior $\mathcal{A}_1$ alphabets

$$\mathcal{A}_0 = \{0, \ldots, s-4\}, \quad \mathcal{A}_1 = \{\underline{3}, \underline{2}, \underline{1}\} \cup \{s-3, s-2, s-1\}\,. \tag{38}$$

For example, for $s = 5$ the interior, respectively exterior alphabets are

$$\mathcal{A}_0 = \{0, 1\}, \quad \mathcal{A}_1 = \{\underline{3}, \underline{2}, \underline{1}\} \cup \{2, 3, 4\}\,. \tag{39}$$

If all $m_z$ belong to $\mathcal{A}_0$ then $\mathsf{M} = \{m_z | z \in \mathbb{Z}^2\}$ is a full shift. Indeed, by the positivity of Green's function (see Appendix A) it follows immediately that $0 \le x_z$, while the condition $\sum_{z'} g_{zz'} = s-4$ implies that $x_z \le 1$, with the equality saturated only if $m_z = s-4$, for all $z \in \mathbb{Z}^2$.

### *4.2. Measures of symbolic blocks*

Let $\mathcal{R} \subset \mathbb{Z}^2$ be a simply connected (convex) region on $\mathbb{Z}^2$ and let $\mathsf{M}_\mathcal{R} = \{m_z | z \in \mathcal{R}\}$ be a block defined on $\mathcal{R}$. We now show that $\mathsf{M}_\mathcal{R}$ determines approximate positions of the points $x_z$, $z \in \mathcal{R}$, within the region $\mathcal{R}$. To start with we define the (exterior) boundary $\partial\mathcal{R}$ of $\mathcal{R}$ as a set of points adjacent to $\mathcal{R}$. More precisely, $z = (n,t)$ belongs to $\partial\mathcal{R}$ if and only if $z \notin \mathcal{R}$ but one of the four neighboring points $(n \pm 1, t)$, $(n, t \pm 1)$ belongs to $\mathcal{R}$, see Figure 4(a). Let then $\mathsf{g}_{zz'}$ be the corresponding Dirichlet Green's function which vanishes at the boundary $\partial\mathcal{R}$. By Green's identity in the discrete setting, see Appendix A, any solution of the equation (36) satisfies

$$x_z = \sum_{z' \in \mathcal{R}} \mathsf{g}_{zz'} m_{z'} + \sum_{z'' \in \partial\mathcal{R}} \mathsf{g}_{z\bar{z}''} x_{z''}, \qquad z \in \mathcal{R}\,, \tag{40}$$

with $\bar{z}''$ being the (unique) adjacent point of $z'' \in \partial\mathcal{R}$ within the domain $\mathcal{R}$. Here, the first term

$$\bar{x}_z := \sum_{z' \in \mathcal{R}} \mathsf{g}_{zz'} m_{z'} \tag{41}$$

can be viewed as the "average coordinate" $\bar{x}(\mathsf{M}_\mathcal{R})$, determined solely by $\mathsf{M}_\mathcal{R}$. From (40) it follows that the difference $|x_z - \bar{x}_z|$ is bounded by

$$|x_z - \bar{x}_z| = \sum_{z'' \in \partial\mathcal{R}} \mathsf{g}_{z\bar{z}''} x_{z''} \le |\partial\mathcal{R}|\, \mathsf{g}_{z\bar{z}''_0}\,,$$

with $\bar{z}''_0$ being the boundary point of $\mathcal{R}$ (i.e., adjacent to $\partial\mathcal{R}$), where the function $\mathsf{g}_{z\bar{z}''}$ attains its maximum value along $\partial\mathcal{R}$ (for a fixed $z$). For an illustration, consider a $[\ell_1 \times \ell_2]$ rectangular region

$$\mathcal{R}^{[\ell_1 \times \ell_2]} = \{(n_0 + i, t_0 + j) | \, i = 0, \ldots, \ell_1 - 1,\ j = 0, \ldots, \ell_2 - 1\}\,, \tag{42}$$

shown in figure 4 (a). If $\ell_1, \ell_2$ are even and the point $z$ is the rectangular center, one has $\ell_{\min} = \min\{\ell_1/2, \ell_2/2\}$. As the Green's function $\mathsf{g}_{z\bar{z}''}$ decays exponentially with $|z - \bar{z}''|$, the distance $|x_z - \bar{x}_z|$ is of the order $|\partial\mathcal{R}|\, e^{-\lambda \ell_{\min}}$ for a large $\ell_{\min}$.

We determine next the measure of the lattice state $\mu(\mathsf{M}_{\mathcal{R}})$. Take $\mathcal{R} = \mathcal{R}^{[\ell_1 \times \ell_2]}$ to be a rectangular region (42). In what follows it is convenient to distinguish points in the interior of $\mathcal{R}$ from the points which belong to the boundary $\partial\mathcal{R}$. While in principle the boundary state space points $x_{z''} \in \partial\mathcal{R}$ are labeled by the symbol pair $z'' = (n, t)$, we find it more convenient to label them by a single index that indicates their position along the border, $x_i = x_{z''}$, where $i$ runs from 1 to $|\partial\mathcal{R}| = 2(\ell_1 + \ell_2)$. For examples, see figure 4, and sections 4.3.1 and 4.3.2. Both the boundary state space points $x_i, i = 1, \dots |\partial\mathcal{R}|$ and the internal points $x_z, z \in \mathcal{R}$ must lie within the unit interval. By (40) this implies:

$$0 \leq x_i < 1, \qquad i = 1, \dots, |\partial\mathcal{R}|\,, \tag{43}$$

$$0 \leq \bar{x}_z + \sum_{i=1}^{|\partial\mathcal{R}|} \mathsf{g}_{z\bar{z}_i} x_i < 1, \qquad z \in \mathcal{R}\,. \tag{44}$$

Accordingly, the admissible set of $x_i, i = 1, \dots |\partial\mathcal{R}|$ form a polytope in the $|\partial\mathcal{R}|$-dimensional Euclidean space: the inequalities (44) cut out the polytope $\mathcal{P}(\mathsf{M}_{\mathcal{R}})$ out of the $\mathcal{D}$-dimensional unit hypercube defined by (43). As in the case of the single cat map, the measures $\mu(\mathsf{M}_{\mathcal{R}})$ can be factorized into product

$$\mu(\mathsf{M}_{\mathcal{R}}) = d(\mathcal{R})\,|\mathcal{P}(\mathsf{M}_{\mathcal{R}})|\,, \tag{45}$$

where $|\mathcal{P}(\mathsf{M}_{\mathcal{R}})|$ is the volume of the polytope defined by (43) and (44). The prefactor $d(\mathcal{R})$ is the Jacobian of the linear connection between boundary coordinates $x_i, i = 1, \dots \mathcal{D}$ and line of the phase space coordinate and momenta at a fixed time $t$, $\{(x_z, p_z), z = (t, n) | \, n = 1, \dots L\}$.

[2017-08-05 Boris] Should I give here more details? - Hope not. Might be a bit messy.

Since the Jacobian of this transformation is independent of any particular block $\mathsf{M}_{\mathcal{R}}$, the factor $d(\mathcal{R})$ depends only on the shape of $\mathcal{R}$, but not on its symbolic content.

### *4.3. Evaluation of measures*

We start by listing the basic properties of the spatiotemporal cat measures $\mu(\mathsf{M}_{\mathcal{R}})$. They largely mimic their counterparts in the single cat case, section 3.5:

*Symmetries.* Besides the invariance under shifts in time and space directions, spatiotemporal cat (36) is separately invariant under the space and time reflections $n \to -n$, $t \to -t$, as well as under exchange $n \longleftrightarrow t$ of space and time. Spatiotemporal cat thus has all the symmetries of the square lattice:

- 2 discrete translation symmetries
- rotations by $\pi/2$:

$$C_4 = \{E, C_{4z}^+, C_{4z}^-, C_{2z}\}\,. \tag{46}$$

- reflection across $x$-axis, $y$-axis, diagonal $a$, diagonal $b$:

$$C_{4v} = \mathrm{D}_4 = \{E, C_{4z}^+, C_{4z}^-, C_{2z}, \sigma_y, \sigma_x, \sigma_{da}, \sigma_{db}, \}\,. \tag{47}$$

In the international crystallographic notation [34], this square lattice is referred to as $p4mm$. It is symmorphic, with point group $p4mm$. In addition, if $\mathsf{M} = \{m_{n,t}\}$ is an admissible state, so is its conjugation symmetry partner $\bar{\mathsf{M}} = \{\bar{m}_{n,t}\}$, where $\bar{m}_{n,t} = s - 4 - m_{n,t}$. All together, the measure is invariant under

$$\mu(\mathsf{M}_\mathcal{R}) = \mu(g \circ \mathsf{M}_\mathcal{R}), \qquad \mu(\mathsf{M}_\mathcal{R}) = \mu(\bar{\mathsf{M}}_\mathcal{R}),$$

where $g$ is an element of space group $p4mm$.

> [2017-09-01 Predrag] Boris wrote "$g$ is an element of dihedral group $\mathrm{D}_4$". Sure it is the order eight $\mathrm{D}_4$, and not the order four $\mathrm{D}_2$? Write out the list of group elements $\mathrm{D}_8 = \{e, \cdots\}$.

> [2017-09-15 Boris] Example $s = 7$. The measures of the following blocks are equal by $\mathrm{D}_4$ symmetry $\mu(\mathsf{M}_\mathcal{R}) = \mu(g \circ \mathsf{M}_\mathcal{R})$:
>
> $$\begin{bmatrix} 1 & 2 \\ 3 & 4 \\ 5 & 6 \end{bmatrix}, \quad \begin{bmatrix} 2 & 4 & 6 \\ 1 & 3 & 5 \end{bmatrix}, \quad \begin{bmatrix} 6 & 5 \\ 4 & 3 \\ 2 & 1 \end{bmatrix}, \quad \begin{bmatrix} 5 & 3 & 1 \\ 6 & 4 & 2 \end{bmatrix}$$
>
> $$\begin{bmatrix} 2 & 1 \\ 4 & 3 \\ 6 & 5 \end{bmatrix}, \quad \begin{bmatrix} 6 & 4 & 2 \\ 5 & 3 & 1 \end{bmatrix}, \quad \begin{bmatrix} 5 & 6 \\ 3 & 4 \\ 1 & 2 \end{bmatrix}, \quad \begin{bmatrix} 1 & 3 & 5 \\ 2 & 4 & 6 \end{bmatrix}$$
>
> The measures of the following blocks are equal by $\mu(\mathsf{M}_\mathcal{R}) = \mu(\bar{\mathsf{M}}_\mathcal{R})$ symmetry
>
> $$\begin{bmatrix} 2 & 1 \\ 4 & 3 \\ 6 & 5 \end{bmatrix}, \quad \begin{bmatrix} 1 & 2 \\ \underline{1} & 0 \\ \underline{3} & \underline{2} \end{bmatrix}.$$

*Interior symbols.* The set of inequalities (44) is satisfied automatically if all symbols from $\mathsf{M}_\mathcal{R}$ belong to the full-shift interior alphabet $\mathcal{A}_0$ in (38). This follows from the positivity of the Green's function $\mathsf{g}_{zz'}$, and the identity:

$$1 = (s-4)\sum_{z'\in\mathcal{R}} \mathsf{g}_{zz'} + \sum_{z''\in\partial\mathcal{R}} \mathsf{g}_{z\bar{z}''}, \qquad z \in \mathcal{R}.$$

As a result, for any block of interior symbols $|\mathcal{P}(\mathsf{M}_\mathcal{R})| = 1$, and the measure

$$\mu(\mathsf{M}_\mathcal{R}) = \frac{1}{d(\mathcal{R})} \tag{48}$$

is independent on the symbolic content of $\mathsf{M}_\mathcal{R}$.

*Rationality.* For any $\mathsf{M}_\mathcal{R}$, $\mu(\mathsf{M}_\mathcal{R})$ is a rational number. This follows from the rationality of every element $\mathsf{g}_{zz'}$, and allows for their exact evaluation by integer arithmetic.

*Normalization.* For a fixed region $\mathcal{R}$:

$$\sum \mu(\mathsf{M}_\mathcal{R}) = \mu(\mathcal{R})\,,$$

where the sum is over all admissible blocks $\mathsf{M}_\mathcal{R}$ over the region $\mathcal{R}$.

The evaluation of measures $\mu(\mathsf{M}_\mathcal{R})$ for the spatiotemporal cat thus boils down to the evaluation of of the polytope volumes $|\mathcal{P}(\mathsf{M}_\mathcal{R})|$, determined by the inequalities (43) and (44). Once the volumes are found for all admissible blocks $\mathsf{M}_\mathcal{R}$, the constant factor $d(\mathcal{R})$ can be extracted from the normalisation condition, by summing up all volumes:

$$1/d(\mathcal{R}) = \sum |\mathcal{P}(\mathsf{M}_\mathcal{R})|\,. \tag{49}$$

While for a single cat map $\partial\mathcal{R}$ is always 2, i.e., the boundary of interval $\mathcal{R}$ consists of the two end points, for the spatiotemporal cat $\mathcal{P}(\mathsf{M}_\mathcal{R})$ is fixed by the $|\partial\mathcal{R}|$ boundary points. The complexity of $|\mathcal{P}(\mathsf{M}_\mathcal{R})|$ calculation for a spatiotemporal cat thus grows with $|\mathcal{R}|$. We illustrate this with calculations for $\mathcal{R} = [1\times1]$ and $[2\times2]$ symbol blocks.

*4.3.1. Example: $\mathcal{R} = [1\times1]$ measure.* Consider a $\mathcal{R} = [1\times1]$ spatiotemporal region, with a single symbol block $\mathsf{M}$, together with the four state space points $x_i = x_z \in \partial\mathcal{R}$ comprising its boundary, figure 4 (b). We need to evaluate the volume of the 4-dimensional polytope $\mathcal{P}(m)$ for each $m \in \mathcal{A}$. $\mathcal{P}(m)$ is contained with the hypercube

$$0 \le x_i < 1, \qquad i = 1,2,3,4,$$

bounded by the inequalities

$$-m \le x_1 + x_2 + x_3 + x_4 < s - m\,. \tag{50}$$

The polytope volume $|\mathcal{P}(m)|$ depends on $m$. For interior alphabet $m \in \mathcal{A}_0$ the hyperplane (50) does not intersect the hypercube and the volume $|\mathcal{P}(m)| = 1$. For $m \in \{\underline{3},\underline{2},\underline{1}\}$ in the exterior $\mathcal{A}_1$ alphabet (38), the corresponding volumes $|\mathcal{P}(m)|$ are $1/4!$, $1/2$, and $23/4!$, respectively. The normalization condition (49) then yields $d = 1/s$. Thus the measures for the symbols from the exterior alphabet $\mathcal{A}_1$ are

$$\begin{aligned}
\mu(\underline{3}) &= \mu(s-3) = 1/4!s \\
\mu(\underline{2}) &= \mu(s-2) = 1/2s \\
\mu(\underline{1}) &= \mu(s-1) = (1-1/4!)/s \\
\mu(m) &= 1/s \text{ for interior alphabet } m \in \mathcal{A}_0\,,
\end{aligned} \tag{51}$$

with the total measure (8) satisfying $\sum_{\mathcal{A}_0} \mu(m) = 1$. The numerical estimates of figure 5 confirm these analytic results.

[2017-08-05 Predrag] to Rana: Figure 5 (b) letters still have the old, now wrong sing. Relabel, harmonize with (38).

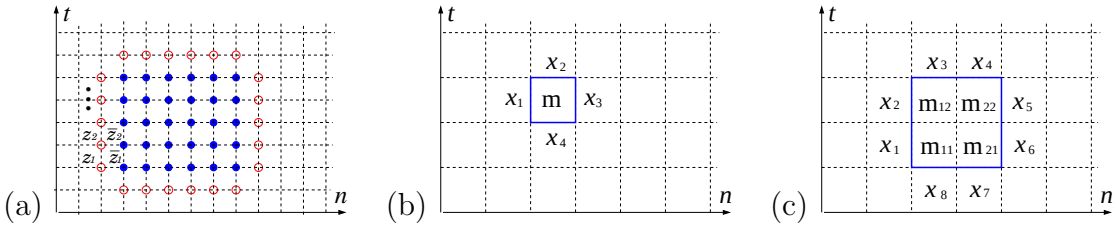


**Figure 4.** The left hand side (a) shows $6 \times 5$ rectangular domain $\mathcal{R}$ on 2-dimensional lattice. The red (empty) circles indicate the (exterior) boundary $\partial\mathcal{R}$. For each point $z_i \in \partial\mathcal{R}$, there exists an associated adjuscent point $\bar{z}_i$ within the domain $\mathcal{R}$. The middle and right hand side figures show block $\mathsf{M}_\mathcal{R}$ for (b) $\mathcal{R} = [1{\times}1]$, and (c) $\mathcal{R} = [2{\times}2]$ regions, together with the corresponding boundary state space points $\partial\mathcal{R} = \{x_1, x_2, x_3, x_4\}$ and $\partial\mathcal{R} = \{x_1, x_2, \cdots, x_8\}$, respectively.

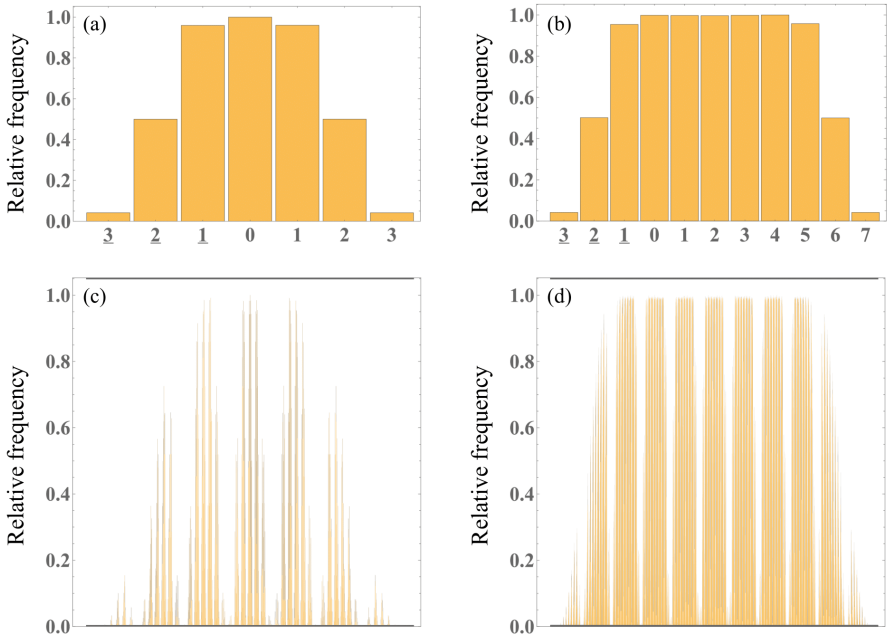


**Figure 5.** Relative frequencies (7) of blocks $\mathsf{M}_\mathcal{R} \in \{m\}$ over the $\mathcal{R} = [1 \times 1]$ spatiotemporal region, obtained by long-time averaging of time evolution of random initial conditions, are in agreement with the analytic results (51). (a) For $s = 4$ the interior alphabet (38) consists of only one letter $\mathcal{A}_0 = \{0\}$, with the corresponding polytope of maximal volume, $|\mathcal{P}(m)| = 1$. (b) For $s = 8$ the frequencies corresponding to the interior alphabet five letters $\mathcal{A}_0 = \{0, 1, 2, 3, 4\}$ are maximal. Relative frequencies (7) of the blocks $\mathsf{M}_\mathcal{R}$ over the $\mathcal{R} = [2{\times}2]$ spatiotemporal region of figure 4, obtained by long-time averaging of time evolution of random initial conditions, ordered along the $\gamma$-axis by the base $s+3$ "decimal" numbers (53): (c) For $s = 4$ there is only one combination of the interior symbols $m_{11} = m_{12} = m_{21} = m_{22} = 0$ which attains the maximum measure. (d) For $s = 8$ the interior alphabet $\mathcal{A}_0$ is composed of 5 symbols and there are $5^4$ distinct blocks that attain the maximum measure. The alphabets are defined in (38).

*4.3.2. Example: $\mathcal{R} = [2\times 2]$ measure.* For the block

$$\mathsf{M} = \begin{bmatrix} m_{12}m_{22} \\ m_{11}m_{21} \end{bmatrix} \tag{52}$$

the eight-dimensional polytope $\mathcal{P}_\mathsf{M}$ is defined by the boundary $\partial\mathcal{R}$ state space points labeled $0 \le x_i < 1, i = 1, \ldots 8$, figure 4 (c), supplemented by the inequalities:

$$0 \le (x_1 + x_8 + m_{11})(s^2 - 2) + (x_3 + x_2 + x_6 + x_7 + m_{12} + m_{21})s + (x_4 + x_5 + m_{22})2 \le P(s)$$
$$0 \le (x_2 + x_3 + m_{12})(s^2 - 2) + (x_1 + x_8 + x_4 + x_5 + m_{11} + m_{22})s + (x_7 + x_6 + m_{21})2 \le P(s)$$
$$0 \le (x_7 + x_6 + m_{21})(s^2 - 2) + (x_1 + x_8 + x_4 + x_5 + m_{22} + m_{11})s + (x_2 + x_3 + m_{12})2 \le P(s)$$
$$0 \le (x_4 + x_5 + m_{22})(s^2 - 2) + (x_3 + x_2 + x_6 + x_7 + m_{12} + m_{21})s + (x_1 + x_8 + m_{11})2 \le P(s)$$

with $P(s) = s(s^2 - 4)$.

[2017-08-05 Predrag] To Boris: do you have analytic results for any of the any $\mathcal{R} = [2\times 2]$ measures? Who ordered $P(s) = s(s^2 - 4)$? Please add them to this section.

[2017-09-15 Boris] After some thinking - We can probably write analytics for $|\mathcal{P}_\mathsf{M}|$ when all except one of the above equations are satisfied automatically. The answer should be some combination of factorials (probably non-inspiring one). If I am not mistaken Li had something on this issue. Otherwise would require quite a work (doable but not trivial). There is however a particular case where things become simple, when the corresponding plane intersects center of the hypercube. This happens, for example if (for even $s > 4$):

$$\mathsf{M} = \begin{bmatrix} s/2-2 & s/2-2 \\ \underline{2} & s/2-1 \end{bmatrix}.$$

In such a case $|\mathcal{P}_\mathsf{M}| = 1/2$ automatically, by symmetry reasoning. The normalization $d(\mathcal{R})$ will be still absent, but one can say that occurrence frequency of such a block is a half of the maximal one, for a block composed of only internal symbols. Do you want to include this? Much easier is to write down the condition for admissibility of M. Namely, any combination of symbols for $2 \times 2$ block that satisfies condition

$$(2 + m_{12})(s^2 - 2) + (4 + m_{22} + m_{11})s + (2 + m_{21})2 \le 0$$

is forbidden i.e., $|\mathcal{P}_\mathsf{M}| = 0$. All other forbidden sequences are obtained by application of the symmetry operations. In principle, in this way we can list all forbidden sequences for some $s$, like 4 or 5.

The volumes of $\mathcal{P}_\mathsf{M}$ evaluated analytically are found to be consistent with the measure of a given block M obtained by numerical simulations of trajectories with random initial conditions.

While in the $\mathcal{R} = [1\times 1]$ case it was possible to plot the single symbol block M measures $\mu(m_j)$ along a single, $j$-labelled axis, as in figure 5, the $\mathcal{R} = [2\times 2]$ has four sites $z \in \{11, 12, 21, 22\}$, and each site owns a measure $\mu(m_z)$ for each of the $s + 3$ letters $m_z$ of the $\mathcal{A}$ alphabet (38). A way to map the array (52) onto a line is to write it as a "decimal" number

$$\gamma(\mathsf{M}_\mathcal{R}) = 0.\gamma_1\gamma_2\gamma_3\gamma_4 \tag{53}$$

in base $s+3$, where $\gamma_k \in \{0, 1, \cdots, s+2\}$ are the symbols $m_{ij}$ shifted into nonnegative numbers,

$$(\gamma_1, \gamma_2, \gamma_3, \gamma_4) = (m_{11}+3, m_{12}+3, m_{21}+3, m_{22}+3)\,.$$

Estimates of the corresponding measures $\mu(\mathsf{M}_\mathcal{R})$ from two long-time numerical Hamiltonian simulations for $T$ large, on a spatially periodic domain of extent ("particle number") $L = 20$, are displayed in this way in figure 5 (c) and (d). The numerics is consistent with relative frequency $\mu(\mathsf{M}_\mathcal{R}) = 1$, if all symbols belong to the interior alphabet. If only a column or row of symbols belongs to the interior alphabet, the relative frequency still appears close to 1. For example, for $s = 8$ the block

$$\begin{bmatrix} 5 & 3 \\ \underline{1} & 0 \end{bmatrix}\,,$$

with the $[3, 0]^T$ column in the interior alphabet, has a relative frequency equal to 0.995755.

[2017-09-06 Predrag] to Rana: "relative frequency equal to 0.995755": how many digits do we trust? we should state only the significant digits.
To Boris: Do you have some analytically small number, like $\mu(\mathsf{M}_\mathcal{R}) = 1/8!s(s^2-1)$ for any of these measures?

[2017-08-05 Predrag] to Rana: If my definition of the labels along $x$-axis in figure 5 (c) and (d) correct? When you replot, and replot you must, make both plots in figure 5 square, with both axes going from 0 to 1.

[2017-01-25 Boris] to Rana: In figure 5 the axis labels are too small. Make them all the same.

[2017-09-01 Li] Figure 5 (c) and (d) is a graph defined on 2-d, how about converting it to a 3-d plot?

## 5. Families of invariant 2-tori

[2017-01-25 Predrag] to Adrian : In figure 8 (also figure 6 if you revert it) and all blocks that follow please remove the matrix bracket, display only the symbols. The pattern is doubly periodic, no reason to bracket it from left and right (but not top and bottom).

[2017-09-01 Li] Figure 6: what about the original version, using numbers, while highlighting shared blocks with background color?

[2017-01-25 Predrag] Gutkin and Osipov refer to the map generated by the action (54) as non-perturbed *coupled cat map*, and to an invariant 2-torus $p$ as a "many-particle periodic orbit" (MPO) if $x_{n,t}$ is doubly-periodic, or "closed," i.e.,

$$x_{n,t} = x_{n+L,t+T}\,, \quad n = 0, 1, 2, \cdots, L-1\,, \quad t = 0, 1, 2, \cdots, T-1\,.$$

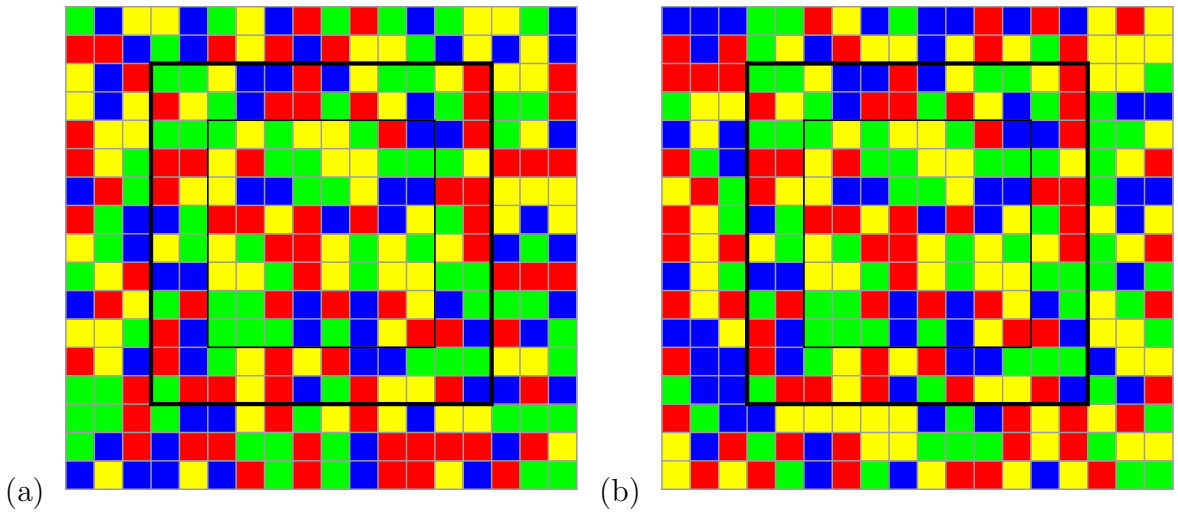

**Figure 6.** (Color online) Symbolic representation (colored tiles) of two $[L\times T] = [18\times 18]$ invariant 2-torus solutions of (36), $s = 7$, that shadow each other within the shared block $\mathsf{M}_{\mathcal{R}} = \mathsf{M}_{\mathcal{R}_0} \cup \mathsf{M}_{\mathcal{R}_1}$ (thick black border). The symbols within $\mathcal{R}$, drawn randomly from the interior alphabet $\mathcal{A}_0$, are the same for both solutions; the symbols outside $\mathcal{R}$, also drawn randomly from $\mathcal{A}_0$, differ. The shared block $\mathcal{R} = \mathcal{R}_0 \cup \mathcal{R}_1$ is split into the interior region $\mathcal{R}_0$ (thin black border) and the border strip $\mathcal{R}_1$ (thick black border).

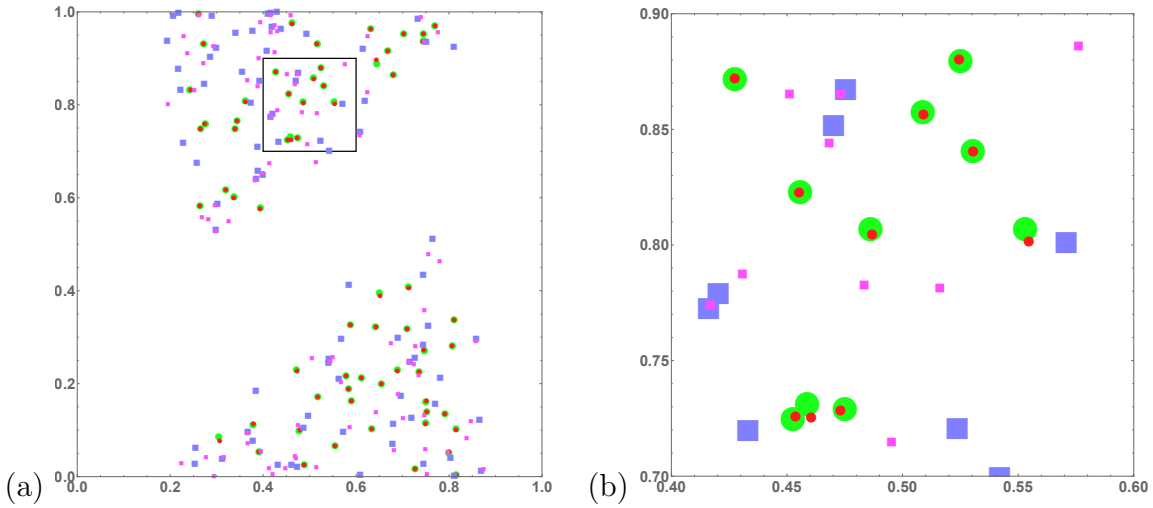


**Figure 7.** (Color online) (a) Phase space representation $(q_z^{(i)}, p_z^{(i)})$, where $i = 1, 2$ refers to the two invariant 2-tori of figure 6. (b) A zoom into small rectangular area shown on the left. The phase space is covered only partially, as symbols in blocks $\mathsf{M}$ are restricted exclusively to the interior alphabet. Only data for $z = (n, t) \in \mathcal{R}$ are shown in the figure. The centers of red (small) circles and green (large) circles are the points $(q_z^{(i)}, p_z^{(i)})$ of the first $(i = 1)$ and the second $(i = 2)$ invariant 2-torus for $z$'s from the interior $\mathcal{R}_0$. The centers of violet (large) and magenta (small) squares show the respective points from the border $\mathcal{R}_1$, see figure 6. All $(q_z^{(1)}, p_z^{(1)})$ and $(q_z^{(2)}, p_z^{(2)})$ in the interior are well paired, while the separations are larger for $z$'s in the border region $\mathcal{R}_1$. This illustrates shadowing being exponentially stronger the closer the point is to the center of $\mathcal{R}$, see (9).

Action of an invariant 2-torus $p$ is

$$S_p = -\frac{1}{2}\sum_{t=1}^{T}\sum_{n=1}^{L} m_{n,t}x_{n,t} \tag{54}$$

[2017-08-02 Boris] The representation figure 6 has changed from digits to colors. Was it try and see, or is it going to stay? In my opinion it is more colorful, but less informative. The reason is a) digits are directly $m_{n,t}$ - no need to translate colors into numbers + make sense without colors (on line). b) the encounters (regions with the same coding) can be visualized by coloring.

[2017-08-11 Predrag] Well, that's a bit subjective - it is unintelligible to a human eye either way. I would keep this one figure as an illustration that color coding is an alternative to number coding.

Methods described above make it an easy task to obtain a particular class of invariant 2-tori for the spatiotemporal cat. Since the interior symbols form a full shift, any $L\times T$ block of interior symbols $\mathsf{M} = \{m_z \in \mathcal{A}_0 | z \in \mathbb{Z}^2_{\rm LT}\}$,

$$\mathbb{Z}^2_{\rm LT} = \{z = (n,t) | n = 1,\dots,L, t = 1,\dots T\}\,,$$

is admissible and generates a invariant 2-torus solution of (36). Its coordinate representation $\Gamma = \{x_z, z \in \mathbb{Z}^2_{\rm LT}\}$, is obtained by taking inverse of (36):

$$x_z = \sum_{z'\in\mathbb{Z}^2_{\rm LT}} \mathsf{g}^0_{zz'} m_{z'}, \qquad m_{z'} \in \mathcal{A}_0, \tag{55}$$

where $\mathsf{g}^0_{zz'}$ is the corresponding Green's function with periodic boundary conditions, see Appendix A. This simple procedure can be exploited to test shadowing properties of invariant 2-torus solutions of the equation (36).

[2019-01-24 Predrag] Some of this invariant 2-torus stuff presumably goes to the kittens paper [27]; this paper does only the Dirichlet b.c..

As the first application, we show in figure 6 two periodic blocks $M_\Gamma$, $M_{\Gamma'}$ composed of interior symbols, which coincide only within the $[\ell\times\ell]$ square region $\mathcal{R}$ marked in blue (color on line). In the accompanying figure 7 we show their spatiotemporal representations $\Gamma = \{x_z, z \in \mathbb{Z}^2_{\rm LT}\}$, $\Gamma' = \{x'_z, z \in \mathbb{Z}^2_{\rm LT}\}$ for the spatiotemporal points $z \in \mathcal{R}$: the distances between $x_z$ and $x'_z$ shrink exponentially as $z$ approaches the center of the square. In other words $\Gamma$ and $\Gamma'$ shadow each other within the region $\mathcal{R}$.

The $\Gamma$ and $\Gamma'$ of the above example shadow each other only partially - outside of the region $\mathcal{R}$ their points are not paired. On the other hand, it turns out to be possible to find different invariant 2-tori solutions of (36) which shadow each other at every point of $\mathbb{Z}^2_{\rm LT}$. Such solutions, referred as partners, play an important role in the semiclassical treatment of the corresponding quantum model, since their action differences are small, see [46–48, 75, 86].

We briefly recall here the construction of partner solutions in $d = 2$ setting, provided first in [48]. Let $\mathsf{M}_\Gamma = \{m_z \in \mathcal{A}_0 | z \in \mathbb{Z}^2_{\rm LT}\}$ be a given $[L\times T]$ symbolic representation of a

invariant 2-torus state $\Gamma$ that satisfies (36), such that it contains exactly the same block of symbols in several distinct regions $\{\mathcal{R}_1, \ldots \mathcal{R}_l\}$, $\mathcal{R}_j \subset \mathbb{Z}^2_{\rm LT}$, related by space-time shifts $t \to t + t_i$, $n \to n + n_i$, $i = 1, \ldots l$. In other words $\mathsf{M}_\Gamma|_{\mathcal{R}_1} = \mathsf{M}_\Gamma|_{\mathcal{R}_2} = \ldots = \mathsf{M}_\Gamma|_{\mathcal{R}_l}$, where $\mathsf{M}_\Gamma|_{\mathcal{R}_i}$ stands for the restriction of $\mathsf{M}_\Gamma$ to region $\mathcal{R}_i$. Furthermore we assume that each $\mathcal{R}_i$ is a multiply connected region of width $\ell$ with a non empty interior $A_i$.

The width of $\mathcal{R}_i$ is defined as follows. Let $A_i$ and $C_i := \mathbb{Z}^2_{\rm LT} \setminus A_i \cup \mathcal{R}_i$ be the interior and the exterior of $\mathcal{R}_i$, respectively. We look for all $\ell$ such that any square $\mathcal{R}$ of the dimension $\ell \times \ell$ having non-zero intersection with $A_i$ i.e., $A_i \cap \mathcal{R} \neq \emptyset$ has zero intersection with $C_i$ i.e., $C_i \cap \mathcal{R} = \emptyset$. The maximum $\ell$ satisfying this requirement is called width of $\mathcal{R}_i$.

Such regions $\mathcal{R}_i, i = 1, \ldots, l$ (which we shall refer to as "$l$-encounters") are shown in figure 10 as blue colored regions. Provided that the interior parts $A_i$, $i = 1, \ldots l$ have different symbolic content i.e., $\mathsf{M}_\Gamma|_{A_i} \neq \mathsf{M}_\Gamma|_{A_j}$ for $i \neq j$, we can construct new invariant 2-tori of (36) by permuting symbol regions $\mathsf{M}_\Gamma|_{A_i}, i = 1, \ldots, l$ . So all together we have $l!$ family of solutions $\Gamma_1, \ldots \Gamma_{l!}$ such that their symbolic representations $\mathsf{M}_{\Gamma_1}, \ldots \mathsf{M}_{\Gamma_{l!}}$ share the following property: each $[\ell \times \ell]$ block of the symbols appears once in each $\mathsf{M}_{\Gamma_i}$. By the shadowing property, this in turn implies that all $\Gamma_1, \ldots \Gamma_{l!}$ pass through approximately the same points of the state space but in a different spatiotemporal 'order'. The degree of their closeness is controlled by the parameter $\ell$. The larger $\ell$ is, the closer two different $\Gamma_i$, $\Gamma_j$ come to each other in the phase space. In figure 9 and figure 11 we illustrate these parings for the family of invariant 2-torus solutions whose symbolic representations are shown in figure 8 and figure 10, respectively.

[2017-03-04 Predrag] figure 8: what does this mean? "Any $4 \times 4$ block of symbols appears one and the same number of times in both representations."

[2017-08-02 Boris] In detail, it means the following: If we scroll/peep through the (upper) torus symbolic representation with $4 \times 4$ window, there are exactly $NT$ different $4 \times 4$ blocks of symbols. Each of them appears (the same number of times), as well, in the symbolic representation of the bottom tori (but for possibly different window positions).

## 6. Summary and discussion

In this paper we have analyzed the spatiotemporal cat (4) linear symbolic dynamics. We now summarize our main findings.

[2016-11-08 Predrag] Say: THE BIG DEAL is
for $d$-dimensional field theory, symbolic dynamics is not one temporal sequence with a huge alphabet, but $d$-dimensional spatiotemporal tiling by a finite alphabet
"Classical foundations of many-particle quantum chaos" I believe could become a game-changer. Corresponding dynamical zeta functions should be sums over invariant 2-tori (as is done in the kittens paper [27]), rather than 1-dimensional periodic orbits

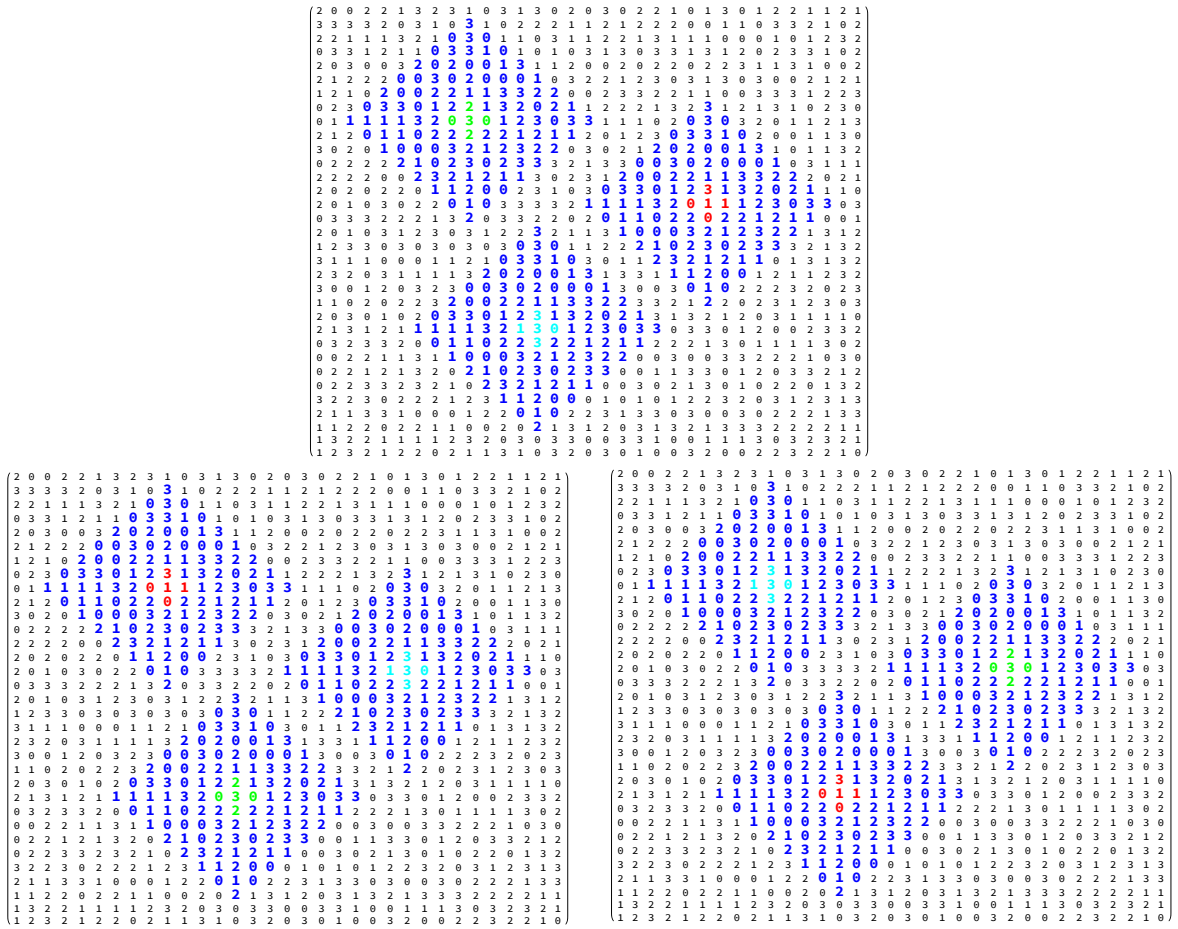

**Figure 8.** (Color online) Symbolic representation of three invariant 2-tori of (36) for $[L\times T] = [33\times 33]$, $s = 7$. They shadow each other in the diamond-shaped regions (blue). The three invariant 2-tori are related by cyclic permutation of the inner regions of symbols, colored red, green and light blue, respectively. Any $[4\times 4]$ diamond block of symbols appears only once in each invariant 2-torus.

[2016-11-20 Boris] All papers that I know were dances around question of uniqueness SRB measure. Either show that measure is unique or opposite way around (phase transitions). We know from the start that system is in the high temperature regime, so the measure is unique.

The finite alphabet of symbols $\mathcal{A}$ encoding system's dynamics has been shown to split into interior $\mathcal{A}_0$ and exterior $\mathcal{A}_1$ parts, where only symbolic sequences containing external symbols require extra grammar rules. Blocks composed of only interior symbols are admissible and attain one and the same measure for a given block shape $\mathcal{R}$. Furthermore, the measure of a general block factorizes into product of a constant factor $d_{\mathcal{R}}$ and the geometric one $\mathcal{P}_{\mathcal{R}}$ which can be interpreted as a volume of certain type of polytopes in the Euclidean space whose dimension is determined by the length of the boundary of $\mathcal{R}$. While $d_{\mathcal{R}}$ is fixed by $\mathcal{R}$, $\mathcal{P}_{\mathcal{R}}$ depends on the symbolic content and attains maximum value 1 for blocks of interior symbols. In addition, it has been shown that

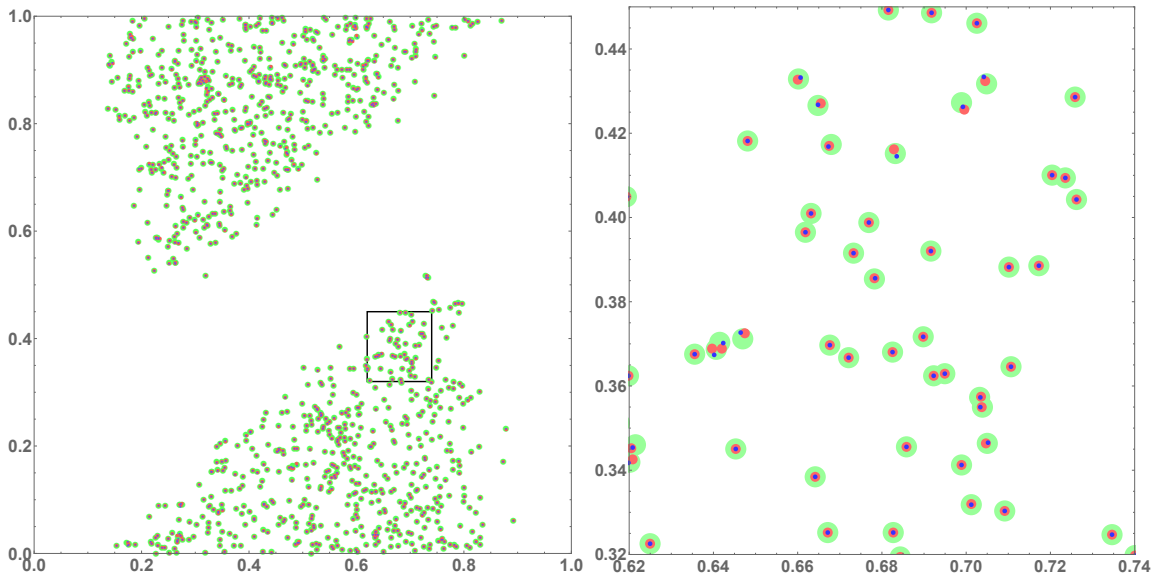


**Figure 9.** (Color online) Hamiltonian coordinate-momentum representation $(q_z^{(i)}, p_z^{(i)})$, $i = 1, 2, 3$ of the three invariant 2-tori of figure 8, shown as centers of green red and blue circles. Note that the above solutions form almost "perfect" triplets except points from the border regions, where some deviations can be observed.

$$\begin{pmatrix}
9&1&1&8&4&7&7&0&5&8&1&7&1&0&6&2&1&2&9&6&7\\
4&7&1&0&2&4&4&1&6&5&4&1&3&2&3&3&9&6&9&0&7\\
4&8&3&8&8&6&9&7&1&5&6&6&6&3&3&6&4&6&9&4&0\\
9&0&4&9&5&0&1&9&3&0&8&1&8&0&1&4&7&3&6&3&4\\
2&9&4&9&9&4&1&9&0&1&1&7&4&7&6&3&4&6&8&2&2\\
4&6&3&7&3&5&6&5&1&5&2&6&3&3&0&7&2&2&4&5&6\\
8&1&2&6&6&4&6&2&7&8&3&3&0&0&1&4&3&4&4&1&8\\
2&6&3&1&1&1&0&3&1&7&3&3&6&7&6&6&5&3&2&4&1\\
4&5&6&6&9&5&3&2&5&0&8&4&3&6&1&2&7&9&0&2&9\\
5&7&3&6&1&1&1&0&2&3&9&5&3&7&5&0&5&9&0&8&7\\
5&7&6&3&9&5&5&3&3&4&8&1&6&5&3&9&6&5&4&1&3\\
1&6&3&7&6&5&9&3&2&3&1&2&9&0&3&8&7&3&3&0&6\\
1&3&4&3&0&2&8&0&6&2&1&7&9&1&5&7&5&1&2&2&0\\
0&6&3&7&8&2&1&1&1&0&8&3&8&8&6&9&7&1&4&0&4\\
0&5&3&4&9&7&4&7&7&9&0&4&9&5&0&1&9&3&2&3&6\\
3&5&2&9&8&3&9&0&7&9&9&4&9&9&4&1&9&0&0&6&8\\
1&5&2&7&4&1&6&8&5&4&6&3&7&2&7&6&5&1&8&8&7\\
9&4&1&6&6&7&1&1&8&9&1&2&6&1&7&6&2&7&2&2&5\\
5&7&1&0&3&3&3&0&6&9&6&3&1&9&2&0&3&1&9&3&2\\
6&1&2&1&1&0&5&0&6&6&5&6&6&9&5&3&2&5&6&4&4\\
1&9&9&2&0&8&6&7&5&9&7&3&6&1&1&1&0&2&8&2&1\\
3&1&8&3&4&3&6&1&9&8&7&6&3&9&5&5&3&3&6&2&3\\
6&2&1&7&6&7&7&3&5&9&4&7&5&5&1&2&9&0&8&6&9\\
7&8&8&9&6&1&1&4&9&3&8&5&4&8&4&2&1&6&3&7&9\\
5&8&7&5&3&8&7&1&8&0&8&5&4&3&0&4&0&3&4&1&7
\end{pmatrix}
\qquad
\begin{pmatrix}
9&1&1&8&4&7&7&0&5&8&1&7&1&0&6&2&1&2&9&6&7\\
4&7&1&0&2&4&4&1&6&5&4&1&3&2&3&3&9&6&9&0&7\\
4&8&3&8&8&6&9&7&1&5&6&6&6&3&3&6&4&6&9&4&0\\
9&0&4&9&5&0&1&9&3&0&8&1&8&0&1&4&7&3&6&3&4\\
2&9&4&9&9&4&1&9&0&1&1&7&4&7&6&3&4&6&8&2&2\\
4&6&3&7&2&7&6&5&1&5&2&6&3&3&0&7&2&2&4&5&6\\
8&1&2&6&1&7&6&2&7&8&3&3&0&0&1&4&3&4&4&1&8\\
2&6&3&1&9&2&0&3&1&7&3&3&6&7&6&6&5&3&2&4&1\\
4&5&6&6&9&5&3&2&5&0&8&4&3&6&1&2&7&9&0&2&9\\
5&7&3&6&1&1&1&0&2&3&9&5&3&7&5&0&5&9&0&8&7\\
5&7&6&3&9&5&5&3&3&4&8&1&6&5&3&9&6&5&4&1&3\\
1&6&3&7&6&5&9&3&2&3&1&2&9&0&3&8&7&3&3&0&6\\
1&3&4&3&0&2&8&0&6&2&1&7&9&1&5&7&5&1&2&2&0\\
0&6&3&7&8&2&1&1&1&0&8&3&8&8&6&9&7&1&4&0&4\\
0&5&3&4&9&7&4&7&7&9&0&4&9&5&0&1&9&3&2&3&6\\
3&5&2&9&8&3&9&0&7&9&9&4&9&9&4&1&9&0&0&6&8\\
1&5&2&7&4&1&6&8&5&4&6&3&7&3&5&6&5&1&8&8&7\\
9&4&1&6&6&7&1&1&8&9&1&2&6&6&4&6&2&7&2&2&5\\
5&7&1&0&3&3&3&0&6&9&6&3&1&1&1&0&3&1&9&3&2\\
6&1&2&1&1&0&5&0&6&6&5&6&6&9&5&3&2&5&6&4&4\\
1&9&9&2&0&8&6&7&5&9&7&3&6&1&1&1&0&2&8&2&1\\
3&1&8&3&4&3&6&1&9&8&7&6&3&9&5&5&3&3&6&2&3\\
6&2&1&7&6&7&7&3&5&9&4&7&5&5&1&2&9&0&8&6&9\\
7&8&8&9&6&1&1&4&9&3&8&5&4&8&4&2&1&6&3&7&9\\
5&8&7&5&3&8&7&1&8&0&8&5&4&3&0&4&0&3&4&1&7
\end{pmatrix}$$

**Figure 10.** (Color online) Symbol blocks of two invariant 2-tori of (36) for $[L \times T] = [25 \times 25]$ which shadow each other at every point. The encounter region of repeated symbolic block-like region is shown in blue. The two solutions are related by permutation of inner regions of symbols colored in red and blue, respectively. Any $4 \times 4$ block of symbols appears one and the same number of times in both representations.

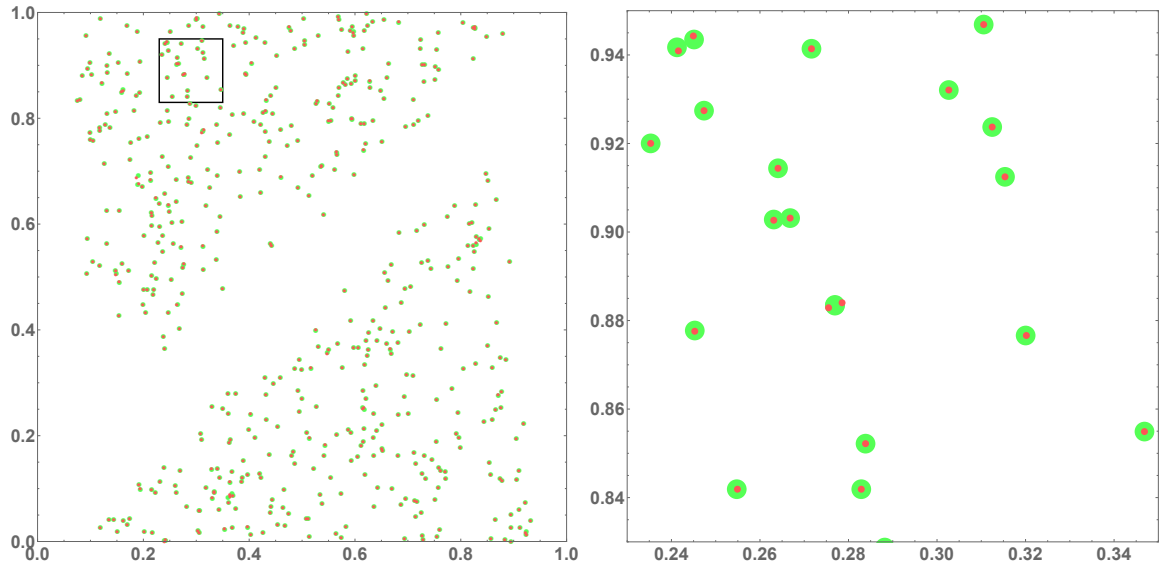


**Figure 11.** (Color online) Coordinate-momentum representation $(q_z^{(i)}, p_z^{(i)}), i = 1, 2$ of the two invariant 2-tori from figure 10.

a local d=2 block of symbols determines approximate positions of the corresponding points in the system phase space within an error decreasing exponentially with the size of the block.

As an application of these results we have constructed several examples of partner invariant 2-tori composed of interior symbols which revisit the same regions in the phase space, but in different spatiotemporal "orders". Such invariant 2-tori shadowing each other are expected to play an important role in the semiclassical treatment of the corresponding quantum models.

### *6.1. Discussion.*

Remarkably, as far as the linear symbolic dynamics is concerned, the above results hold both for the single cat map and its coupled lattice generalization. In both cases the proofs rely only upon ellipticity of the operator $\Box$ and the linearity of the equations. It is very plausible that the same results hold for the lattices $\mathbb{Z}^d$ of an arbitrary dimension $d$. Furthermore, the restriction to the integer valued matrices in the definitions of maps appears unnecessary. Cat map is a smooth version of the sawtooth map, defined by the same equation (16), but for a real (not necessarily integer) value of $s$. The linear symbolic dynamics for single saw map has been analyzed in [76] and its extension to a coupled $\mathbb{Z}^d$ model along the lines of the present paper seems to be straightforward. Also, in the current paper we sticked to the Laplacian form of $\Box$. Again this seems to be too restrictive and extension to other elliptic operators of higher order should be possible. Such operators are necessarily appear within the models with higher range of interactions.

A physically necessary extension of current setting would be addition of an external

periodic potential $V$ to (4), rendering this a nonlinear problem,

$$(\Box - s + 2d + V'(x_z))x_z = m_z, \qquad z \in \mathbb{Z}^d\,. \tag{56}$$

As long as the perturbation $V$ is sufficiently weak, this lattice map can be conjugated to the linear spatiotemporal cat, with $V = 0$. This approach has been used in [48] to construct partner invariant 2-tori for perturbed cat map lattices. On the other hand, for a sufficiently strong perturbation, such a conjugation to linear system is no longer possible. Finally, let us note that the lattice models like (56) can be seen as discretized versions of PDEs arising from the Hamiltonian field theories. In this respect it would be of interest to study whether our results can be extended to the continuous, PDE setting.

[2016-11-01 Boris] **"Deeper insight" into $d = 2$ symbolic dynamics**: Relevance to semiclassics.

There is much to say about the cat map quantization, starting with the work of Hannay and Berry [50], the analysis of the use of the periodic orbits of the cat map in its quantization by Keating [31, 62], and subsequent developments such as Keating and Mezzadri [63, 64], but in this work we have restricted our considerations to purely classical deterministic spatiotemporal dynamics.

**Acknowledgments**

Work of B. G. and P. C. was supported by the family of late G. Robinson, Jr..

## Appendix A. Lattice Green's functions

### *Appendix A.1. Green's function for 1-dimensional lattice*

Consider the single cat map equation (16) with a delta function source term

$$(-\Box + s - 2)\mathsf{g}_{i,j} = \delta_{i,j}, \qquad i, j \in \mathbb{Z}^1\,. \tag{A.1}$$

The corresponding free, infinite lattice Green's function $\mathsf{g}_{i,j} = \mathsf{g}_{i-j}$ is given by [73, 76]

$$\mathsf{g}_t = \frac{1}{\pi}\int_0^\pi \frac{\cos(tx)}{s - 2\cos x}dx = \Lambda^{-|t|}/(\Lambda - \Lambda^{-1})\,, \tag{A.2}$$

with $s = \Lambda + \Lambda^{-1}$, $\Lambda > 1$, as may be verified by substitution.

*Dirichlet boundary conditions:* In this case the Green's function $\mathsf{g}$ satisfies (A.1), but, in addition, is subject to the Dirichlet boundary conditions:

$$\mathsf{g}_{0,j} = \mathsf{g}_{i,0} = \mathsf{g}_{\ell+1,j} = \mathsf{g}_{i,\ell+1} = 0\,.$$

It is possible to determine $\mathsf{g}$ in two different ways. The first one is to use the fact that $\mathsf{g}_{i,j} = (\mathcal{D}^{-1})_{i,j}$, where $\mathcal{D}$ is tridiagonal $[\ell \times \ell]$ matrix

$$\mathcal{D} = \begin{pmatrix} s & -1 & 0 & 0 & \dots & 0 & 0 \\ -1 & s & -1 & 0 & \dots & 0 & 0 \\ 0 & -1 & s & -1 & \dots & 0 & 0 \\ \vdots & \vdots & \vdots & \vdots & \ddots & \vdots & \vdots \\ 0 & 0 & \dots & \dots & \dots & -1 & s \end{pmatrix}.$$

Since $\mathcal{D}$ is of a tridiagonal form, its inverse can be found explicitly.

An alternative way to evaluate $\mathsf{g}_{i,j}$ is to use Green's function $g$ and take anti-periodic sum (similar method can be used for periodic and Neumann boundary conditions)

$$\mathsf{g}_{i,j} = \sum_{n=-\infty}^{\infty} \mathsf{g}_{i,j+2n(\ell+1)} - \mathsf{g}_{i,-j+2n(\ell+1)}.$$

This approach has an advantage of being easily extendable to $\mathbb{Z}^2$ case. After substituting $g$ and taking the sum one obtains

$$\mathsf{g}_{i,j} = \begin{array}{ll} \frac{U_{i-1}(s/2)U_{\ell-j}(s/2)}{U_\ell(s/2)} & \text{for } i \le j \\ \frac{U_{j-1}(s/2)U_{\ell-i}(s/2)}{U_\ell(s/2)} & \text{for } i > j. \end{array} \tag{A.3}$$

where $U_n(s/2) = \frac{\sinh(n+1)\lambda}{\sinh\lambda}$ are Chebyshev polynomials of the second kind, and $e^\lambda = \Lambda$.

Note that the Green's function is strictly negative for both boundary conditions.

*Appendix A.2. Green's function for 2-dimensional square lattice*

The free Green's function $g(z,z') = g(z-z',0) = \mathsf{g}_{n,t}$, $z - z' = (n,t) \in \mathbb{Z}^2$ solves the equation

$$(-\Box + s - 4)g(z,z') = \delta_{z,z'}\,. \tag{A.4}$$

The solution is given by the double integral [72]

$$\mathsf{g}_{n,t} = \frac{1}{\pi^2}\int_0^\pi \int_0^\pi \frac{\cos(nx)\cos(ty)}{s - 2\cos x - 2\cos y} dxdy\,, \tag{A.5}$$

an expression which can, in turn, be recast into single integral form,

$$\begin{aligned} \mathsf{g}_{n,t} &= \frac{1}{2\pi^3}\int_{-\infty}^{+\infty} d\eta \int_0^\pi \int_0^\pi \frac{\cos(nx)\cos(ty)}{(s/2 - 2\cos x - i\eta)(s/2 - 2\cos y + i\eta)} dxdy \\ &= \frac{1}{2\pi}\int_{-\infty}^{+\infty} d\eta \, \frac{\mathcal{L}(\eta)^{-n}\mathcal{L}^*(\eta)^{-t}}{|\mathcal{L}(\eta) - \mathcal{L}(\eta)^{-1}|^2}\,, \end{aligned} \tag{A.6}$$

where

$$\mathcal{L}(\eta) + \mathcal{L}(\eta)^{-1} = s/2 + i\eta, \qquad |\mathcal{L}(\eta)| > 1\,.$$

The above equation can be thought as the integral over a product of two $\mathbb{Z}^1$ functions:

$$\mathsf{g}_{n,t} = \frac{1}{2\pi}\int_{-\infty}^{+\infty} d\eta \, \mathsf{g}_n(s/2 + i\eta)\mathsf{g}_t(s/2 - i\eta)\,. \tag{A.7}$$

An alternative representation is given by modified Bessel functions $I_n(x)$ of the first kind [72]:

$$\mathsf{g}_{n,t} = \int_0^{+\infty} d\eta\, e^{-s\eta} I_n(\eta) I_t(\eta)\,, \tag{A.8}$$

which enables the evaluation of the diagonal elements explicitly, as a Legendre function,

$$\mathsf{g}_{n,n} = \frac{1}{2\pi i} Q_{n-1/2}(s^2/8-1), \qquad s^2/8-1>1\,.$$

The representation (A.7) demonstrates that $\mathsf{g}_{n,t}$ is positive for any $n$ and $t$.

*Dirichlet boundary conditions.* Consider next the Green's function $\mathsf{g}_{zz'} \equiv \mathsf{g}(z,z')$, $z=(n,t)\in\mathbb{Z}^2$, $z'=(n',t')\in\mathbb{Z}^2$ which satisfies (A.4) within the rectangular domain $\mathcal{R}=\{(n,t)\in\mathbb{Z}^2 | 1\le n\le \ell_1, 1\le t\le \ell_2\}$ and vanishes at its boundary $\partial\mathcal{R}$, see figure 4(a). By applying the same method as in the case of one-dimensional lattices we get

$$\begin{aligned}\mathsf{g}(z,z') = \sum_{j_1,j_2=-\infty}^{+\infty} & \mathsf{g}_{n-n'+2j_1(\ell_1+1),t-t'+2j_2(\ell_2+1)} + \mathsf{g}_{n+n'+2j_1(\ell_1+1),t+t'+2j_2(\ell_2+1)} \\ & - \mathsf{g}_{n-n'+2j_1(\ell_1+1),t+t'+2j_2(\ell_2+1)} - \mathsf{g}_{n+n'+2j_1(\ell_1+1),t-t'+2j_2(\ell_2+1)},\end{aligned}$$

where $\mathsf{g}_{n,t}$ is the free Green's function defined by (A.5). Substituting (A.7) yields

$$\mathsf{g}(z,z') = \frac{1}{2\pi}\int_{-\infty}^{+\infty} d\eta\, \mathsf{g}_{n,n'}(s/2+i\eta)\mathsf{g}_{t,t'}(s/2-i\eta)\,. \tag{A.9}$$

*Exponential decay of Green's function.* We are now going to show that the Green's function $\mathsf{g}(z,z')$ decays exponentially as distance between points $z$ and $z'$ grows. The starting point is (A.9) by which

$$|\mathsf{g}(z,z')|^2 \le \int_{-\infty}^{+\infty}\frac{d\eta}{2\pi}|\mathsf{g}_{n,n'}(s/2+i\eta)|^2 \int_{-\infty}^{+\infty}\frac{d\eta}{2\pi}|\mathsf{g}_{t,t'}(s/2-i\eta)|^2. \tag{A.10}$$

[2017-07-18 Boris] TO BE CONTINUED

*Appendix A.3. A lattice Green's function identity*

Consider the equation

$$(-\Box + s - 2d)\, x(z) = m(z)\,, \tag{A.11}$$

where $x(z)$, $m(z)$ are $C^2$ functions of coordinates $z\in\mathbb{R}^d$. For $s<2d$ this is the inhomogeneous Helmholtz equation, whose general solution is a sum of complex exponentials. For $s>2d$, the case studied here, the equation is known as the screened Poisson equation [38], or Yukawa equation, whose general solution is a sum of exponentials.

[2017-11-19 Predrag] Dropped this: " In the homogeneous case, the screened Poisson equation is the same as the time-independent KleinGordon equation. "

Let $g(z,z')$, $z,z' \in \mathcal{R}$ be the corresponding Green's function on a bounded, simply connected domain $\mathcal{R} \subset \mathbb{R}^d$,

$$(-\Box + s - 2d)\, g(z,z') = \delta^{(d)}(z-z'), \tag{A.12}$$

satisfying some boundary condition (e.g., periodic, Dirichlet or Neumann) at $\partial\mathcal{R}$. The Green's function identity allows us to connect the values of $x_z$ inside of $\mathcal{R}$ with the ones attained at the boundary (an arbitrary Soviet citation):

$$\begin{aligned} x(z) = & \int_{\mathcal{R}} g(z,z')m(z')dz' \\ & - \int_{\partial\mathcal{R}} \nabla_n\, g(z,z'')x(z'')\, dz'' + \int_{\partial\mathcal{R}} \nabla_n\, x(z'')g(z,z'')\, dz''\,. \end{aligned} \tag{A.13}$$

The analogous theorem holds in the discrete setting as well. For the sake of simplicity, we will restrict our considerations to $d = 1, 2$.

*1-dimensional lattice.* Let $\mathsf{g}_{t,t'}$ be a Green's function on $\mathbb{Z}^1$ satisfying (A.1) and some boundary condition at the end points 0, $\ell+1$. To prove the Green's theorem for a solution $x_t$ of (16) we multiply each side of this equation by $\mathsf{g}_{t,t'}$ and sum up over the index $t$, running from 1 to $\ell$. In a similar way, the two sides of (A.1) can be multiplied with $x_t$ and summed up over the same interval. After subtraction of two equations we obtain

$$\begin{aligned} x_t &= \sum_{t'=1}^{\ell} m_{t'}\mathsf{g}_{t',t} - x_\ell \mathsf{g}_{\ell+1,t} + x_0\mathsf{g}_{1,t} - x_1\mathsf{g}_{0,t} + x_{\ell+1}\mathsf{g}_{\ell,t}, \\ &= \sum_{t'=1}^{\ell} m_{t'}\mathsf{g}_{t',t} - x_\ell \partial_n\mathsf{g}_{\ell,t} - x_1\partial_n\mathsf{g}_{1,t} + \partial x_1\mathsf{g}_{1,t} + \partial x_\ell \mathsf{g}_{\ell,t}, \end{aligned}$$

with $\partial_n\phi(\ell) := \phi(\ell+1) - \phi(\ell)$, $\partial_n\phi(1) := \phi(0) - \phi(1)$ being the normal derivatives at the two boundary points. This equation is exactly of the same form as (A.13). For the Green's function $\mathsf{g}$ with the Dirichlet boundary condition it simplifies further to:

$$x_t = \sum_{t'=1}^{\ell} m_{t'}\mathsf{g}_{t',t} + x_0\mathsf{g}_{1,t} + x_{\ell+1}\mathsf{g}_{\ell,t}\,. \tag{A.14}$$

*2-dimensional lattice.* Let $x_z$ be a solution of (36) within a domain $\mathcal{R}$. After multiplication of two sides of (36) with a Green's function satisfying (A.4) and summing up over the region $\mathcal{R}$ we get

$$\sum_{z'\in\mathcal{R}} g(z,z')\left(\sum_{i=1}^{4} x_{z'+e_i} - s x_{z'}\right) = \sum_{z'\in\mathcal{R}} g(z,z')m_{z'}\,,$$

with $e_{1,2} = (0,\pm 1), e_{3,4} = (\pm 1, 0)$ being the four vectors connecting the neighboring sites of the lattice. In the same way, we obtain from (A.4)

$$\sum_{z'\in\mathcal{R}} x_{z'}\left(\sum_{i=1}^{4} g(z+e_i,z') - s g(z,z')\right) = \sum_{z'\in\mathcal{R}} \delta(z,z')x_{z'} = -x_z\,.$$

The subtraction of two equations yields

$$x_z = \sum_{z'\in\mathcal{R}} g(z,z')m_{z'} - \sum_{z''\in\partial\mathcal{R}} \nabla_n g(z,z'')x_{z''} + \sum_{z''\in\partial\mathcal{R}} \nabla_n x_{z''} g(z,z'')\,, \quad \text{(A.15)}$$

with $\nabla_n\phi_z := \sum_{e_i\notin\mathcal{R}} \phi_{z+e_i} - \phi_z$. For a Green's function satisfying Dirichlet boundary conditions, (A.15) can be simplified further, as illustrated by the following example of.

*Example: Rectangular domain.* Given a rectangular domain $\mathcal{R} = \mathcal{R}^{[\ell_1\times\ell_2]}$, let $\mathsf{g}(z,z'')$ be the corresponding Dirichlet Green's function vanishing at the boundary $\partial\mathcal{R}$. Since $\mathsf{g}(z,z'') = 0$ for all $z''\in\partial\mathcal{R}$, equation (A.15) can be written down in the following form

$$x_z = \sum_{z'\in\mathcal{R}} \mathsf{g}(z,z')m_{z'} + \sum_{z''\in\partial\mathcal{R}} \mathsf{g}(z,\bar{z}'')x_{z''}\,, \quad \text{(A.16)}$$

where $\bar{z}''\in\mathcal{R}$ is a point of $\mathcal{R}$, adjacent to $z''\in\partial\mathcal{R}$, see figure 4(a). Note that the rectangular corners are associated with two points of the boundary $\partial\mathcal{R}$. Otherwise, the relationship between $\bar{z}''$ and $z''$ is one-to-one.

## Appendix B. Spatiotemporal cat, Hamiltonian formulation

[2017-09-14 Boris] We should add here the discussion of entropy.
PC 2017-11-20 added.

The Hamiltonian setup of the spatiotemporal cat (36) is discussed in detail in [48]. In this paper we use it to generate spatiotemporally chaotic patterns by time evolution of random initial conditions on a cylinder infinite in time direction, but $L$-periodic in the space direction.

In one spatial dimension the momentum field at the lattice site ($n$'th "particle") $q_n$ is given by $p_{n,t} = x_{n,t} - x_{n,t-1}$, and the Hamiltonian cat map (13) at each lattice site is coupled to its nearest neighbors by

$$\begin{aligned} x_{n,t+1} &= p_{n,t} - x_{n+1,t} + a\,x_{n,t} - x_{n-1,t} - m^x_{n,t+1} \\ p_{n,t+1} &= bp_{n,t} + (ab-1)\,x_{n,t} - b\,(x_{n+1,t} + x_{n-1,t}) - m^p_{n,t+1}\,, \end{aligned} \quad \text{(B.1)}$$

where $(x_{n,t}, p_{n,t})$ are the coordinate and momentum of the $n$'th "particle" at the discrete time $t$, and $m^x_{n,t}, m^p_{n,t}$ are the corresponding winding numbers necessary to bring $(x_{n,t+1}, p_{n,t+1})$ to the unit interval. As for the single cat map, integers $a$ and $b$ are arbitrary; the Lagrangian form (3) of the map only depends on their sum $s = a + b$. Hamiltonian winding numbers [48] are connected to the Lagrangian ones by $m_{n,t} = -b\,m^x_{n,t} + m^x_{n,t+1} - m^p_{n,t}$.

In the Hamiltonian setup, the $d = 2$ spatiotemporal cat is thus viewed as a $\mathbb{Z}^1$ chain of linearly coupled cat maps acting on the phase space $V$, a direct product of the 2-dimensional tori $V = \otimes_n \mathbb{T}^2_n$, $n\in\mathbb{Z}^1$. Each torus $\mathbb{T}^2_n$ is equipped with the phase space coordinate pair $(x_n, p_n)\in(0,1]\times(0,1]$ corresponding to the position and momentum of the $n$'th "particle". The law of time evolution (B.1) is time-translation invariant as well as space-translation, i.e., invariant under shifts $\sigma : n\to n+1$.

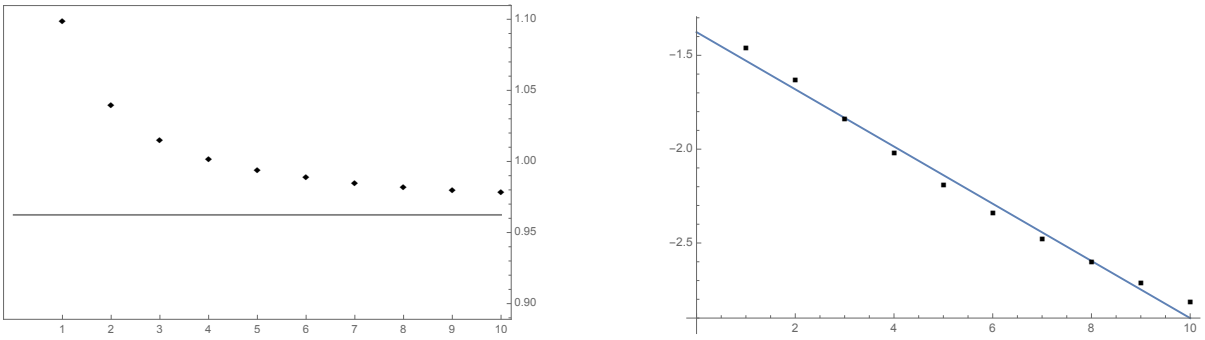


**Figure B1.** Entropies $h_\ell$ and $\log\Lambda$ vs. the length $|\ell|$ of periodic orbits used to estimate them. **To Rana: In this figure should be the data for several different $s$ (3 and something) of $h^1_\ell$**

Along with the infinite chain we will consider the spatial finite counterpart of the model, with $L$ Hamiltonian cat maps coupled cyclically, and (B.1) subject to the periodic boundary conditions $(x_n, p_n) = (x_{n+L}, p_{n+L})$. This defines a linear map $V_L \to V_L$ on the $2L$-dimensional phase space $V_L = \otimes_{n=1}^{L} \mathbb{T}^2_n$:

$$Z_{t+1} = \mathcal{B}_L Z_t \mod 1\,, \qquad Z_t = (x_{1,t}, p_{1,t}, \dots x_{L,t}, p_{L,t})^T\,, \tag{B.2}$$

where $Z_t \in V_L$, and $\mathcal{B}_L$ is the $[2L\times 2L]$ matrix

$$\mathcal{B}_L = \begin{pmatrix} A & B & 0 & \dots & 0 & B \\ B & A & B & \dots & 0 & 0 \\ 0 & B & A & \dots & 0 & 0 \\ \vdots & \vdots & \vdots & \ddots & \vdots & \vdots \\ 0 & 0 & 0 & \dots & A & B \\ B & 0 & 0 & \dots & B & A \end{pmatrix}, \qquad \begin{aligned} A &= \begin{pmatrix} a & 1 \\ ab-1 & b \end{pmatrix} \\ B &= -\begin{pmatrix} 1 & 0 \\ b & 0 \end{pmatrix} \end{aligned}\,.$$

The spectrum of the Lyapunov exponents (linear stability of the Hamiltonian spatiotemporal cat (B.1), posed as $t = 0$ initial problem, evolving in time) is given by the $\mathcal{B}_L$ eigenvalues (see eq. (3.6) of [48]):

$$\Lambda_k + \Lambda_k^{-1} = s - 2\cos(2\pi k/L), \qquad k = 1, \dots L\,, \tag{B.3}$$

$s = a + b \in \mathbb{Z}$. Accordingly, the map is fully hyperbolic iff $s > 4$, with all Lyapunov exponents $\lambda_k^{\pm} = \pm\log|\Lambda_k|$ paired as $\lambda_k^{+} = -\lambda_k^{-}$, $\lambda_k^{+} > 0$, for all $k$. Since the matrix $\mathcal{B}_L$ is symplectic, in the fully hyperbolic case the map (B.2) preserves the measure $d\mu_L = \prod_{i=1}^{L} dx_i dp_i$ on $V_L$. In the limit $L \to \infty$, $\mu_L$ induces the corresponding measure $\mu$ on $V$, invariant under both time evolution and discrete spatial lattice translations.

### *Appendix B.1. Cat map entropy*

Given measures $\mu(b)$ of blocks $b$ of an arbitrary finite length $|b| = \ell$ one can estimate observables of the dynamical system with increasing precision as $\ell$ grows. In the following we apply our central result (29) to estimation of the metric entropy of the cat map.

The metric entropy of the cat map with respect to measure $\mu$ can be represented as the limit

$$h_\mu = \lim_{\ell\to\infty} h_\ell, \tag{B.4}$$

where

$$h_\ell = -\frac{1}{\ell}\sum_{|b|=\ell} \mu(b)\log\mu(b)\,.$$

By using the decomposition (29) $h_\ell$ can be split as $h_\ell = h^1_\ell + h^0_\ell$ into "geometric" and "internal" parts:

$$h^1_\ell = \frac{\sum_{|b|=\ell}|\mathcal{P}_b|\log|\mathcal{P}_b|}{\ell\sum_{|b|=\ell}|\mathcal{P}_b|}, \qquad h^0_\ell = \frac{1}{\ell}\log U_\ell(s/2).$$

The "interior" part $h^0_\ell$ converges to $\log\Lambda$ with the rate $O(1/\ell)$.

[2016-11-08 Predrag] this looks wrong to me - $\log\Lambda$ applies to the whole set, not this Smale horseshoe repeller.

[2017-07-31 Boris] Do not see too much room for being wrong here: $h^0_\ell \to \log\Lambda$ just by definition (easy to see). The point here is that $|\mathcal{P}_b|$ are kind of uniform - either close to 1 or to 0. In other words elements of the partition $\mathcal{M}$ have by and large similar size. This is probably very different from Adler-Weiss partitions. We could add some remark in this spirit to the text.

[2017-08-01 Boris] To Rana and all: I guess we are lacking a relevant picture for figure B1. What is plotted there right now is $h_\ell$ and $\log\Lambda$ (for which value of $s$?). It would be better if we plot just $h^1_\ell$ for several different $s$ (to see that it converges to 0 with some rate. Speculation- I expect some power-law convergence, something of the type $\sim \ell^{-1/2}$ ).

[2017-09-05 Li] I'm looking at numerical data. The number of total admissible rules of single cat map takes an exponential law: $\sim 2.63^n$ for s=3, $\sim 3.74^n$ for s=4 for example. i.e., effectively 2.63/3.74 symbols are needed for s=3/s=4. They agree with that from the topological entropy and Lyapunov exponent, which are $(3+\sqrt{5})/2, 2+\sqrt{3}$, respectively. Intuitively this should hold (that log[ number of admissible rules]/n = topological entropy), but is it well-known/justified in symbolic dynamics?

[2017-09-16 Predrag] we know the exact, Adler-Weiss answer, in terms of a golden mean - state it. The half-assed linear codes is an arbitrary, infinite sequence of approximations to the exact answer.

Since $\log\Lambda$ is precisely the value of $h_\mu(\phi)$, the metric entropy [87], it yields for the geometrical part: $\lim_{\ell\to\infty} h^1_\ell = 0$. In figure B1 we verify this directly by numerical calculations for several different $s$.

*Appendix B.2. Spatiotemporal cat entropy*

[2017-02-18 Predrag] We have not touched upon "new kinds of determinants, new relations between propagation of temporal vs. spatial disturbances." But we should - spatiotemporal cat offers a much more accessible, first illustration of the space-time duality than the spin chain papers.

[2017-07-29 Boris] Should we discuss determinants? Some material exists but it is outside of the present paper.

[2017-08-11 Predrag] Up to you - but it is an obvious question - what replaces the linear stability of the old-fashioned time-evolving solutions (so called "dynamical systems theory" with its Lyapunov exponents etc) in the new, spatiotemporal reformulation? You can write it up as a sequel to this paper, if you think that is too much stuff for one paper.

Recall that for single, temporal cat map the constant $d(\mathcal{R})$ was given explicitly by the Jacobian (30). In the case of spatiotemporal cat we were unable to derive any simple formula for $d(\mathcal{R})$, even in the case of rectangular regions. On the other hand, by the same argument as in the single cat map case, it might be expected that in the limit of large regions $\mathcal{R}$ the asymptotics of $d(\mathcal{R})$ should be determined by the metric entropy. In other words, we expect that for large regions $\mathcal{R}$

$$\frac{1}{|\mathcal{R}|}\log d(\mathcal{R}) \sim -h\,, \qquad \text{as } |\mathcal{R}|\to\infty\,,$$

where $h$ is the spatiotemporal metric entropy (B.5) of the spatiotemporal cat.

[2017-08-28 Predrag] "metric entropy (B.5) of the spatiotemporal cat" is a forward reference.

By the translational invariance of the spatially $L$-periodic spatiotemporal cat, each invariant 2-torus has the one and the same spectrum of the Lyapunov exponents $\lambda_k$, $k=1,\ldots,2L$, given by the eigenvalues (B.3) $\Lambda_k = e^{\lambda_k}$ of the matrix $\mathcal{B}_L$. Accordingly, the map is fully hyperbolic iff $s=a+b>4$. In this case all solutions of (B.3) are paired such that $\lambda_k^+ = -\lambda_k^-$ and $\lambda_k^+ > 0$ for all $k$. The metric entropy of $\Phi_L$ for a finite $L$ is given by the sum of all positive exponents:

$$h(\Phi_L) = \sum_{k=1}^{L} \log \lambda_k^+\,.$$

For the infinite lattice the corresponding spatiotemporal entropy of $\Phi$ with respect to $\mu$ is given by the limit $h_\mu(\Phi) = \lim_{L\to\infty} \frac{1}{L} h(\Phi_L)$ leading to

$$h_\mu(\Phi) = \frac{1}{\pi^2}\int_0^\pi\int_0^\pi dx\,dy\,\log(s-4+4\sin^2 x+4\sin^2 y)\,. \tag{B.5}$$

[2017-09-14 Predrag] Might want to note that this entropy (extensive with time $T$) is for the time evolution only, and unrelated to the determinants computed in evaluation the lattice Greens function, and to the spatiotemporal entropy that uses the weights of admissible spatiotemporal patterns, and is extensive with the area $[L\times T]$.

**References**


[1] R. L. Adler and B. Weiss, "Entropy, a complete metric invariant for automorphisms of the torus", Proc. Natl. Acad. Sci. USA **57**, 1573–1576 (1967).

[2] V. I. Arnol'd and A. Avez, *Ergodic Problems of Classical Mechanics* (Addison-Wesley, Redwood City, 1989).

[3] R. Artuso, "Diffusive dynamics and periodic orbits of dynamic systems", Phys. Lett. A **160**, 528–530 (1991).

[4] R. Artuso and P. Cvitanović, "Deterministic diffusion", in *Chaos: Classical and Quantum* (Niels Bohr Inst., Copenhagen, 2016).

[5] R. Artuso and R. Strepparava, "Reycling diffusion in sawtooth and cat maps", Phys. Lett. A **236**, 469–475 (1997).

[6] J.-C. Ban and S.-S. Lin, "Patterns generation and transition matrices in multi-dimensional lattice models", Discrete Continuous Dyn. Syst. Ser. A **13**, 637–658 (2005).

[7] J.-C. Ban, S.-S. Lin, and Y.-H. Lin, "Patterns generation and spatial entropy in two-dimensional lattice models", Asian J. Math. **11**, 497–534 (2007).

[8] J.-C. Ban, W.-G. Hu, S.-S. Lin, and Y.-H. Lin, *Zeta functions for two-dimensional shifts of finite type*, Vol. 221, Memoirs Amer. Math. Soc. (Amer. Math. Soc., Providence RI, 2013).

[9] J.-C. Ban, W.-G. Hu, S.-S. Lin, and Y.-H. Lin, Verification of mixing properties in two-dimensional shifts of finite type, 2015.

[10] M. Baranger, K. T. R. Davies, and J. H. Mahoney, "The calculation of periodic trajectories", Ann. Phys. **186**, 95–110 (1988).

[11] E. Behrends, "The ghosts of the cat", Ergod. Theor. Dynam. Syst. **18**, 321–330 (1998).

[12] E. Behrends and B. Fielder, "Periods of discretized linear Anosov maps", Ergod. Theor. Dynam. Syst. **18**, 331–341 (1998).

[13] N. Bird and F. Vivaldi, "Periodic orbits of the sawtooth maps", Physica D **30**, 164–176 (1988).

[14] M. Blank and G. Keller, "Random perturbations of chaotic dynamical systems: stability of the spectrum", Nonlinearity **11**, 1351–1364 (1998).

[15] M. L. Blank, *Discreteness and Continuity in Problems of Chaotic Dynamics* (Amer. Math. Soc., Providence RI, 1997).

[16] R. Bowen, *Equilibrium States and the Ergodic Theory of Anosov Diffeomorphisms* (Springer, Berlin, 1975).

[17] M. Boyle, R. Pavlov, and M. Schraudner, "Multidimensional sofic shifts without separation and their factors", Trans. Amer. Math. Soc. **362**, 4617–4653 (2010).

[18] F. Brini, S. Siboni, G. Turchetti, and S. Vaienti, "Decay of correlations for the automorphism of the torus $T^2$", Nonlinearity **10**, 1257–1268 (1997).

[19] L. A. Bunimovich and Y. G. Sinai, "Spacetime chaos in coupled map lattices", Nonlinearity **1**, 491 (1988).

[20] B. V. Chirikov, "A universal instability of many-dimensional oscillator system", Phys. Rep. **52**, 263–379 (1979).

[21] S.-N. Chow, J. Mallet-Paret, and E. S. Van Vleck, "Pattern formation and spatial chaos in spatially discrete evolution equations", Random Comput. Dynam. **4**, 109–178 (1996).

[22] S.-N. Chow, J. Mallet-Paret, and W. Shen, "Traveling waves in lattice dynamical systems", J. Diff. Equ. **149**, 248–291 (1998).

[23] F. Christiansen, P. Cvitanović, and V. Putkaradze, "Spatiotemporal chaos in terms of unstable recurrent patterns", Nonlinearity **10**, 55–70 (1997).

[24] S. C. Creagh, "Quantum zeta function for perturbed cat maps", Chaos **5**, 477–493 (1995).

[25] P. Cvitanović, "Counting", in *Chaos: Classical and Quantum* (Niels Bohr Inst., Copenhagen, 2016).

[26] P. Cvitanović and J. F. Gibson, "Geometry of turbulence in wall-bounded shear flows: Periodic orbits", Phys. Scr. T **142**, 014007 (2010).

[27] P. Cvitanović and H. Liang, Spatiotemporal cat: An exact classical chaotic field theory, in preparation, 2019.

[28] P. Cvitanović, P. Gaspard, and T. Schreiber, "Investigation of the Lorentz gas in terms of periodic orbits", Chaos **2**, 85–90 (1992).

[29] P. Cvitanović, R. L. Davidchack, and E. Siminos, "On the state space geometry of the Kuramoto-Sivashinsky flow in a periodic domain", SIAM J. Appl. Dyn. Syst. **9**, 1–33 (2010).

[30] P. Cvitanović, R. Artuso, R. Mainieri, G. Tanner, and G. Vattay, *Chaos: Classical and Quantum* (Niels Bohr Inst., Copenhagen, 2018).

[31] I. Dana, "General quantization of canonical maps on a two-torus", J. Phys. A **35**, 3447 (2002).

[32] R. L. Devaney, *An Introduction to Chaotic Dynamical systems*, 2nd ed. (Westview Press, 2008).

[33] X. Ding, H. Chaté, P. Cvitanović, E. Siminos, and K. A. Takeuchi, "Estimating the dimension of the inertial manifold from unstable periodic orbits", Phys. Rev. Lett. **117**, 024101 (2016).

[34] M. S. Dresselhaus, G. Dresselhaus, and A. Jorio, *Group Theory: Application to the Physics of Condensed Matter* (Springer, New York, 2007).

[35] F. J. Dyson and H. Falk, "Period of a discrete cat mapping", Amer. Math. Monthly **99**, 603–614 (1992).

[36] B. Fernandez and P. Guiraud, "Route to chaotic synchronisation in coupled map lattices: Rigorous results", Discrete Continuous Dyn. Syst. Ser. B **4**, 435–456 (2004).

[37] B. Fernandez and M. Jiang, "Coupling two unimodal maps with simple kneading sequences", Ergod. Theor. Dynam. Syst. **24**, 107–125 (2004).

[38] A. L. Fetter and J. D. Walecka, *Theoretical Mechanics of Particles and Continua* (Dover, New York, 2003).

[39] S. Friedland, "On the entropy of $Z^d$ subshifts of finite type", Linear Algebra Appl. **252**, 199–220 (1997).

[40] I. García-Mata and M. Saraceno, "Spectral properties and classical decays in quantum open systems", Phys. Rev. E **69**, 056211 (2004).

[41] G. Giacomelli, S. Lepri, and A. Politi, "Statistical properties of bidimensional patterns generated from delayed and extended maps", Phys. Rev. E **51**, 3939–3944 (1995).

[42] J. F. Gibson and P. Cvitanović, Movies of plane Couette, tech. rep. (Georgia Inst. of Technology, 2015).

[43] J. F. Gibson, J. Halcrow, and P. Cvitanović, "Visualizing the geometry of state-space in plane Couette flow", J. Fluid Mech. **611**, 107–130 (2008).

[44] F. Ginelli, P. Poggi, A. Turchi, H. Chaté, R. Livi, and A. Politi, "Characterizing dynamics with covariant Lyapunov vectors", Phys. Rev. Lett. **99**, 130601 (2007).

[45] S. Grossmann and H. Fujisaka, "Diffusion in discrete nonlinear dynamical systems", Phys. Rev. A **26**, 1779–1782 (1982).

[46] B. Gutkin and V. Osipov, "Clustering of periodic orbits and ensembles of truncated unitary matrices", J. Stat. Phys. **153**, 1049–1064 (2013).

[47] B. Gutkin and V. Osipov, "Clustering of periodic orbits in chaotic systems", Nonlinearity **26**, 177 (2013).

[48] B. Gutkin and V. Osipov, "Classical foundations of many-particle quantum chaos", Nonlinearity **29**, 325–356 (2016).

[49] B. Gutkin, L. Han, R. Jafari, A. K. Saremi, and P. Cvitanović, Linear encoding of the spatiotemporal cat map, in preparation, 2018.

[50] J. H. Hannay and M. V. Berry, "Quantization of linear maps on a torus – Fresnel diffraction by a periodic grating", Physica D **1**, 267–290 (1980).

[51] M. Hochman and T. Meyerovitch, "A characterization of the entropies of multidimensional shifts of finite type", Ann. Math. **171**, 2011–2038 (2010).

[52] B. Hof, C. W. H. van Doorne, J. Westerweel, F. T. M. Nieuwstadt, H. Faisst, B. Eckhardt, H. Wedin, R. R. Kerswell, and F. Waleffe, "Experimental observation of nonlinear traveling waves in turbulent pipe flow", Science **305**, 1594–1598 (2004).

[53] W. G. Hoover and K. Aoki, "Order and chaos in the one-dimensional $\phi^4$ model : N-dependence and the Second Law of Thermodynamics", Commun. Nonlinear Sci. Numer. Simul. **49**, 192–201 (2017).

[54] W.-G. Hu and S.-S. Lin, "Nonemptiness problems of plane square tiling with two colors", Proc. Amer. Math. Soc. **139**, 1045–1059 (2011).

[55] W.-G. Hu and S.-S. Lin, "On spatial entropy of multi-dimensional symbolic dynamical systems", Discrete Continuous Dyn. Syst. Ser. A **36**, 3705–3717 (2016).

[56] W. Just, "Analytical approach for piecewise linear coupled map lattices", J. Stat. Phys. **90**, 727–748 (1998).

[57] W. Just, "Equilibrium phase transitions in coupled map lattices: A pedestrian approach", J. Stat. Phys. **105**, 133–142 (2001).

[58] K. Kaneko, "Transition from torus to chaos accompanied by frequency lockings with symmetry breaking: In connection with the coupled-logistic map", Prog. Theor. Phys. **69**, 1427–1442 (1983).

[59] K. Kaneko, "Period-doubling of kink-antikink patterns, quasiperiodicity in antiferro-like structures and spatial intermittency in coupled logistic lattice: Towards a prelude of a "field theory of chaos"", Prog. Theor. Phys. **72**, 480–486 (1984).

[60] H. Kantz and P. Grassberger, "Chaos in low-dimensional Hamiltonian maps", Phys. Let. A **123**, 437–443 (1987).

[61] J. P. Keating, "Asymptotic properties of the periodic orbits of the cat maps", Nonlinearity **4**, 277 (1991).

[62] J. P. Keating, "The cat maps: quantum mechanics and classical motion", Nonlinearity **4**, 309–341 (1991).

[63] J. P. Keating and F. Mezzadri, "Pseudo-symmetries of Anosov maps and spectral statistics", Nonlinearity **13**, 747–775 (2000).

[64] J. P. Keating, F. Mezzadri, and J. M. Robbins, "Quantum boundary conditions for torus maps", Nonlinearity **12**, 579 (1999).

[65] T. Kreilos and B. Eckhardt, "Periodic orbits near onset of chaos in plane Couette flow", Chaos **22**, 047505 (2012).

[66] P. Kurlberg and Z. Rudnick, "Hecke theory and equidistribution for the quantization of linear maps of the torus", Duke Math. J. **103**, 47–77 (2000).

[67] S. Lepri, A. Politi, and A. Torcini, "Chronotopic Lyapunov analysis. I. A detailed characterization of 1D systems", J. Stat. Phys. **82**, 1429–1452 (1996).

[68] S. Lepri, A. Politi, and A. Torcini, "Chronotopic Lyapunov analysis. II. Towards a unified approach", J. Stat. Phys. **88**, 31–45 (1997).

[69] A. J. Lichtenberg and M. A. Lieberman, *Regular and Chaotic Dynamics*, 2nd ed. (Springer, New York, 2013).

[70] J. Mallet-Paret and S. N. Chow, "Pattern formation and spatial chaos in lattice dynamical systems. I", IEEE Trans. Circuits Systems I Fund. Theory Appl. **42**, 746–751 (1995).

[71] J. Mallet-Paret and S. N. Chow, "Pattern formation and spatial chaos in lattice dynamical systems. II", IEEE Trans. Circuits Systems I Fund. Theory Appl. **42**, 752–756 (1995).

[72] P. A. Martin, "Discrete scattering theory: Green's function for a square lattice", Wave Motion **43**, 619–629 (2006).

[73] B. D. Mestel and I. Percival, "Newton method for highly unstable orbits", Physica D **24**, 172 (1987).

[74] F. Mezzadri, "On the multiplicativity of quantum cat maps", Nonlinearity **15**, 905–922 (2002).

[75] S. Müller, S. Heusler, P. Braun, F. Haake, and A. Altland, "Semiclassical foundation of universality in quantum chaos", Phys. Rev. Lett. **93**, 014103 (2004).

[76] I. Percival and F. Vivaldi, "A linear code for the sawtooth and cat maps", Physica D **27**, 373–386 (1987).

[77] I. Percival and F. Vivaldi, "Arithmetical properties of strongly chaotic motions", Physica D **25**, 105–130 (1987).

[78] Y. B. Pesin and Y. G. Sinai, "Space-time chaos in the system of weakly interacting hyperbolic systems", J. Geom. Phys. **5**, 483–492 (1988).

[79] S. D. Pethel, N. J. Corron, and E. Bollt, "Symbolic dynamics of coupled map lattices", Phys. Rev. Lett. **96**, 034105 (2006).

[80] S. D. Pethel, N. J. Corron, and E. Bollt, "Deconstructing spatiotemporal chaos using local symbolic dynamics", Phys. Rev. Lett. **99**, 214101 (2007).

[81] A. Politi and A. Torcini, "Towards a statistical mechanics of spatiotemporal chaos", Phys. Rev. Lett. **69**, 3421–3424 (1992).

[82] A. Politi, A. Torcini, and S. Lepri, "Lyapunov exponents from node-counting arguments", J. Phys. IV **8**, 263 (1998).

[83] A. N. Quas and P. B. Trow, "Subshifts of multi-dimensional shifts of finite type", Ergod. Theor. Dynam. Syst. **20**, 859–874 (2000).

[84] D. Ruelle, "A measure associated with Axiom-A attractors", Amer. J. Math. **98**, 619–654 (1976).

[85] M. Schell, S. Fraser, and R. Kapral, "Diffusive dynamics in systems with translational symmetry: A one–dimensional–map model", Phys. Rev. A **26**, 504–521 (1982).

[86] M. Sieber and K. Richter, "Correlations between periodic orbits and their rle in spectral statistics", Phys. Scr. **2001**, 128 (2001).

[87] Y. G. Sinai, "On the concept of entropy of a dynamical system", Dokl. Akad. Nauk. SSSR **124**, 768–771 (1959).

[88] J. Slipantschuk, O. F. Bandtlow, and W. Just, "Complete spectral data for analytic Anosov maps of the torus", Nonlinearity **30**, 2667 (2017).

[89] R. Sturman, J. M. Ottino, and S. Wiggins, *The Mathematical Foundations of Mixing* (Cambridge Univ. Press, 2006).

[90] T. Ward, "Automorphisms of $Z^d$-subshifts of finite type", Indag. Math. **5**, 495–504 (1994).

[91] A. P. Willis, P. Cvitanović, and M. Avila, "Revealing the state space of turbulent pipe flow by symmetry reduction", J. Fluid Mech. **721**, 514–540 (2013).

[92] A. Wirzba and P. Cvitanović, "Appendix: Discrete symmetries of dynamics", in *Chaos: Classical and Quantum* (Niels Bohr Inst., Copenhagen, 2016).

[93] Wolfram Research, Inc., *Mathematica 11* (2017).

[94] A. Zee, *Quantum Field Theory in a Nutshell*, 2nd ed. (Princeton Univ. Press, Princeton NJ, 2010).

## Appendix C. Inserts, varied temptations

B. Fernandez and P. Guiraud [36]
B. Fernandez and M. Jiang [37]
W. Just [56, 57]

the cat map is linear and the trivial trajectory located at the origin can be regarded as distinguished

## Appendix D. Symbolic dynamics: a glossary

**Predrag 2019-01-19** : This entire Appendix has been moved to the kittens paper [27] `siminos/kittens/symbolic.tex`.

## Appendix E. Nonlinearity journal tips

### *Appendix E.1. Naming your files*

Please name all your files, both figures and text, as follows:

- Use only characters from the set a to z, A to Z, 0 to 9 and underscore (_).
- Do not use spaces or punctuation characters in file names.
- Do not use any accented characters such as á, ê, ñ, ö.
- Include an extension to indicate the file type (e.g., `.tex`, `.eps`, `.txt`, etc).
- Use consistent upper and lower case in filenames and in your LaTeX file. If your LaTeX file contains the line `\includegraphics{fig1.eps}` the figure file must be called `fig1.eps` and not `Fig1.eps` or `fig1.EPS`. If you are on a Unix system, please ensure that there are no pairs of figures whose names differ only in capitalization, such as `fig_2a.eps` and `fig_2A.eps`, as Windows systems will be unable to keep the two files in the same directory.

### *Appendix E.2. Preparing your article*

Footnotes should be avoided whenever possible and can often be included in the text as phrases or sentences in parentheses. If required, they should be used only for brief notes that do not fit conveniently into the text. The use of displayed mathematics in footnotes should be avoided wherever possible and no equations within a footnote should be numbered. The standard LaTeX macro `\footnote` should be used. Note that in `iopart.cls` the `\footnote` command produces footnotes indexed by a variety of different symbols, whereas in published articles we use numbered footnotes. This is not a problem: we will convert symbol-indexed footnotes to numbered ones during the production process.

### *Appendix E.3. The abstract*

The abstract should be self-contained—there should be no references to figures, tables, equations, bibliographic references etc.

### *Appendix E.4. Some matters of style*

It will help the readers if your article is written in a clear, consistent and concise manner. During the production process we will try to make sure that your work is presented to its readers in the best possible way without sacrificing the individuality of your writing.

(i) We recommend using '-ize' spellings (diagonalize, renormalization, minimization, etc) but there are some common exceptions to this, for example: devise, promise and advise.
Do not include 'eq.', 'equation' etc before an equation number or 'ref.' 'reference' etc before a reference number.

*Appendix E.5. Two-line constructions*

For simple fractions in the text the solidus `/`, as in $\lambda/2\pi$, should be used instead of `\frac` or `\over`, using parentheses where necessary to avoid ambiguity, for example to distinguish between $1/(n-1)$ and $1/n-1$. Exceptions to this are the proper fractions $\frac{1}{2}$, $\frac{1}{3}$, $\frac{3}{4}$, etc, which are better left in this form. In displayed equations horizontal lines are preferable to solidi provided the equation is kept within a height of two lines. A two-line solidus should be avoided where possible; the construction $(\ldots)^{-1}$ should be used instead. For example use:

$$\frac{1}{M_{\mathrm{a}}}\left(\int_0^\infty \mathrm{d}\omega\,\frac{|S_o|^2}{N}\right)^{-1} \qquad \text{instead of} \qquad \frac{1}{M_{\mathrm{a}}}\Big/\int_0^\infty \mathrm{d}\omega\,\frac{|S_o|^2}{N}.$$

*Appendix E.6. Roman and italic in mathematics*

In mathematics mode there are some cases where it is preferable to use a Roman font; for instance, a Roman d for a differential d, a Roman e for an exponential e and a Roman i for the square root of $-1$. To accommodate this and to simplify the typing of equations, `iopart.cls` provides some extra definitions. `\rmd`, `\rme` and `\rmi` now give Roman d, e and i respectively for use in equations, e.g. $\mathrm{i}x\mathrm{e}^{2x}\mathrm{d}x/\mathrm{d}y$ is obtained by typing `$\rmi x\rme^{2x}\rmd x/\rmd y$`.

Certain other common mathematical functions, such as cos, sin, det and ker, should appear in Roman type. Standard LaTeX provides macros for most of these functions (in the cases above, `\cos`, `\sin`, `\det` and `\ker` respectively); `iopart.cls` also provides additional definitions for Tr, tr and O (`\Tr`, `\tr` and `\Or`, respectively).

Subscripts and superscripts should be in Roman type if they are labels rather than variables or characters that take values. For example in the equation

$$\epsilon_m = -g\mu_{\mathrm{n}}Bm$$

$m$, the $z$ component of the nuclear spin, is italic because it can have different values whereas n is Roman because it is a label meaning nuclear ($\mu_{\mathrm{n}}$ is the nuclear magneton).

*Appendix E.7. Special characters for mathematics*

Bold italic characters can be used in our journals to signify vectors (rather than using an upright bold or an over arrow). To obtain this effect when using `iopart.cls`, use `\bi{#1}` within maths mode, e.g. $\boldsymbol{ABCdef}$. Similarly, in `iopart.cls`, if upright bold characters are required in maths, use `\mathbf{#1}` within maths mode, e.g. $\mathbf{XYZabc}$. The calligraphic (script) uppercase alphabet is obtained with `\mathcal{AB}` or `\cal{CD}` ($\mathcal{ABCD}$).

The package `iopams.sty` uses the definition `\boldsymbol` in `amsbsy.sty` which allows individual non-alphabetical symbols and Greek letters to be made bold within equations. The bold Greek lowercase letters $\boldsymbol{\alpha}\ldots\boldsymbol{\omega}$,are obtained with the commands `\balpha` ... `\bomega` (but note that bold eta, $\boldsymbol{\eta}$, is `\bfeta` rather than `\beta`) and the capitals, $\boldsymbol{\Gamma}\ldots\boldsymbol{\Omega}$, with commands `\bGamma` ... `\bOmega`. Bold versions of the

**Table E1.** Other macros defined in `iopart.cls` for use in maths.

| Macro | Result | Description |
|---|---|---|
| `\fl` | | Start line of equation full left |
| `\case{#1}{#2}` | $\frac{\#1}{\#2}$ | Text style fraction in display |
| `\Tr` | Tr | Roman Tr (Trace) |
| `\tr` | tr | Roman tr (trace) |
| `\Or` | O | Roman O (of order of) |
| `\lshad` | $[\![$ | Text size left shadow bracket |
| `\rshad` | $]\!]$ | Text size right shadow bracket |

following symbols are predefined in `iopams.sty`: bold partial, $\boldsymbol{\partial}$, `\bpartial`, bold 'ell', $\boldsymbol{\ell}$, `\bell`, bold imath, $\boldsymbol{\imath}$, `\bimath`, bold jmath, $\boldsymbol{\jmath}$, `\bjmath`, bold infinity, $\boldsymbol{\infty}$, `\binfty`, bold nabla, $\boldsymbol{\nabla}$, `\bnabla`, bold centred dot, $\boldsymbol{\cdot}$, `\bdot`. Other characters are made bold using `\boldsymbol{\symbolname}`.

*Appendix E.8. Alignment of displayed equations*

The `iopart.cls` class file aligns left and indents each line of a display. To make any line start at the left margin of the page, add `\fl` at start of the line (to indicate full left).

Using the `eqnarray` environment equations will naturally be aligned left and indented without the use of any ampersands for alignment, see equations (E.1) and (E.2)

$$\alpha + \beta = \gamma^2, \tag{E.1}$$

$$\alpha^2 + 2\gamma + \cos\theta = \delta. \tag{E.2}$$

Where some secondary alignment is needed, for instance a second part of an equation on a second line, a single ampersand is added at the point of alignment in each line (see (E.3) and (E.4)).

$$\alpha = 2\gamma^2 + \cos\theta + \frac{XY\sin\theta}{X + Y\cos\theta} \tag{E.3}$$

$$= \delta\theta PQ\cos\gamma. \tag{E.4}$$

Two points of alignment are possible using two ampersands for alignment (see (E.5) and (E.6)). Note in this case extra space `\qquad` is added before the second ampersand in the longest line (the top one) to separate the condition from the equation.

$$\alpha = 2\gamma^2 + \cos\theta + \frac{XY\sin\theta}{X + Y\cos\theta} \qquad \theta > 1 \tag{E.5}$$

$$= \delta\theta PQ\cos\gamma \qquad \theta \leq 1. \tag{E.6}$$

For a long equation which has to be split over more than one line the first line should start at the left margin, this is achieved by inserting `\fl` (full left) at the start of

the line. The use of the alignment parameter `&` is not necessary unless some secondary alignment is needed.

$$\alpha + 2\gamma^2 = \cos\theta + \frac{XY\sin\theta}{X + Y\cos\theta} + \frac{XY\sin\theta}{X - Y\cos\theta} + + \left(\frac{XY\sin\theta}{X + Y\cos\theta}\right)^2 + \left(\frac{XY\sin\theta}{X - Y\cos\theta}\right)^2. \tag{E.7}$$

The plain TEX command `\eqalign` can be used within an `equation` environment to obtain a multiline equation with a single centred number, for example

$$\begin{aligned} &\alpha + \beta = \gamma^2 \\ &\alpha^2 + 2\gamma + \cos\theta = \delta. \end{aligned} \tag{E.8}$$

*Appendix E.9. Miscellaneous*

Exponential expressions, especially those containing subscripts or superscripts, are clearer if the notation exp(...) is used, except for simple examples. For instance $\exp[\mathrm{i}(kx - \omega t)]$ and $\exp(z^2)$ are preferred to $\mathrm{e}^{\mathrm{i}(kx-\omega t)}$ and $\mathrm{e}^{z^2}$, but $\mathrm{e}^x$ is acceptable.

The square root sign $\sqrt{}$ should only be used with relatively simple expressions, e.g. $\sqrt{2}$ and $\sqrt{a^2 + b^2}$; in other cases the power 1/2 should be used; for example, $[(x^2 + y^2)/xy(x - y)]^{1/2}$.

It is important to distinguish between $\ln = \log_\mathrm{e}$ and $\lg = \log_{10}$. Braces, brackets and parentheses should be used in the following order: $\{[(\,)]\}$.

Decimal fractions should always be preceded by a zero: for example 0.123 **not** .123. For long numbers use thin spaces after every third character away from the position of the decimal point, unless this leaves a single separated character: e.g. 60 000, 0.123 456 78 but 4321 and 0.7325.

Equations should be followed by a full stop (periods) when at the end of a sentence.

*Appendix E.10. Equation numbering and layout in* `iopart.cls`

If the command `\eqnobysec` is included in the preamble, equation numbering by section is obtained, e.g. (2.1), (2.2), etc. Refer to equations in the text using the equation number in parentheses. It is not normally necessary to include the word equation before the number; and abbreviations such as eqn or eq should not be used. In `iopart.cls`, there are alternatives to the standard `\ref` command that you might find useful—see table E2.

Sometimes it is useful to number equations as parts of the same basic equation. This can be accomplished in `iopart.cls` by inserting the commands `\numparts` before the equations concerned and `\endnumparts` when reverting to the normal sequential numbering. For example using `\numparts \begin{eqnarray} ... \end{eqnarray} \endnumparts`:

$$T_{11} = (1 + P_\mathrm{e})I_{\uparrow\uparrow} - (1 - P_\mathrm{e})I_{\uparrow\downarrow}, \tag{5.9$a$}$$

$$T_{-1-1} = (1 + P_e)I_{\downarrow\downarrow} - (1 - P_e)I_{\uparrow\downarrow}, \tag{5.9b}$$
$$S_{11} \quad = (3 + P_e)I_{\downarrow\uparrow} - (3 - P_e)I_{\uparrow\uparrow}, \tag{5.9c}$$
$$S_{-1-1} = (3 + P_e)I_{\uparrow\downarrow} - (3 - P_e)I_{\downarrow\downarrow}. \tag{5.9d}$$

Equation labels within the `\eqnarray` environment will be referenced as subequations, e.g. (5.9*a*).

### *Appendix E.11. Miscellaneous extra commands for displayed equations*

The `\cases` command has been amended slightly in `iopart.cls` to increase the space between the equation and the condition. Equation (5.10) demonstrates simply the output from the `\cases` command

$$X = \begin{cases} 1 & \text{for } x \geq 0 \\ -1 & \text{for } x < 0 \end{cases} \tag{5.10}$$

To obtain text style fractions within displayed maths the command `\case{#1}{#2}` can be used instead of the usual `\frac{#1}{#2}` command or `{#1 \over #2}`.

When two or more short equations are on the same line they should be separated by a 'qquad space' (`\qquad`), rather than `\quad` or any combination of `\,`, `\>`, `\;` and `\ `.

### *Appendix E.12. Preprint references*

Preprints may be referenced but if the article concerned has been published in a peer-reviewed journal, that reference should take precedence. If only a preprint reference can be given, it is helpful to include the article title. Examples are:

[1] Neilson D and Choptuik M 2000 *Class. Quantum Grav.* **17** 761 (arXiv:gr-qc/9812053)
[2] Sundu H, Azizi K, Süngü J Y and Yinelek N 2013 Properties of $D^*_{s2}(2573)$ charmed-strange tensor meson arXiv:1307.6058

### *Appendix E.13. Cross-referencing*

`label` may contain letters, numbers or punctuation characters but must not contain spaces or commas. It is also recommended that the underscore character `_` is not used in cross referencing.

Thus labels of the form `eq:partial`, `fig:run1`, `eq:dy'`, etc, may be used. When several references occur together in the text `\cite` may be used with multiple labels with commas but no spaces separating them; the output will be the numbers within a single pair of square brackets with a comma and a thin space separating the numbers. Thus `\cite{label1,label2,label4}` would give [1, 2, 4]. Note that no attempt is made by the style file to sort the labels and no shortening of groups of consecutive numbers is done. Authors should therefore either try to use multiple labels in the correct order, or use a package such as `cite.sty` that reorders labels correctly.

**Table E2.** Alternatives to the normal references command `\ref` available in `iopart.cls`, and the text generated by them. Note it is not normally necessary to include the word equation before an equation number except where the number starts a sentence. The versions producing an initial capital should only be used at the start of sentences.

| Reference | Text produced |
|---|---|
| `\eref{<label>}` | (`<num>`) |
| `\Eref{<label>}` | Equation (`<num>`) |
| `\fref{<label>}` | figure `<num>` |
| `\Fref{<label>}` | Figure `<num>` |
| `\sref{<label>}` | section `<num>` |
| `\Sref{<label>}` | Section `<num>` |
| `\tref{<label>}` | table `<num>` |
| `\Tref{<label>}` | Table `<num>` |

*Appendix E.14. Tables and table captions*

Tables are numbered serially and referred to in the text by number (table 1, etc, **not** tab. 1). Each table should have an explanatory caption which should be as concise as possible. If a table is divided into parts these should be labelled (*a*), (*b*), (*c*), etc but there should be only one caption for the whole table, not separate ones for each part.

The standard form for a table in `iopart.cls` is:

```
\begin{table}
\caption{\label{label}Table caption.}
\begin{indented}
\item[]\begin{tabular}{@{}llll}
\br
Head 1&Head 2&Head 3&Head 4\\
\mr
1.1&1.2&1.3&1.4\\
2.1&2.2&2.3&2.4\\
\br
\end{tabular}
\end{indented}
\end{table}
```

(i) The caption comes before the table. It should have a period at the end.

(ii) Tables are normally set in a smaller type than the text. The normal style is for tables to be indented. This is accomplished by using `\begin{indented}` ... `\end{indented}` and putting `\item[]` before the start of the tabular environment. Omit these commands for any tables which will not fit on the page when indented.

(iii) The default is for columns to be aligned left and adding `@{}` omits the extra space before the first column.

(iv) Tables have only horizontal rules and no vertical ones. The rules at the top and bottom are thicker than internal rules and are set with `\br` (bold rule). The rule

**Table E3.** A simple example produced using the standard table commands and `\lineup` to assist in aligning columns on the decimal point. The width of the table and rules is set automatically by the preamble.

| *A* | *B* | *C* | *D* | *E* | *F* | *G* |
|---|---|---|---|---|---|---|
| 23.5 | 60 | 0.53 | −20.2 | −0.22 | 1.7 | 14.5 |
| 39.7 | −60 | 0.74 | −51.9 | −0.208 | 47.2 | 146 |
| 123.7 | 0 | 0.75 | −57.2 | — | — | — |
| 3241.56 | 60 | 0.60 | −48.1 | −0.29 | 41 | 15 |

separating the headings from the entries is set with `\mr` (medium rule). These are special `iopart.cls` commands.

(v) Numbers in columns should be aligned on the decimal point; to help do this a control sequence `\lineup` has been defined in `iopart.cls` which sets `\0` equal to a space the size of a digit, `\m` to be a space the width of a minus sign, and `\-` to be a left overlapping minus sign. `\-` is for use in text mode while the other two commands may be used in maths or text. (`\lineup` should only be used within a table environment after the caption so that `\-` has its normal meaning elsewhere.) See table E3 for an example of a table where `\lineup` has been used.

*Appendix E.15. Simplified coding and extra features for tables*

The basic coding format can be simplified using extra commands provided in the `iopart` class file. The commands up to and including the start of the tabular environment can be replaced by

```
\Table{\label{label}Table caption}
```

and this also activates the definitions within `\lineup`. The final three lines can also be reduced to `\endTable` or `\endtab`. Similarly for a table which does not fit on the page when indented `\fulltable{\label{label}caption}` ... `\endfulltable` can be used. LaTeX optional positional parameters can, if desired, be added after `\Table{\label{label}caption}` and `\fulltable{\label{label}caption}`.

`\centre{#1}{#2}` can be used to centre a heading `#2` over `#1` columns and `\crule{#1}` puts a rule across `#1` columns. A negative space `\ns` is usually useful to reduce the space between a centred heading and a centred rule. `\ns` should occur immediately after the `\\` of the row containing the centred heading (see code for table E4). A small space can be inserted between rows of the table with `\ms` and a half line space with `\bs` (both must follow a `\\` but should not have a `\\` following them).

Units should not normally be given within the body of a table but given in brackets following the column heading; however, they can be included in the caption for long column headings or complicated units. Where possible tables should not be broken over pages. If a table has related notes these should appear directly below

**Table E4.** A table with headings spanning two columns and containing notes. To improve the visual effect a negative skip (\ns) has been put in between the lines of the headings. Commands set-up by \lineup are used to aid alignment in columns. \lineup is defined within the \Table definition.

| Nucleus | Thickness ($mg\,cm^{-2}$) | Composition | Separation energies | |
|---|---|---|---|---|
| | | | $\gamma$, n (MeV) | $\gamma$, 2n (MeV) |
| $^{181}$Ta | $19.3 \pm 0.1$[a] | Natural | 7.6 | 14.2 |
| $^{208}$Pb | $3.8 \pm 0.8$[b] | 99% enriched | 7.4 | 14.1 |
| $^{209}$Bi | $2.86 \pm 0.01$[b] | Natural | 7.5 | 14.4 |

[a] Self-supporting.
[b] Deposited over Al backing.

the table rather than at the bottom of the page. Notes can be designated with footnote symbols (preferable when there are only a few notes) or superscripted small roman letters. The notes are set to the same width as the table and in normal tables follow after `\end{tabular}`, each note preceded by `\item[]`. For a full width table `\noindent` should precede the note rather than `\item[]`. To simplify the coding `\tabnotes` can, if desired, replace `\end{tabular}` and `\endtabnotes` replaces `\end{indented}\end{table}`.

### *Appendix E.16. Inclusion of graphics files*

Below each figure should be a brief caption describing it and, if necessary, interpreting the various lines and symbols on the figure. As much lettering as possible should be removed from the figure itself and included in the caption. If a figure has parts, these should be labelled (*a*), (*b*), (*c*), etc and all parts should be described within a single caption. Table E5 gives the definitions for describing symbols and lines often used within figure captions (more symbols are available when using the optional packages loading the AMS extension fonts).

### *Appendix E.17. Supplementary Data*

Supplementary data enhancements typically consist of video clips, animations or data files, tables of extra information or extra figures. See guidelines on supplementary data file formats, 'Author Guidelines' link at `http://authors.iop.org`.

Software, in the form of input scripts for mathematical packages (such as Mathematica notebook files), or source code that can be interpreted or compiled (such as Python scripts or Fortran or C programs), or executable files, can sometimes be accepted as supplementary data, but the journal may ask you for assurances about the software and distribute them from the article web page only subject to a disclaimer. Contact the journal in the first instance if you want to submit software.

**Table E5.** Control sequences to describe lines and symbols in figure captions.

| Control sequence | Output | Control sequence | Output |
|---|---|---|---|
| `\dotted` | ····· | `\opencircle` | ○ |
| `\dashed` | - - - - | `\opentriangle` | △ |
| `\broken` | – – – | `\opentriangledown` | ▽ |
| `\longbroken` | — — — | `\fullsquare` | ■ |
| `\chain` | — · — | `\opensquare` | □ |
| `\dashddot` | — · · — | `\fullcircle` | ● |
| `\full` | ——— | `\opendiamond` | ◊ |

**Table E6.** Macros defined within `iopart.cls` for use with figures and tables.

| Macro name | Purpose |
|---|---|
| `\Figures` | Heading for list of figure captions |
| `\Figure{#1}` | Figure caption |
| `\Tables` | Heading for tables and table captions |
| `\Table{#1}` | Table caption |
| `\fulltable{#1}` | Table caption for full width table |
| `\endTable` | End of table created with `\Table` |
| `\endfulltab` | End of table created with `\fulltable` |
| `\endtab` | End of table |
| `\br` | Bold rule for tables |
| `\mr` | Medium rule for tables |
| `\ns` | Small negative space for use in table |
| `\centre{#1}{#2}` | Centre heading over columns |
| `\crule{#1}` | Centre rule over columns |
| `\lineup` | Set macros for alignment in columns |
| `\m` | Space equal to width of minus sign |
| `\-` | Left overhanging minus sign |
| `\0` | Space equal to width of a digit |

## Appendix F. Cats' GHJSC16blog

Internal discussions of [49] edits: Move good text not used in [49] to this file, for possible reuse later.

**2016-11-18 Predrag** A theory of turbulence that has done away with *dynamics*? We rest our case.

**2016-10-05 Predrag** My approach is that this is written for field theorists, fluid dynamicists etc., who do not see any reason to look at cat maps, so I am trying to be pedagogical, motivate it as that chaotic counterpart of the harmonic oscillator, something that field theorists fell comfortable with (they should not, but they do).

**2016-11-13 Predrag** The next thing to rethink: Green's functions for periodic lattices are in ChaosBook sections D.3 Lattice derivatives and on, for the Hermitian Laplacian and $s = 2$. For real $s > 2$ cat map, the potential is inverted harmonic oscillator, the frequency is imaginary (Schrödinger in imaginary time), eigenvectors real - should be a straightforward generalization. Have done this already while studying Ornstein-Uhlenbeck with Lippolis and Henninger - the eigenfunctions are Hermite polynomials times Gaussians.

**2016-11-13 Predrag** The claim "the cat map $A = \begin{pmatrix} a & c \\ d & b \end{pmatrix}$ is assumed to be time-reversal invariant, i.e. $c = d$." seems to be in conflict with Boris choice $A = \begin{pmatrix} s-1 & 1 \\ s-2 & 1 \end{pmatrix}$
We write (16) as

$$(\Box + 2 - s)x_t = m_t \,, \tag{6.1}$$

Percival and Vivaldi [76] write their Eq. (3.6)

$$(\Box + 2 - s)x_t = -b_t \tag{6.2}$$

so their "stabilising impulses" $b_t$ (defined on interval $x \in [-1/2, 1/2)$) have the opposite sign to our "winding numbers" $m_t$ (defined on $x \in [0, 1)$).
Did not replace Arnol'd by PerViv choice.

$$A = \begin{pmatrix} 0 & 1 \\ -1 & s \end{pmatrix} \,, \tag{6.3}$$

$$\begin{aligned} x_{t+1} &= p_t \mod 1 \\ p_{t+1} &= -x_t + s\,p_t \mod 1 \end{aligned} \tag{6.4}$$

Predrag's formula, removed by Boris 2017-01-15:

$$\begin{aligned} x_{t+1} &= (s-1)\,x_t + p_t \\ p_{t+1} &= (s-2)\,x_t + p_t \end{aligned} \mod 1 \,, \tag{6.5}$$

Predrag's formula, removed by Boris 2017-01-15:
As the 3-point discretization of the second time derivative $d^2/dt^2$ (central difference operator) is $\Box\, x_t \equiv x_{t+1} - 2x_t + x_{t-1}$ (with the time step set to $\Delta t = 1$), the *temporal* cat map (1) can be rewritten as the discrete time Newton equation for inverted harmonic potential,

$$(\Box + 2 - s)\, x_t = m_t\,. \tag{6.6}$$

Predrag's formula, replaced by a more abstract form by Boris 2017-01-15:
a $d$-dimensional spatiotemporal pattern $\{x_z\} = \{x_{n_1 n_2 \cdots n_d}\}$ requires *$d$-dimensional* spatiotemporal block $\{m_z\} = \{m_{n_1 n_2 \cdots n_d}\}$,
for definiteness written as

$$A = \begin{pmatrix} 2 & 1 \\ 1 & 1 \end{pmatrix}\,, \tag{6.7}$$

**2016-08-20 Predrag** " The fact that even Dyson [35] counts cat map periods should give us pause - clearly, some nontrivial number theory is afoot. "
Not sure whether this is related to cat map symbolic dynamics that we use, dropped for now: " Problems with the discretization of Arnol'd cat map were pointed out in [14, 15]. [14] discusses two partitions of the cat map unit square. "
" and resist the siren song of the Hecke operators [66, 74] "

While stability multipliers depend only on the trace $s$, the state space eigenvectors depend on the explicit matrix $A$, and so do "winding numbers" $m_t$ (which also depend on the defining interval $x \in [-1/2, 1/2)$, Percival and Predrag choice, or Boris choice $x \in [0, 1)$. Time-reversed has different eigenvectors (orthogonal to the forward-time ones), so I am not even sure how time reversed $m_t$ look.

**2016-05-21 Predrag** Behrends [11, 12] *The ghosts of the cat* is fun - he uncovers various regular patterns in the iterates of the cat map.

**2016-09-27 Boris Cat maps and spatiotemporal cats**
In the spatiotemporal cat, "particles" (i.e., a cat map at each periodic lattice site) are coupled by the next-neighbor coupling rules:

$$q_{n,t+1} = p_{n,t} + (s-1)q_{n,t} - q_{n+1,t} - q_{n-1,t} - m^q_{n,t+1}$$

$$p_{n,t+1} = p_{n,t} + (s-2)q_{n,t} - q_{n+1,t} - q_{n-1,t} - m^p_{n,t+1}$$

The symbols of interest can be found by:

$$m_{n,t} = q_{n,t+1} + q_{n,t-1} + q_{n+1,t} + q_{n-1,t} - s\, q_{n,t}\,.$$

**2016-10-27 Boris** Gutkin and Osipov [48] write: "In general, calculating periodic orbits of a non-integrable system is a non-trivial task. To this end a number of methods have been developed," and then, for a mysterious reasons, they refer to [10].

**2016-10-27 Boris** Added to section 5 the following references: M. Sieber and K. Richter [86], S. Müller, S. Heusler, P. Braun, F. Haake and A. Altland [75], B. Gutkin, V.Al. Osipov [47], B. Gutkin, V.Al. Osipov [46] (Predrag added [48] as well).

**2016-11-07 Predrag** The dynamical systems literature tends to focus on *local* problems: bifurcations of a single time-invariant solution (equilibrium, relative equilibrium, periodic orbit or relative periodic orbit) in low-dimensional settings (3-5 coupled ODEs, 1-dimensional PDE). The problem that we face is *global*: organizing and relating *simultaneously* infinities of unstable relative periodic orbits in $\infty$-dimensional state spaces, orbits that are presumed to form the skeleton of turbulence (see [42] for a gentle introduction) and are typically not solutions that possess the symmetries of the problem. In this quest we found the standard equivariant bifurcation theory literature not very helpful, as its general focus is on bifurcations of solutions, which admit all or some of the symmetries of the problem at hand.

**2016-11-17 Predrag** a simple generalization of a Bernoulli map to a Hamiltonian setting
finite grammars whenever all partition borders map onto partition borders.
If one neglects the width of the stretched-out area, get sawtooth maps, with infinity of finite grammars.

Adler and Weiss [1] discovered that certain mappings from the torus to itself, called hyperbolic toral automorphisms have Markov partitions, and in fact these partitions are parallelograms. One famous example is the Arnol'd Cat Map
(Axiom A; Anosov)
are a family of analytic hyperbolic automorphisms of the two-dimensional torus which
The "linear code" was introduced and worked out in detail in influential papers of Percival and Vivaldi [13, 76, 77].
For $d = 1$ lattice, $s = 5$ the spatial period 1 fixed point is equivalent to the usual $s = 3$ Arnol'd cat map.
The cat map partitions the state space into $|\mathcal{A}|$ regions, with borders defined by the condition that the two adjacent labels $k, k+1$ simultaneously satisfy (16),

$$x_1 - sx_0 + x_{-1} - \epsilon = k\,, \tag{6.8}$$

$$x_1 - sx_0 + x_{-1} + \epsilon = k+1\,, \tag{6.9}$$

$$x_2 - sx_1 + x_0 = m_1\,, \tag{6.10}$$

$$x_1 - sx_0 + x_{-1} = m_0\,, \tag{6.11}$$

$$(x_0, x_1) = (0,0) \to (0,0)\,, \quad (1,0) \to (0,-1)\,, \quad (0,1) \to (1,s)\,, \quad (1,1) \to (1,s-1)$$

**2016-11-05 Predrag** Dropped this:

Note the two symmetries of the dynamics [61]: The calculations generalize directly to any cat map invariant under time reversal [63].

**2016-11-11 Boris "Deeper insight" into $d = 2$ symbolic dynamics** Information comes locally (both in space and time). Allows to understand correlations between invariant 2-tori. Connection with field theories.

To Predrag: we have similar results on $2 \times 1$ blocks, but I think $1 \times 1$, $2 \times 2$ is enough. Agree?

**2016-12-08 Predrag**: I agree

**2016-12-06 Boris** Confused about Predrag's claim that [23, 43] tile " spatially and temporally infinite domains"(?) In both papers the spatial extension of the system is finite, and the attractors have relatively small dimensions.

**2016-12-08 Predrag**: I rewrote that now, is it clearer?

**2016-12-06 Boris** Is this clai true: "Temporally chaotic systems are exponentially unstable with time: double the time, and roughly twice as many periodic orbits are required to describe it to the same accuracy. For large spatial extents, the complexity of the spatial shapes also needs to be taken into account. A spatiotemporally chaotic system is *extensive* in the sense that ..." Double the time and the number of periodic orbits is squared?

**2016-12-08 Predrag**: It is true only for discrete time, complete binary dynamics, but any other statement brings in more confusing words. I do not want to say "entropy" here. I rewrote it now.

**2016-12-06 Boris** Predrag's statement "Essentially, as the stretching is uniform, distinct admissible symbol patterns count all patterns of a given size, and that can be accomplished by construction the appropriate finite size transition matrices [25]." is true only for symbolic dynamics based on Markov partitions. Wrong e.g., for linear coding.

**2016-12-08 Predrag**: I rewrote that now, is it correct?

**2016-12-12 Predrag** My claim (in a conversation with Boris) that spatiotemporal cat symbolic dynamics is "$d$-dimensional" was nonsensical. I have now removed this from the draft: " The key innovation of [48] is the realization (an insight that applies to all coupled-map lattices, and all PDEs modeled by them, not only the system considered here) that $d$-dimensional spatiotemporal orbit $\{x_z\}$ requires $d$-*dimensional* symbolic dynamics code $\{m_z\} = \{(m_1, m_2, \cdots, m_d)\}$, rather than a *single* temporal symbol sequence (as one is tempted to do when describing a finite coupled $N^{d-1}$-"particle" system)."

Li Han text: " To generate such state space partitions, we start with length $\ell = 1$. Consider first the symbol $m_0 = sx_0 - (x_1 + x_{-1}) = \lfloor sx_0 - x_1 \rfloor$, where $\lfloor \cdots \rfloor$ is the floor function. $m_0$ has symbol boundaries which are equally spaced parallel lines of slope $s$ and passing through $(x_0, x_1) = (0, 0), (1, 1)$. We then look at the time-evolved images of these symbol regions under forward map (18). The transformed

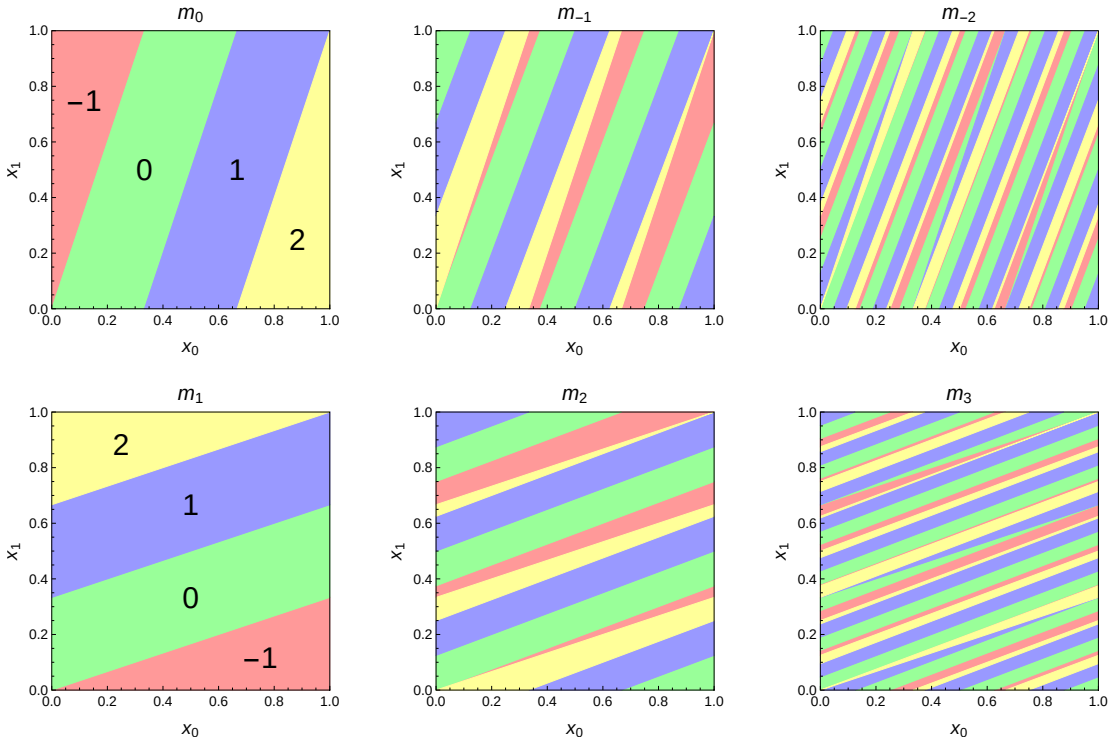


**Figure F1.** (Color online) Newtonian Arnol'd cat map $(x_0, x_1)$ state space partition into (a) 4 regions labeled by $m_0$. , obtained from $(x_{-1}, x_0)$ state space by one iteration (the same as figure 1). (b) 14 regions labeled by past block $m_{-1}m_0$. , obtained from $(x_{-2}, x_{-1})$ state space by two iterations. (c) 44 regions, past block $m_{-2}m_{-1}m_0$. (d) 4 regions labeled by $.m_1$ , obtained from $(x_2, x_1)$ state space by one backward iteration. (e) 14 regions labeled by future block $.m_1m_2$ , obtained from $(x_3, x_2)$ state space by two backward iterations. (f) 44 regions, future block $m_3m_2m_1$. Each color has the same total area (1/6 for $m_t = \underline{1}, 2$, and 1/3 for $m_t = 0, 1$). All boundaries are straight lines with rational slopes.

region therefore means that at coordinate $(x_{t+1}, Fx_{t+2})$ the point has symbol $m_t$, which in turn implies that when interpreted back to $(x_0, x_1)$ state space, a point is associated with symbol $m_{-1}$. As a result, we can generate all length-1 state spaces corresponding to symbols $m_t$, $t = 0, \pm1, \pm2, \cdots$ on the $(x_0, x_1)$ state space simply by applying the forward map (18) or its inverse. We plot such length-1 diagrams in figure 2 for symbols $m_0, m_{-1}, m_{-2}$ (top), and $m_1, m_2, m_3$ (bottom), and call them different blocks. Note that any of the blocks can be used to recover the 1-symbol measure $f_1(m)$ by calculating the total of respective region areas, while with blocks $m_0 = \lfloor sx_0 - x_1 \rfloor$ and $m_1 = \lfloor sx_1 - x_0 \rfloor$ the computations are the easiest, which have symbol boundaries of slopes $s$ and $1/s$ respectively.

The fact that $\mu(m \in \mathcal{A}_0)$ are all equal and twice of $\mu(m \in \mathcal{A}_1)$ is also obvious from the $m_0, m_1$ blocks of length-1 state spaces.

A length-$\ell$ state space is then the superposition of any $\ell$ consecutive blocks of length-1 diagrams, while a choice that is symmetric about block $m_0$ or $m_0$ and $m_1$ will make the amount of calculations minimal. We have evaluated $\mu(m)$ up to $\ell = 12$

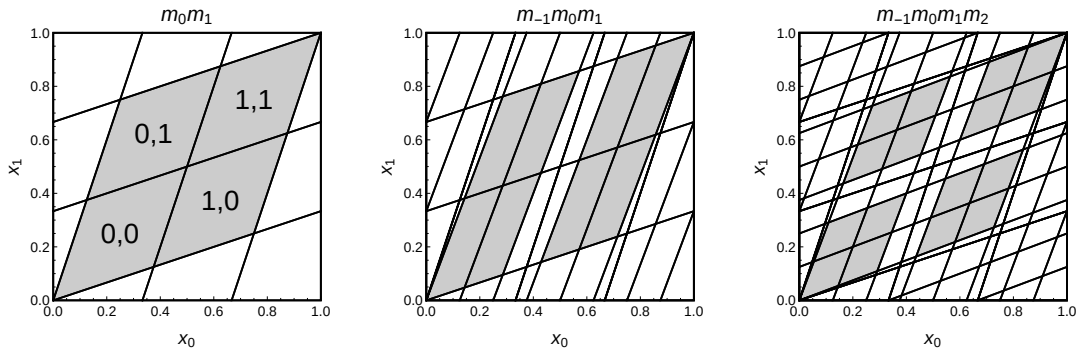


**Figure F2.** Newtonian Arnol'd cat map $(x_0, x_1)$ state space partition into (a) 14 regions labeled by block $b = m_0.m_1$, the intersection of one past (figure F1 (a)) and one future iteration (figure F1 (d)). (b) block $b = m_{-1}m_0.m_1$, the intersection of two past (figure F1 (b)) and one future iteration (figure F1 (d)). (c) block $b = m_{-1}m_0.m_1m_2$, the intersection of two past (figure F1 (b)) and two future iterations (figure F1 (e)). Note that while some regions involving external alphabet (such as _22_ in (a)) are pruned, the interior alphabet labels a horseshoe, indicated by the shaded regions. Their total area is (a) $4 \times 1/8$, (b) $8 \times 1/21$, and (c) $16 \times 1/55$.

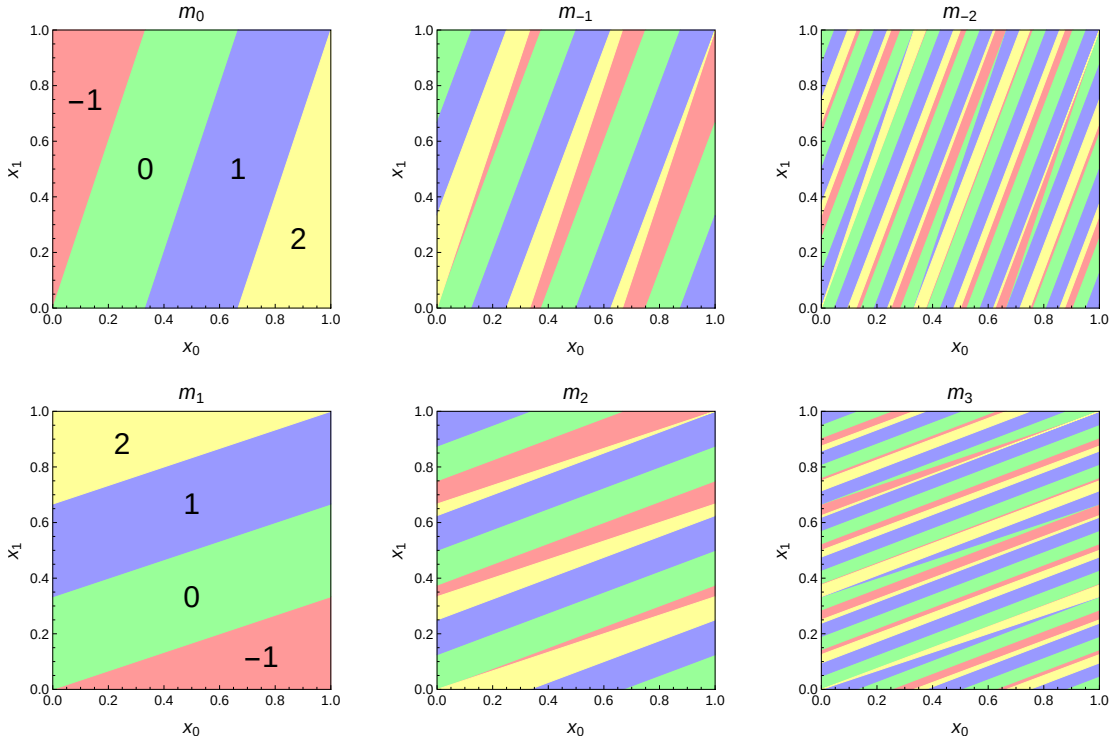


**Figure F3.** (Color online) $\ell = 1$ state spaces on $(x_0, x_1)$ state space with respect to symbols $m_t$, $t = 0, -1, -2, 1, 2, 3$ for $s = 3$. In each block values of $m_t = -1, 0, 1, 2$ are shaded with light red, green, blue, and yellow, respectively, and each color has the same total area (1/6 for $m_t = -1, 2$, 1/3 for $m_t = 0, 1$) in all blocks. All boundary lines are straight lines with rational slopes, while the slopes tend to irrational values set by stable/unstable directions of the cat map exponentially fast in the limit $t \to \pm\infty$.

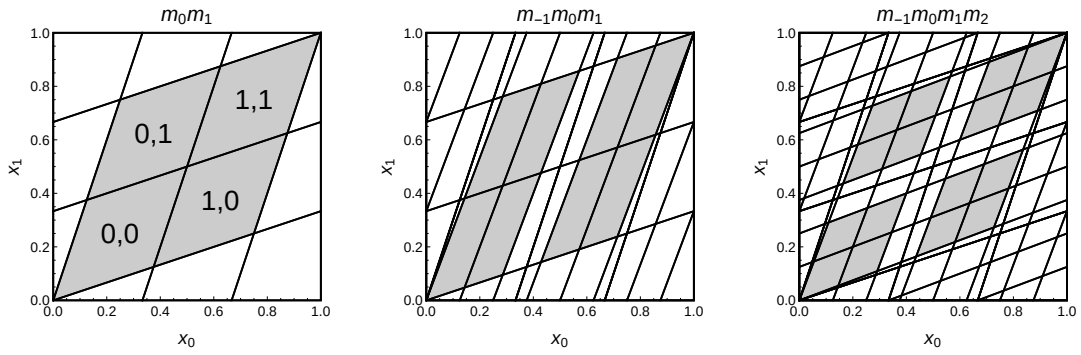


**Figure F4.** $\ell = 2, 3, 4$ state spaces on $(x_0, x_1)$ state space for $s = 3$, using blocks $m_0m_1$, $m_{-1}m_0m_1$, and $m_{-1}m_0m_1m_2$ from the $\ell = 1$ diagrams. Shaded diamonds or rectangles correspond to sequences of all interior symbols $(0, 1)^{\otimes\ell}$, having a total area of $4 \times 1/8$, $8 \times 1/21$, $16 \times 1/55$ respectively from left to right.

from both (29) and symbolic diagrams for $s = 3, 4, 5$, and they are consistent. In figure 2 we plot the symbolic diagrams for 2, 3, and 4 consecutive symbols using blocks $m_{0,1}$, $m_{-1,0,1}$, and $m_{-1,0,1,2}$ of figure 2. Sequences of all interior symbols correspond to congruent parallelogram regions whose opposite sides are exactly parallel, and for even $\ell$ the regions are diamonds whose sides are of equal length. Sequences of symbols from both $\mathcal{A}_0$ and $\mathcal{A}_1$ are not all admissible, which is the topic of next section. Here we note that the corresponding regions of such sequences have general polygon shapes and are not parallelograms, no matter which consecutive set of blocks we use.

All boundary lines are straight lines with rational slopes, while the slopes tend to irrational values set by stable/unstable directions of the cat map exponentially fast in the limit $t \to \pm\infty$.

From (29) the measure $\mu(b)$ for a block $b = m_1m_2 \cdots m_\ell$ is proportional to the area of the polygon defined by inequalities (27).

The full list of measures $\mu(m_1m_2 \cdots m_\ell)$ has a tensor structure of tensor rank $\ell$ with each index running over $\mathcal{A}$ and can be interpreted as a joint probability function.
"

Boris results.tex text: " whose lower left corner is the $(n, t)$ lattice site

$$\mathcal{R}_{n,t} = \{(n + i, t + j)|i = 0, \ldots, \ell_1 - 1, j = 0, \ldots, \ell_2 - 2\}\,,$$

It is straightforward to see that when $\mathsf{M}$ is such that all symbols $m_z$ belong to $\mathcal{A}_0 = \{0, \ldots, s - 4\}$ then $\mathsf{M}$ is always admissible. By positivity of Green's function (see Appendix A) it follows immediately that $0 < x_z$ while the condition $\sum_{z' \in \mathbb{Z}} \mathsf{g}_{zz'} = s - 2$ implies that $x_z \leq 1$.
"

Predrag text, recycle: " Here the piecewise linearity of the spatiotemporal cat enables us to go far analytically. Essentially, as the cat map stretching is uniform, distinct admissible symbol blocks count all blocks of a given shape (they all have the

same stability, and thus the same dynamical weight), and that can be accomplished by linear, Green's function methods. "

Predrag removed Boris poetry: " The alphabet separation into interior and external parts nicely illustrates the transition of the model from the correlated regime to the uncorrelated Bernoulli process as parameter $s$ in (4) tends to $\infty$. Indeed, the number of external symbols in $\mathcal{A}_1$ is fixed within a given differential operator $\Box$ structure, while the number of interior symbols in $\mathcal{A}_0$ grows linearly with the parameter $s$ controlling the strength of chaos in a single map. For single cat map this transition can be achieved by merely increasing the time step of time evolution. Increasing the time step from 1 to 2 leaves the form of equation (16) intact, but renormalizes the constant $s \to s^2-1$. This reflects the fact that $\phi^2$ is more "chaotic" than $\phi$. With an increase of $k$ the map $\phi^k$ resembles more and more uncorrelated Bernoulli process. Similar transition can be observed in the coupled $\mathbb{Z}$ map lattices, with a caveat that switch from $\Phi$ to $\Phi^k$ renormalizes not only the constant $s$, but $\Box$ itself. The resulting equation of motion will contain an elliptic operator $\Box^{(k)}$ of higher order. Still, it is straightforward to see that the number of external symbols is controlled by the order of the operator $\Box^{(k)}$ which grows linearly with $k$. On the other hand, the number of interior symbols grows in the same way as the constant $s$ i.e., exponentially. "

Replaced $N$ (for $N$ "particles") by $L$ (for spatial extent) throughout

**2016-11-20 Boris** The spatiotemporal symbols follow from the Newtonian equations in $d$ spatiotemporal dimensions

$$\begin{aligned} m_{n,j} &= (q_{n,j+1} - 2q_{n,j} + q_{n,j-1}) + (q_{n+1,j} - 2q_{n,j} + q_{n-1,j}) - (s-4)q_{n,j} \\ m &= [\Box + 2d1 - s1]\, q\,. \end{aligned} \tag{6.12}$$

**2017-01-03 Predrag** I changed the sign of $m_{n,t}$ in (36), as in (4), do all cats approve?

**2017-07-31 Boris** Changed it back. Our present convention is the opposite one!

**2017-02-16 Predrag** To me, the Green's functions look strictly positive. Must harmonize definitions (A.1), (A.2), (A.4), (4) and (16), originating in Boris' flip-flop $m_t \to -m_t$

Is there a reference to Green's functions in terms of Chebyshevs?

**2017-08-02 Boris** Yes, and it is OK with our present convention - Green's functions must be positive.

**2017-07-31 Boris** "As every Anosov automorphism is topologically conjugate to a linear cat map ..." Is it really true ?

**2017-08-11 Predrag** That's what I read in some of the articles cited. But no need to say it here, so now this is removed from our article.

**2016-11-13 Predrag** to all cats - where we write (16), Percival and Vivaldi [76] write their Eq. (3.6) $(\Box + 2 - s)x_t = -b_t$ so their "stabilising impulses" $b_t$ have the opposite sign to our "winding numbers" $m_t$ (defined on $x \in [0,1)$).

To all cats: keep checking that after your flip of signs of $m_t$'s Eqs. (4), (16), (22) and (6.12) are consistent.

**2017-07-31 Boris** Changed time ago. They should have the same sign as Percival and Vivaldi i.e., our $m$ are positive!

**2017-08-05 Predrag** dropped this: " We illustrate this by first reviewing the $d = 1$ case (introduced in [76]), but the focus of the paper is the $d = 2$ case (introduced in [48]). "

**2016-12-15 Predrag** I worry a bit as whether it make sense. It works for a single letter, $\mathcal{R} = [1 \times 1]$. Have to argue that for larger blocks $\mathcal{N}(\mathsf{M}_\mathcal{R}|\mathsf{M}_{[L\times T]})$ does not grow exponentially or as a power of $LT$? Perhaps obvious... Anyway, $\mathcal{N}$ is never mentioned again in the paper.

**2017-07-29 Boris** Looks like a misunderstanding here. I have tried to make the text more clear. We should distinguish between frequencies in (4) and measures $\mu(\mathsf{M}_\mathcal{R})$, at least on the level of definitions. They coincide for systems with unique ergodic measure. For me the normalization looks correct. Note that $LT$ is just the total number of patterns within $\mathsf{M}_{[L\times T]}$ (minus boundary "effects"). $\mathcal{N}$ is never mentioned but we use it together with (8) to build histograms on fig. 5.

**2017-08-11 Predrag** I now get it. $LT$ is the area of $\mathcal{R}$. The total number of blocks grows exponentially with the size of $\mathcal{R}$ and is bounded from above by $(LT)^{|\mathcal{A}|}$. You are saying that the number of times a *single* admissible block $\mathsf{M}_\mathcal{R}$ shows up over a region $[L\times T]$ grows linearly with the area $LT$, and so does the sum over frequencies of all distinct admissible blocks $\mathsf{M}'_\mathcal{R}$? These "frequencies" are *relative*, in the sense that correct normalization is not (8), but

$$\mu(\mathsf{M}_\mathcal{R}) = \frac{f(\mathsf{M}_\mathcal{R})}{\sum_{\mathsf{M}'_\mathcal{R}} f(\mathsf{M}'_\mathcal{R})}\,. \tag{6.13}$$

**2017-08-05 Predrag** Cylinder sets are subtle: if we were counting only *admissible* $\mathsf{X}$, the cylinder set would be much smaller. But we almost never know all inadmissible states.

**2016-11-07 Predrag** There is also a large literature on multi-dimensional shifts [6–9, 17, 21, 22, 39, 51, 54, 55, 70, 71, 83, 90] that does not seem to directly relevant to the 2-dimensional spatiotemporal symbolic dynamics studied here?

**2017-08-02 Boris** I have checked the consistency of the symbol definitions ($m \to -m$ issue). Double check might be needed in captions, but otherwise OK. Rule-of-thumb - internal symbols are non-negative, Green's functions are positive.

**2017-07-31 Boris** Li subsection *Blocks of length $\ell$,* was siminos/cats/catGenerL.tex 2017-02-17, mostly contained repetitions of the previous stuff. Did not think we needed it. Few usable things could be brought to other places. Agree?

**2017-08-23 Predrag** Done.

**2017-08-05 Boris** We probably do not need to write again explicitely here the (4). Not sure about the above disassembling of map: $[\Box + 2d\,1]$ and $-s1$ is the on-site

cat map dynamics. Sounds too mysterious.

**2017-08-26 Predrag** Removed: " The term $\Box + 2d\,1$ is the standard statistical mechanics diffusive inverse propagator that counts paths on a $d$-dimensional lattice [92], and $-s1$ is the on-site cat map dynamics (for the Hamiltonian formulation, see Appendix B). 2CB

**2017-08-05 Boris** Something unclear here (at least for me). "The iteration of a map $g(x_t)$ generates a group of *time translations*". Why translations? $g$ is a (time) map acting on all sites of lattice independently (no interaction). Note: I think the models in [78] and [19] are of the same type. Both can be thought of as products of two maps: " Interactions" · "Single particle propagations" (i.e., product of $g$'s)
**2017-09-04 Predrag**: You are right, I have rewritten that text now.

**2016-11-07 Predrag** dropped " this is another path to a deeper understanding of foundations of statistical mechanics; ordered phases, chaotic phases, and the phase transitions that separate them. "

**2017-08-28 Predrag** For the Dirichlet (as opposed to periodic) boundary condition, which breaks the translational symmetry, we take the very unphysical b.c. $x_z = 0$ for $z \in \mathcal{R}$. Finite windows into turbulence that we describe by our symbol blocks never have such edges. Methinks...

**2017-09-12 Boris** This equation

$$\begin{aligned} x_{n,t+1} &= p_{n,t} + (s-3)x_{n,t} - (x_{n+1,t} - 2x_{n,t} + x_{n-1,t}) - m^x_{n,t+1} \\ p_{n,t+1} &= p_{n,t} + (s-4)x_{n,t} - (x_{n+1,t} - 2x_{n,t} + x_{n-1,t}) - m^p_{n,t+1}\,. \end{aligned} \tag{6.14}$$

seems wrong. We use (B.1).

[2017-09-14 Boris] Recall that (the Dirichlet) $\mathsf{g}_{zz''}$ is a function of both $z$ and $z''$ and not just of the distance between them $|z - z''|$.

**2017-09-04 Predrag** "integer $s > 4$" is not the correct condition, for $d = 2$ $s = 4$ is already hyperbolic. For $d = 2$ $s = 4$ is presumably already hyperbolic. To add to the confusion, in his report Adrien computes for $s = 3$, the case with no interior alphabet symbols. So $s > 2$ is the correct hyperbolicity condition for all $d$? Give the correct condition on $s$, explain it.

**2017-09-12 Boris** Here are the answers to this and co. questions over the paper.

(i) The system is uniformly (fully) hyperbolic for $s > 2d$. This means all eigenvalues of linearized map (see (B.3) for $d = 2$) are either $|\Lambda| < 1$ (stable subspaces) or $|\Lambda| > 1$ (unstable subspaces).

(ii) For $s = 2d$ the system is partially hyperbolic. This means everything as above except two Lyapunovs for which $\Lambda = 1$ (neutral subspaces).

(iii) For $|s| < 2d$ system is non-hyperbolic. Apparently for everything in this paper 1 & 2 is OK. But

(iv) drastically changes everything (suspect a phase transition in physics jargon i.e., non-unique SRB measure). So whatever we consider in the paper should be for $s \geq 2d$.

**2017-09-26 Boris** Dropped this: " with the corresponding probability of occurrence of a fixed symbol block $\mathsf{M}_{\mathcal{R}}$ given by

$$\mu(\mathsf{M}_{\mathcal{R}}|\mathsf{M}_{[L\times T]}) = \frac{f(\mathsf{M}_{\mathcal{R}}|\mathsf{M}_{[L\times T]})}{\sum_{\mathsf{M}'_{\mathcal{R}}} f(\mathsf{M}'_{\mathcal{R}}|\mathsf{M}_{[L\times T]})}\,, \qquad \sum_{\mathsf{M}_{\mathcal{R}}} \mu(\mathsf{M}_{\mathcal{R}}|\mathsf{M}_{[L\times T]}) = 1\,,$$

where the sum goes over all distinct admissible blocks $\mathsf{M}'_{\mathcal{R}}$."
The point is that

$$\sum_{\mathsf{M}_{\mathcal{R}}} \mathcal{N}(\mathsf{M}_{\mathcal{R}}|\mathsf{M}_{[L\times T]}) = LT - \text{ "Terms linear in L and T"}.$$

So no need in an artificial normalization - normalization in (8) would follow anyhow. Also I prefer not to use $\mu$ at this point, but rather leave it till (8). There it looks OK, since the explanation on $\mu$ follows immediately after.

**2017-09-14 Boris** A comment on $s = 2d$ case (do not know how much of it we need for the paper). Our results in this paper require in principle $s > 2d$ (all Lyapunovs are positive). However certain things still work (by whatever reason) for $s = 2d$ as two figs in section Appendix B.2 show. In this case the total momentum $\sum_{n=1}^{L} p_{n,t}$ is preserved. This can be seen from the invariance of (4) under translation $x_{n,t} \to x_{n,t} + \alpha$. So the system is not ergodic and linear encoding is not one to one (different trajectories might have the same symbolic representation). However, it is (probably) ergodic on the shell $\sum_{n=1}^{L} p_{n,t} = const$. This is probably the reason why our formulas for frequencies of $\mathsf{M}_{\mathcal{R}}$ still work.

**2017-09-14 Boris** Replaced this eq.

$$\mathsf{M} \cup \partial\mathcal{R} = \begin{bmatrix} & x_{12} & \\ x_{01} & m_{11} & x_{21} \\ & x_{10} & \end{bmatrix} = \begin{bmatrix} & x_2 & \\ x_1 & m_{11} & x_3 \\ & x_4 & \end{bmatrix} \tag{6.15}$$

by the first plot in figure 4.

**2017-12-01 Predrag** removed "X, being a solution, is by definition an admissible spatiotemporal block." from subsection*Statement of the problem.

**2016-11-15, 2017-08-28 Predrag** A side issue: When I look at the intersection of the diagonal with the partition strips in by inspecting figure 2, I find that the Fibonacci numbers 1,2,3,5, ... give the numbers of periodic points, in agreement with the Adler-Weiss Markov partition. So the linear code is not a generating partition, but periodic orbits do the right thing anyway.

**2018-04-05 to Adrien from Predrag** I think figure 7 is really hard to explain to a reader; why these axes, how did all points get mapped into the same unit square, why there are huge empty swaths - all stuff that distracts from the main point which is that $x_z$'s within the center of the shared symbol block are exponentially close.

I think we can simplify this greatly, using the fact that the damped Poisson equation (35) is linear, so one can subtract patterns in order to visualize their distance.

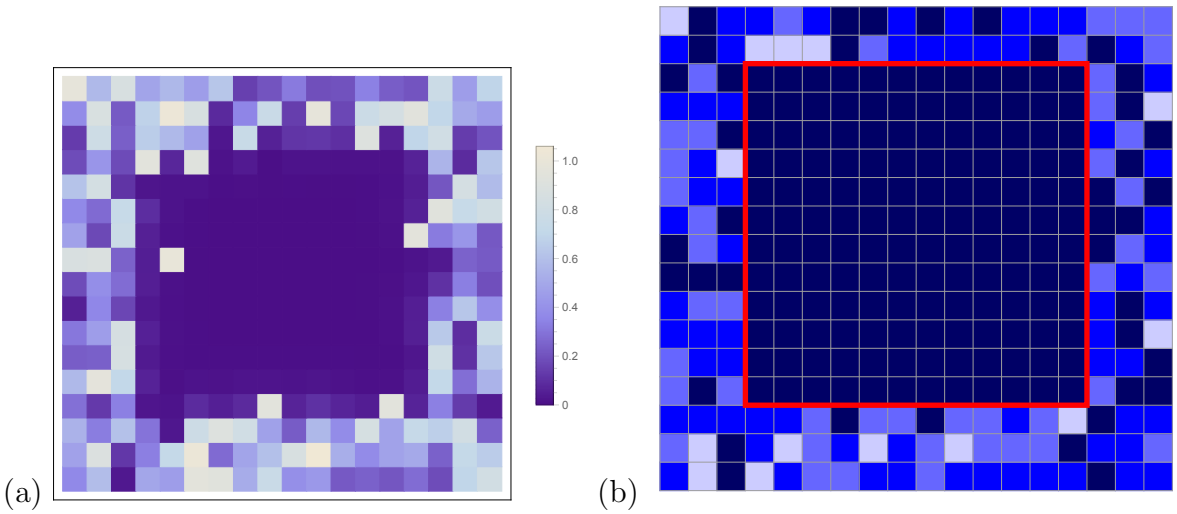


**Figure F5.** (Color online) (a) $\mathsf{X}_{2,z} - \mathsf{X}_{1,z}$ , the site-wise distance between the invariant 2-tori fields corresponding to the $[18 \times 18]$ symbol blocks $\mathsf{M}_1$, $\mathsf{M}_2$ (colored tiles) of figure 6 (a), respectively (b). (b) The plot of the logarithm of the site-wise distance $\ln|\mathsf{X}_{2,z} - \mathsf{X}_{1,z}|$ emphasizes the exponential falloff of the distance around the center of the shared block $\mathcal{R} = \mathcal{R}_0 \cup \mathcal{R}_1$. As $\mathsf{X}_z$ take rational values, for finite $[L \times T]$ invariant 2-tori, and sufficiently close $\mathsf{X}_{2,z}$, $\mathsf{X}_{1,z}$ the cancelations can be exact.

In order to have a 2-dimensional visualisation for each block, color the symbol $\mathsf{M}_j$ $[L_1 \times L_2]$ block with discrete color alphabet $\mathcal{A}_0$, as in figure 6, and the corresponding state $\mathsf{X}_j$ $[L_1 \times L_2]$ block with colors chosen from a continuum color strip.
As this is a linear problem, you can also represent closeness of two $[L_1 \times L_2]$ blocks by using this coloring scheme for $\mathsf{M}_2 - \mathsf{M}_1$ and $\mathsf{X}_2 - \mathsf{X}_1$.
For pairs of distinct 2-tori which share the same region of $m_z$'s, or a single 2-torus in which the same region of $m_z$'s appears twice, the states $x_z$ in the center of the region should be exponentially close, in order to demonstrate that they shadow each other.
So, replace figure 7 by (a) $\mathsf{M}_2 - \mathsf{M}_1$ from figure 6 (it will be all the same color in the shared region), and (b) plot $\mathsf{X}_2 - \mathsf{X}_1$. Mark the lattice point $z$ with the minimal value of $|x_z^{(2)} - x_z^{(1)}|$ on this graph, and in the text state the minimal value of $|x_z^{(2)} - x_z^{(1)}|$. You can also state the mean Euclidean (or L2) distance between the two invariant 2-tori:

$$d_{\mathsf{X}_2-\mathsf{X}_1} = \left( \frac{1}{LT} \sum_z (x_z^{(2)} - x_z^{(1)})^2 \right)^{1/2} , \tag{6.16}$$

or distance averaged over the lattice points restricted a region $\mathcal{R}$.

**2018-04-13 Adrien** After reconstructing the orbits separately, I plotted the distance between the positions in $(q, p)$ space for each lattice site $z$, see the new figure F5, meant to replace the current figure 7. Still have to use sensible color ranges, and compute figure F5 (b).

**2018-04-13 to Adrien from Predrag** Also of interest might be the color-coded plot of value of $x_{q,p}$ for at least one of them. Would be nice to check -at least once- whether there is any relation to the corresponding $m_{q,p}$ (probably there is no relation).

We'll have to rethink coloring (should be the same as $m_{q,p}$, more or less).

As the distance decreases exponentially towards the center, you probably want a color plot of $\ln|x^{(}_{q,p}2) - x^{(}_{q,p}1)|$ to resolve the small distances towards the center of the square.

Note to Predrag - send this paper to Vladimir Rosenhaus vladr@kitp.ucsb.edu